University of Ulm
Institute of Pathology

Head of the Department: Prof. Dr. med. Peter Möller

Analysis of Amyloid beta (Aβ) protein in Amyloid precursor protein (APP) transgenic mouse models of Alzheimer's disease (AD) and in human brains

Doctoral Thesis

for

Ph.D. degree in Human Biology

from the

Faculty of Medicine

of the

University of Ulm

Ajeet Rijal Upadhaya

from

Lalitpur/Nepal

2012

Dean of the Faculty of Medicine: Prof. Dr. Thomas Wirth

1. Fist Supervisor: Prof. Dr. Dietmar Rudolf Thal

2. Second Supervisor: Prof. Dr. Christine von Arnim

Day of the defence: 22.06.2012

Table of contents

Abbreviations iii

1 Introduction 1

1.1 Neuropathology and biochemistry of AD 3
1.1.1 Amyloid beta (Aβ) 3
1.1.1.1 Classification of Aβ plaques 7
1.1.2 Aβ aggregation 8
1.1.3 Aβ deposition in the aging brain and AD 10
1.1.4 Neurofibrillary pathology 12
1.1.4.1 Staging of neurofibrillary pathology 13
1.1.5 Neuronal and synaptic loss in aging brain and AD 14

1.2 Aβ toxicity 15

1.3 Transgenic mouse models of Alzheimer's disease 16

1.4 Aims of the study 20

2 Material and Methods 22

2.1 Animal models 25

2.2 Morphological Analysis of Traced Neurons 26

2.3 Immunohistochemistry for mouse brains 27

2.4 Determination of plaque and CAA distribution in the mouse brain 28

2.5 Neuropathology and human sample characterization 28

2.6 Protein extraction from mouse and human postmortem brain 29

2.7 Measurement of total protein concentration (BCA measurement) 31

2.8 Immunoprecipitation 31

2.9 Blue native (BN) and SDS Polyacrylamide gel-electrophoresis (SDS-PAGE) 31

2.10 Electron microscopy of immunoprecipitated oligomeric and fibrillar/protofibrillar proteins from human AD and control brains 33

2.11 Analysis of synthetic $A\beta_{42}$- and $A\beta_{40}$-aggregates in native state and after SDS-denaturation 33

2.12 Aβ ELISA 34

2.13 Electron Microscopy and Analysis of Synaptic Density and Dystrophic Dendrites 34

2.14 Stereological assessment of the number of hippocampal neurons 36

2.15 Photoconversion of DiI-traced neurons and subsequent immuno EM 36

2.16 Statistical analysis 37

3 Results 38

3.1 Neurodegeneration in APP23 mice but not in APP51/16 mice 38

3.2 Aβ-aggregates and deposits in APP23 and APP51/16 mice 41

3.3 Oligomeric, protofibrillar and fibrillar Aβ-aggregates in human AD, ADRP, and

control brain **45**

3.4 High-molecular weight $A\beta_{42}$ aggregates predominate in the soluble/dispersible fraction of native brain homogenates from human and APP23 and APP51/16 mice **47**

3.5 SDS-treatment destroys native high-molecular weight $A\beta_{42}$ and $A\beta_{40}$ aggregates **50**

3.6 A11-antibody and B10AP-antibody fragments specifically precipitate oligomeric and protofibrillar/fibrillar proteins including Aβ oligomers, Aβ protofibrils and Aβ fibrils in AD cases **52**

3.7 Quantitative differences in dispersible Aβ oligomer, protofibril and fibril levels distinguish APP23 from APP51/16 mice and AD from control/ADRP brain **55**

4 Discussion 60

4.1 High-molecular weight Aβ-oligomers and protofibrils are the predominant Aβ-species in the native soluble/dispersible protein fraction of the AD brain. **60**

4.2 Dispersible, SDS-denaturable high-molecular weight Aβ aggregates are associated with dendritic degeneration in amyloid precursor protein transgenic mouse models and with Alzheimer's disease **63**

4.3 Conclusion and Future perspective **67**

5 Summary 69

6 References 71

7 Appendix 86

8 Acknowledgement 91

Abbreviations

Aβ	Amyloid beta
ABC complex	Avidin biotin peroxidase complex
ANOVA	Analysis of variance
ADDL	Aβ-derived diffusible ligand
AD	Alzheimer's disease
ADRP	AD related pathology
AGD	Argyrophilic grain disease
AICD	APP intracellular domain
APH-1	Anterior pharynx defective protein-1
APOE	Apolipoprotein E
APP	Amyloid precursor protein
BACE	β-site APP-cleaving enzyme
BDA	Biotinylated dextrane amine
CAA	Cerebral amyloid angiopathy
CA1	Cornus Ammonis
cDNA	Complementary deoxyribonucleic acid
Cg	Cingulate cortex
D	(amino acid) Aspartic acid
CTF	C-terminal fragment
DAB	3, 3-diaminobenzidine
dd$H_2$0	Double destilled hydrogen oxide
DiI	1,1'-dioctadecyl-3,3,3',3'-tetramethylindolcarbocyanine perclorate
ELISA	Enzyme linked inmunoabsorvent assay
H_2O_2	Hydrogen peroxide
hAPP	Human amyloid precursor protein
HCl	Hydrogen chloride
hiMW	High molecular weight
hPrP	Hamster prion protein promoter
I	(amino acid) Isoleucine
Ig	Immunoglobulin
K	Lysine
kDa	KiloDalton

KI	Knock-in
L	(amino acid) Leucine
loMW	Low molecular weight
LTP	Long term potentiation
LRP-1	Low density lipoprotein receptor-related protein
LR White	London Resin White
M	(amino acid) Methionine
M	(concentration) molar
M1	Primary motor cortex
M2	Secondary motor cortex
MgCl2	Magnesium chloride
mRNA	Messenger ribonucleic acid
MW	Molecular weight
N	(amino acid) Asparagine
n	Number of animals
Na_2EDTA	Disodium ethylenediaminetetraacetic acid
Na_2HPO4	Disodium hydrogen phosphate
NaCl	Sodium Chloride
NaH_2PO_4	Sodium dihydrogen phosphate
NaOH	Sodium hydroxide
NFP	Neurofibrillary pathology
NFT	Neurofibrillary tangles
NMDA	N-methyl-D-aspartic acid
P	(amino acid) Proline
p3	Peptide produce by cleavage of APP by α- and β secretases
PBS	Phosphate buffer solution
PCR	Polymerase chain reaction
PHF	Paired helical filament
pHMG	p-Hydroxymethyl CoA reductase
PDGF-β	Platelet derived growth factor-β
PDAPP	Platelet derived APP
PCR	Polymerase Chain Reaction
PEN-2	Presenilin enhancer protein-2
PFA	Paraformaldehyde

PS	Presenilin
S1	Primary somatosensory cortex
SDS	Sodium dodecyl sulfate
TAE	Tris acetate EDTA
TBS	Tris buffer solution
Thy	Thymocyte
Tris HCl	Tris hydrochloride
UV	Ultraviolet
V	(amino acid) Valine

1 Introduction

Alzheimer's disease (AD) is a neurodegenerative disorder that is clinically characterized by deficits in memory, thinking skills, and retaining new information. In the end stage, it destroys the ability to carry out the simplest tasks of daily life (Storandt et al., 1984; Knopman and Ryberg, 1989; Welsh et al., 1991; Petersen et al., 1994; Grober and Kawas, 1997). AD symptoms include impairments in memory, executive functioning, perceptual speed, verbal ability, visuospatial skill and attention (Lamy et al., 1989; Backman et al., 2004; 2005; Twamley et al., 2006). Epidemiologically, AD is the most common cause of dementia in the elderly and represents 50-70% of all dementia cases (Lamy et al., 1989; Ferri et al., 2005). Other major causes of dementia are cerebrovascular disease (CVD), Parkinson's disease with dementia (PDD), dementia with Lewy bodies (DLB), and frontotemporal dementia (FTD). AD mainly affects older individuals, although in some cases the onset of disease occurs at the age of 65 or earlier. After age 65, the likelihood of developing AD doubles every five years (Lamy et al., 1989). According to 2010 World Alzheimer Report, there are estimated 35.6 million people living with AD-related dementia worldwide, presumably increasing to 65.7 million by 2030 and 115.4 million in 2050.

The neurodegenerative changes of AD develop long before clinical manifestation of the disease (Katzman, 1994; Thal et al., 2004; Braak et al., 2011). As the pathological changes of AD gradually accumulate, clinical symptoms also start to appear. Afterwards, cognitive deficits become evident and increase in parallel with progressive neurodegeneration (Salmon and Bondi, 2009). The term mild cognitive impairment (MCI) is used to refer to very mild cognitive deficits not fulfilling the criteria of dementia (Arnaiz and Almkvist, 2003). However, as not every person with MCI develops AD, it is still debated whether MCI corresponds to different diagnostic entities or truly represents the first step of a progressive neurodegenerative disorder leading to AD (Petersen et al., 2001). AD is caused by multiple genetic and environmental risk factors. Some risk factors are genetically determined, whereas others are associated with individual lifestyle. Some studies have shown that individuals with low education levels have a two-fold to three-fold higher risk of developing dementia and AD (Zhang, 1990; Friedland, 1993; Katzman, 1993; Stern et al., 1995; Callahan et al., 1996). High cholesterol levels and high blood pressure may also increase the risk for developing AD (Elias et al., 1993; Hofman et al., 1997; Clarke et al., 1998). Young adults who experience moderate or severe head injury have more than double the risk of developing AD and other forms of dementia later in life (Plassman et al.,

2000). Some researchers suspect that increased exposure to certain substances, such as aluminum, may make some persons more susceptible to AD.

Age, however, is the primary risk factor for AD along with a family history of dementia. It is not clear why the progression of the disease varies among individuals. Most AD cases develop clinical symptoms beginning at 60 years or older. This type of AD is termed as late-onset-AD (LOAD) (Brookmeyer et al., 1998) and represents more than 90% of all AD cases with no obvious genetic inheritance. In contrast, familial AD (FAD) represents a group of individuals who develop clinical and histopathological symptoms of AD traceable to inherited gene mutations. Approximately 10% of all Alzheimer cases are early-onset familial forms of autosomal dominance or recessive inheritance, usually with an onset before age 60 (Hardy, 1997; Blennow et al., 2006).

In FAD, about 90% of patients show autosomal dominant mutations in at least three different genes that encode either the amyloid precursor protein (APP) gene on chromosome 21, the presenilin 1 (PSEN1) gene on chromosome 14, or the presenilin 2 (PSEN2) gene on chromosome 1 (Goate et al., 1991; Levy-Lahad et al., 1995; Sherrington et al., 1995; Raux et al., 2005; Rovelet-Lecrux et al., 2006). The first genetic mutation connected with early-onset AD was in the APP gene located on the long (q) arm of chromosome 21 at position 21. Mutations in the γ-secretase cleaveage site of APP increase the possibility that APP C-terminal fragments are cleaved, thereby leading to the production of $A\beta_{40}$ and $A\beta_{42,}$ that are the most abundant species of Aβ in AD-related neuritic plaques (Younkin, 1995; Scheuner et al., 1996), and prone to form fibrils (Suzuki et al., 1994; Tamaoka et al., 1994; Selkoe, 1999). The relative amount of $A\beta_{42}$ formed is particularly noteworthy because this longer form of Aβ is far more prone to oligomerize and form fibrils than the more abundantly produced $A\beta_{40}$ peptide (Burdick et al., 1992; Jarrett et al., 1993; Selkoe, 1999; Walsh and Selkoe, 2007). Production of Aβ also depends on the available amount of APP. Overproduction of APP in Down's syndrome due to triplication of APP (Lejeune et al., 1959) leads to Aβ plaque deposition and manifestation of clinical and pathological AD in persons in their late 40s or early 50s (Wisniewski et al., 1985; Rumble et al., 1989). Moreover, APP overproduction is also linked to autosomal dominant early-onset FAD-related dementia with cerebral amyloid angiopathy (CAA), which is the consequence of APP locus duplications (Rovelet-Lecrux et al., 2006; Thinakaran and Koo, 2008).

Currently, the only known genetic high risk factor for sporadic AD is the APOE ε4 allele (Corder et al., 1993; Schmechel et al., 1993; Strittmatter et al., 1993). Carriers of the

APOE ε4 allele were found to have the highest risk of developing AD (Roses, 1996). Between 40% and 80% of patients with AD possess at least one APOE ε4 allele, indicating that there must be other risk factors as well (Goate et al., 1991; Mahley et al., 2006). APOE ε4 increases the risk of AD by three times in heterozygotes and by 15 times in homozygotes (Blennow et al., 2006).

AD shows a typical pathology with accumulation of abnormal protein aggregates in the form of plaques and neurofibrillary tangles (NFT). In the following introductory sections, the pathology and biochemistry of AD will be described and discussed.

1.1 Neuropathology and biochemistry of AD

The clinical symptoms of AD are associated with progressive degenerative changes in multiple brain regions (Braak and Braak, 1991a, c; Thal et al., 2000b; Thal et al., 2000c; Small et al., 2003). Macroscopically, the AD brain shows general atrophy beginning in the medial temporal lobe (MTL) with reduction of volume, thickness, and length of the cortical ribbon and ventricular dilatation (Duyckaerts and Dickson, 2003). Approximately, 300 g of brain weight is lost in AD brains at autopsy compared with age-matched controls. The degree of cortical atrophy varies among individuals but seems to correlate with cognitive decline (Mouton et al., 1998).

Microscopically, AD is characterized by extracellular deposition of Aβ in the form of plaques, and about 80-100% of AD cases are associated with CAA, which is characterized by the deposition of Aβ in leptomeningeal and cortical arteries, veins, arterioles, venules, and capillaries (Schlote, 1965; Mandybur, 1986; Natte et al., 1999). In addition, NFT and neuropil threads (NT) consisting of intraneuronal aggregates of abnormally phosphorylated tau protein are also observed in AD brains (Alzheimer, 1907; Masters et al., 1985a; Braak and Braak, 1991b; Dickson, 1997; Esiri et al., 1997; Duyckaerts and Dickson, 2003). Accumulation of plaques and NFTs in AD finally leads to neuronal and synaptic loss in the brain (DeKosky and Scheff, 1990; Terry et al., 1991; Masliah et al., 1992; Gomez-Isla et al., 1997; Selkoe, 2002). In sections 1.1.1-1.1.5, the production of Aβ, its accumulation in the brain in various forms of aggregates, the generation of NFTs, and synaptic as well as neuronal loss will be explained in detail, including its role in the progression of AD.

1.1.1 Amyloid beta (Aβ)

Aβ is a 36-43 amino acid long peptide of 4 kDa MW. The two major forms of monomeric Aβ are $A\beta_{1-40}$ and $A\beta_{1-42}$ (Glenner and Wong, 1984; Masters et al., 1985b; Iwatsubo et al.,

1994). Aβ is synthesized as a part of a large integral membrane protein, i.e., amyloid precursor protein (APP) by sequential proteolytic cleavage (Goldgaber et al., 1987; Robakis et al., 1987; Tanzi et al., 1987; Kang et al., 1997). The protein structure and cellular functions of APP are consistent with its potential role as a cell-surface receptor implicated in cell adhesion (Kang et al., 1987), although a natural ligand for APP remains to be established. APP is an internal type I transmembrane glycoprotein that has a β-peptide spanning transmembrane region between a large amino terminal extracellular/luminar domain (ectomain) and a short cytoplasmic tail. Three different isoforms of APP have been described, namely: APP695 (neuronal isoform), APP770 (peripheral isoforms), and APP751 (glial isoforms), which develop as a result of alternative splicing (Kang et al., 1987; Kitaguchi et al., 1988; Ponte et al., 1988; Tanzi et al., 1988). The amyloid cascade hypothesis (Hardy and Selkoe, 2002) postulates that accumulation of Aβ, specifically $A\beta_{42,}$ in the brain is the primary event in AD pathogenesis subsequently leading to the aggregation of Aβ. The rest of the disease process, including formation of neurofibrillary tangles containing tau protein, is proposed to result from an imbalance between Aβ production and Aβ clearance. The amyloid cascade hypothesis, however, has been of considerable debate for many years (Braak and Braak, 1991a; Korczyn, 2008; Pimplikar, 2009; Karran et al., 2011)

The proteolytic processing of APP consists of cleavage of APP by three proteases named as α, β, and γ-secretases (Fig. 1). The entire process can be categorized into two distinct pathways (Fig. 1): (1) the non-amyloidogenic pathway and (2) the amyloidogenic pathway, which leads to the production of the Aβ peptide. In the non-amyloidogenic pathway, APP cleavage is initiated by an α-secretase within the Aβ sequence (between residues K16 and L17 of Aβ), thus precluding Aβ peptide generation (Esch et al., 1990; Sisodia et al., 1990; Pasternack et al., 1992). The α-cleavage leads to the generation of a large soluble N-terminal fragment (sAPPα) released into the lumen of the organelles or into the extracellular space, and to the retention of 83-amino-acid long C-terminal membrane-bound fragment (α-CTF or APP-CTFα or C83), which has neurotrophic and possibly neuroprotective properties. The C-terminal membrane-bound α-CTF is subsequently cleaved by γ-secretase [a multimeric protein complex that includes presenilin-1 (PSEN1) or PSEN2 (Sherrington et al., 1995), nicastrin (Yu et al., 2000), anterior pharynx defective protein (APH)-1, and presenilin enhancer 2 (PEN2) (Francis et al., 2002; Kaether et al., 2006)] within the transmembrane domain and gives rise to an N-terminal truncated Aβ 3kDa p3 peptide (Haass et al., 1993), which is found only in a few cored neuritic plaques

in late-stage AD cases (Iwatsubo et al., 1996; Thal et al., 2005) and in the APP intracellular domain (AICD) (Cao and Sudhof, 2001; Cupers et al., 2001; Kimberly et al., 2001). In the amyloidogenic pathway, on the other hand, APP is first cleaved by β-secretase (between M-596 and D-597 position of full length APP695), which leads to the production and release of sAPPβ and a membrane-bound C-terminal (β-CTF or C99) fragment (Roch et al., 1993; Vassar and Citron, 2000). The intramembranous C99 fragment is further cleaved by γ-secretase at several sites to produce various forms of Aβ species, such as $Aβ_{36}$, $Aβ_{38}$, $Aβ_{40}$, $Aβ_{42}$, $Aβ_{43}$ (Li et al., 2003; Citron, 2004; Iwatsubo, 2004; Ma et al., 2005), and the C-terminal fragment, i.e., AICD (Haass et al., 1992).

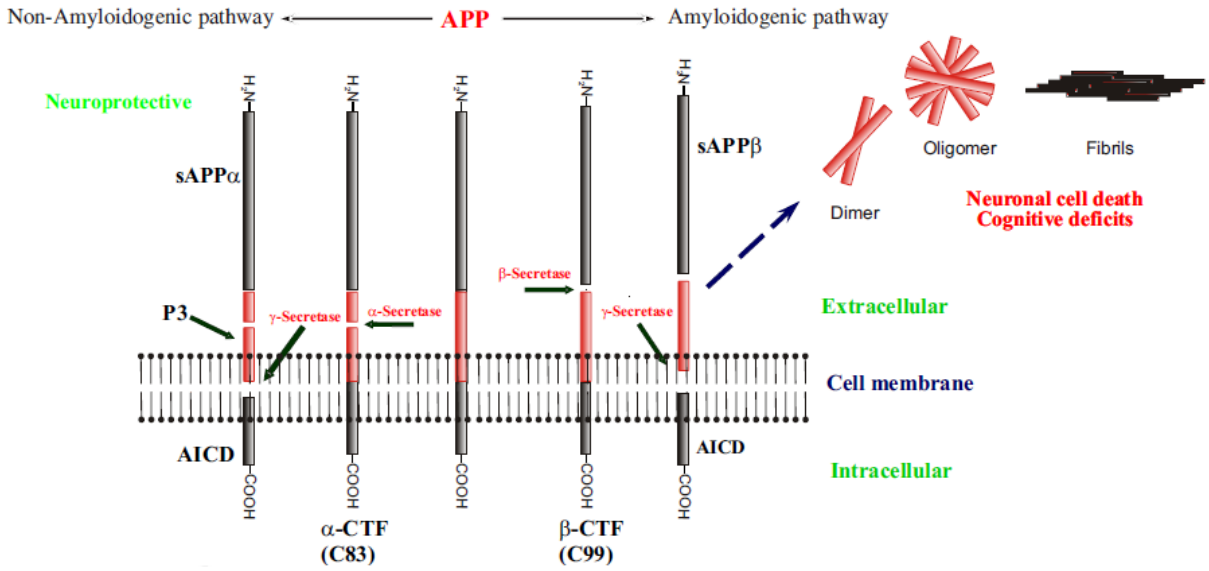

Figure 1: Schematic representation of Amyloid precursor protein (APP) cleavage pathways within the membrane. The non-amyloidogenic processing of APP by α- and γ-cleavage results in the generation of soluble APPα (sAPPα), peptide p3 and APP intracellular domain (AICD). The amyloidogenic processing of APP by β- and γ-secretases cleavage produces sAPPβ, Aβ and AICD.

In FAD, mutations in the APP gene or in the PSEN1 and PSEN2 genes interfere with the normal processing of APP, resulting in an increased production and subsequently increased aggregation of $Aβ_{42}$ (Hardy, 1997; Bertram and Tanzi, 2003; Masters and Beyreuther, 2003). However, in sporadic AD no increase in Aβ production has been detected but a reduction of Aβ clearance (Masters and Beyreuther, 2003; Miller et al., 2003; Koistinaho et al., 2004; Holtzman, 2011). Aβ-peptides in the brain occur in several compartments and different clearance mechanisms exist. Extracellular Aβ can be cleared by drainage into the perivascular space (PVS) after binding to apoE protein (Weller et al., 1998; Thal et al., 2007; Rolyan et al., 2011), by endocytosis through microglia and astrocytes (Akiyama et

al., 1996; Funato et al., 1998; Yamaguchi et al., 1998; Thal et al., 2000a) or by active transport across the blood-brain barrier (BBB) (Deane et al., 2008; Bell and Zlokovic, 2008).

Intracellular Aβ peptides may undergo enzymatic degradation by neprilysin and/or insulin-degrading enzyme (IDE) (Iwata et al., 2000; Miller et al., 2003). In the event that extracellular soluble Aβ increases in the brain, there is a high risk that it aggregates and forms oligomers of various sizes, protofibrils, and, finally, amyloid fibrils as found in plaques (Masters and Beyreuther, 2003). Such an increased aggregation of Aβ may be due to an increase of Aβ production or to decreased Aβ clearance. As a result, Aβ accumulates within neurons and in the extracellular space of the brain and forms of plaques as well as CAA. In AD pathology Aβ plaques are frequently observed in the frontal and temporal cortex (Terry et al., 1991; Arriagada et al., 1992; Masliah et al., 1994; Gomez-Isla et al., 1997; Ingelsson et al., 2004) including the individuals with no dementia. The development of dementia is associated with end-stage NFT pathology, more abundant neocortical Aβ deposition and an expansion of Aβ and NFT pathology throughout the brain including brainstem and cerebellum in the late stages AD (Braak and Braak, 1991b; Thal et al., 2002; Thal et al., 2008).

Plaques contain fibrillar aggregates of Aβ with amyloid properties. The term “amyloid” is used for a specific structure of any polypeptide or protein, which is rich in β-pleated sheet structure and can be stained with the Congo red dye showing apple-green birefringence when viewed under polarized light (Virchow, 1854, 1855; Glenner et al., 1973; Glenner, 1980; Bennhold, 1992; Kelly, 1996; Lansbury, 1999). The Aβ protein was identified in 1984/85 as the main component of vascular amyloid deposits (Glenner and Wong, 1984) and in amyloid plaques in the AD brain (Masters et al., 1985). All types of cerebral, nonvascular, or intraneuronal Aβ deposits are typically referred to as “plaques” regardless of their morphology (Duyckaerts and Dickson, 2003). Depending on their location in the brain and the point in time at which they appear, Aβ deposits can be distinguished by their morphology and protein content (Thal et al., 2006). Aβ plaques associated with dystrophic neurites are referred to as neuritic plaques (Braak et al., 1989). Two major protein components of Aβ plaques and vascular Aβ deposits are $A\beta_{40}$ and $A\beta_{42}$ (Glenner and Wong, 1984; Masters et al., 1985a; Iwatsubo et al., 1994). In addition, Aβ plaques also contain N-terminal truncated forms of Aβ. The most common forms of N-terminal truncated Aβ peptides are $A\beta_{3\text{-}40/42}$, $A\beta_{11\text{-}40/42,}$ and p3 ($A\beta_{17\text{-}40/42}$) (Saido et al., 1995; Saido

et al., 1996). Other proteins occurring in plaques are the apoE, α_2-macroglobulin, interleukin1α, interleukin 6, components of the complement system, α_2-macroglobulin receptor/low density lipoprotein receptor-related protein (LRP-1), and collageneous Alzheimer amyloid component/collagen XXV (Griffin et al., 1989; McGeer et al., 1989; Namba et al., 1991; Strauss et al., 1992; Rebeck et al., 1993; Thal et al., 1997; Hashimoto et al., 2002).

1.1.1.1 Classification of Aβ plaques

Extracellular amyloid plaques in the human brain vary in shape and size as well as in protein composition (Duyckaerts and Dickson, 2003; Thal et al., 2006). According to the protein composition and morphology of the plaques, different types can be distinguished (Duyckaerts and Dickson, 2003; Thal et al., 2006) (Table 1, Fig. 2). Aβ deposits can be assigned to one of the following classes: diffuse plaques, subpial band-like Aβ-deposits, lake-like amyloid, fleecy amyloid, cored plaques (or classical plaques), core-only plaques, and white matter plaques (Thal et al., 2000). Of all known plaque forms, diffuse plaques and cored plaques (classical) are very commonly present in AD (Masters et al., 1985a; D'Andrea et al., 2002).

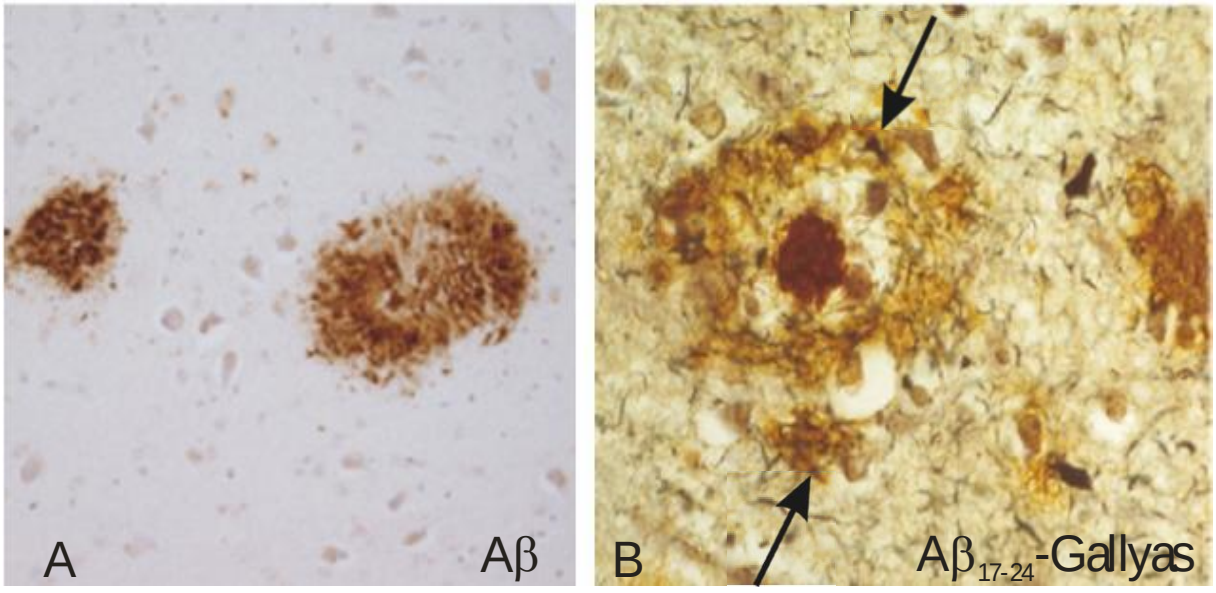

Figure 2: Amyloid beta (Aβ) deposits. Diffuse (**A**) and classical cored (**B**) plaques are the most common forms of Aβ deposits in AD. They are clearly distinguished morphologically. **A**: Diffuse plaques consist of noncompact Aβ deposits and represent the first type of plaques seen in the human brain. **B**: Classical cored plaques are characterized by a compact amyloid cored and a surrounding halo of diffuse Aβ representing the "mature" form of senile plaques. Here, dystrophic neurites (indicated by arrows) were observed in association with the plaque indicating the neuritic nature of this classical cored neuritic plaque. Reproduced with permission from (Thal et al., 2006)

Table 1: List of plaque types (Thal et al., 2000)

Plaque Type	Morphological determination	Campbell-Switzer/ Aβ $_{17-24}$	Gallyas silver staining
Diffuse plaque	**a)** Diffuse non-neuritic plaque: Sharply delineated, evenly distributed Aβ-deposits; occasionally enclosed neuronal perikarya of normal appearance (Fig. 2A) **b)** Diffuse neuritic plaque: Diffuse plaque which contains Gallyas-positive dystrophic neurites	+ +	- +
Subpial band-like Aβ	Sharply-delineated, evenly distributed band-like Aβ within the subpial portion of the molecular layer of the temporal and entorhinal cortex	+	-
Lake-like amyloid	Sharply delineated, evenly distributed Aβ deposits within the parvopyramidal layer of the presubicular region containing neuronal perikarya of normal appearance (10, 17, 23)	+	-
Fleecy amyloid	bordered cloud-like deposits consisting of N-terminal truncated Aβ	+	-
Cored plaque (5 classical plaque)	**a)** Cored non-neuritic plaque: Sharply delineated Aβ deposits with an amyloid core in the center surrounded by a corona of diffuse Aβ deposits. Between core and corona is a small gap without Aβ. This non-neuritic plaque is free of dystrophic neurites containing neurofibrillary lesions as detectable with the Gallyas silver method. **b)** Cored neuritic plaque: Cored plaque which contains Gallyaspositive dystrophic neuritis (Fig. 2B)	+ +	- +
Core-only plaque	Pure, sharply delineated amyloid cores without associated diffuse Aβ deposits	+	-
White matter plaque	**a)** Diffuse type: Sharply delineated, evenly distributed Aβ deposits within the white matter **b)** Globular type: Sharply delineated Aβ deposits in the white matter which contain globular aggregates of Aβ. Few plaques contain Gallyas-positive dystrophic neurites	+ +	- +

1.1.2 Aβ aggregation

Among the two principal forms of Aβ comprising 40 or 42 amino acid residues, $A\beta_{42}$ has gained particular attention because it oligomerizes and forms amyloid fibrils more readily than the more abundantly produced $A\beta_{40}$ peptide (Burdick et al., 1992; Jarrett et al., 1993). In the normal human brain Aβ-protein is present in small amounts as a natural product in the brain parenchyma and in cerebrospinal fluid (CSF) (Haass et al., 1992; Seubert et al., 1992; Walsh et al., 2000). Thus, the mere presence of Aβ alone does not explain neurotoxic effects causing neurodegeneration. The current concept of AD pathogenesis hypothesizes that the ordered self-association of Aβ molecules into oligomers, protofibrils, and fibrils is critical for the alteration of neurons in AD (Pike et al., 1991; Busciglio et al., 1992; Geula et al., 1998). Within amyloid plaques that pathologically characterize AD, insoluble fibrils of 6-10 nm diameters occur. In vitro synthetic Aβ can form amyloid fibrils similar to those present in senile plaques (Castano et al., 1986; Kirschner et al., 1987). One may hypothesize that aggregation of Aβ into fibrillar forms is essential for its toxicity, but this theory does not explain the relatively weak correlation between the severity of dementia and the density of fibrillar amyloid plaques in AD cases (Katzman, 1986; Terry

et al., 1991; Dickson et al., 1995). Furthermore, there was no close spatial relationship between Aβ plaques and degenerating commissural neurons in APP23 mice (Capetillo-Zarate et al., 2006). These results indicate that Aβ-induced degeneration of neurons in the brain is not due to a simple increase in Aβ plaques but to qualitative changes in the status of Aβ aggregation. This conclusion is also supported by other studies showing that the aggregation of Aβ to soluble oligomers, protofibrils, and/or fibrils is required for Aβ toxicity (Podlisny et al., 1995; Kayed et al., 2003; Kim et al., 2003; Cleary et al., 2005) and it goes beyond the findings of other authors who have reported that Aβ plaques induce local dendritic or neuritic degeneration (Tsai et al., 2004; Brendza et al., 2005; Spires et al., 2005).

The aggregation of Aβ appears to begin with the formation of small soluble oligomers (e.g. dimers or trimers) that could act as seeds and, thereby, promote rapid fibril growth (Harper and Lansbury, 1997; Soto and Estrada, 2008).

Studies of the involvement of soluble but non-fibrillar Aβ in AD have been conducted utilizing various approaches, such as synthetic Aβ peptides, cell culture systems in which APP is over-expressed, APP-transgenic mice, human CSF, and the postmortem brain. The *in vivo* study of Aβ plaque formation induced by inoculation of amyloid containing brain homogenates into monkeys or APP-transgenic mice suggests that protein fibrillization is nucleation-dependent oligomerization process (Koo et al., 1999; Kumar et al., 2011). In the beginning monomeric Aβ undergoes misfolding process which then initiates self-association property to form oligomeric nuclei or seeds (Ni et al., 2011). After the formation of the nuclei, assembly of larger aggregates and fibril elongation is much more favourable process and proceeds rapidly (Jarrett et al., 1993; Harper and Lansbury, 1997; Walker et al., 2002; Meyer-Luehmann et al., 2006; Geula et al., 2008; Meyer-Luehmann et al., 2008). Biophysical studies also support this finding (Rochet and Lansbury, 2000; Chiti and Dobson, 2006).

As discussed above, certain mutations within the Aβ domain which are responsible for early-onset AD may promote formation of oligomeric assemblies and fibrillization (Kirkitadze et al., 2001; Murakami et al., 2003; Tomiyama et al., 2010). However, such disease causing mutations in the Aβ domain are very rare and only account for a minority of cases of early-onset AD.

The mechanism that drives formation of oligomeric nuclei within wild-type Aβ and subsequently promoting AD pathogenesis remains largely unclear. Some studies of

pyroglutamate modified variants of Aβ point to a critical role of N-terminal modification in the aggregation process (Schilling et al., 2006; Schilling et al., 2008). When expressed within neurons, AβpE$_{3-42}$ induces neurodegeneration and concomitant neurological deficits in a transgenic mouse model (Wirths et al., 2009). Posttranslational modifications of Aβ, such as phosphorylation (Kumar and Walter, 2011), glycosylation, or addition of other protein subunits (Kirkitadze et al., 2001), are under discussion as well.

Fibrillogenesis of Aβ is thought to involve a series of conformational alterations, and under certain circumstances, progress to oligomers and ultimately to mature 7-10 nm wide amyloid fibrils. However, in vivo, fibril formation includes the formation of thermodynamically unstable amyloidogenic transition intermediates, known as protofibrils, which go on to self-association and stabilization, ultimately giving way to mature fibrils (Harper and Lansbury, 1997; Teplow, 1998). This protofibrillar intermediate structure has already been shown to induce acute electrophysiological changes and progressive neurotoxicity in cortical neurons (Hartley et al., 1999). Aβ dimers and other loMWAβ oligomers have toxic properties when administered to cell/tissue cultures or into the brain of rats (Lesne et al., 2006; Shankar et al., 2008; Reed et al., 2009; McDonald et al., 2010). Non-fibrillar oligomers, such as dimers and other loMWAβ are capable of inducing cognitive changes (Lesne et al., 2006) and alterations of long-term potentiation (Wang et al., 2002; Shankar et al., 2008).

1.1.3 Aβ deposition in the aging brain and AD

Aβ deposits have been found not only in the brain of AD patients but also in cognitively normal elderly (Price and Morris, 1999; Hardy and Selkoe, 2002; Oddo et al., 2004). In the non-demented elderly, AD-related Aβ deposits are restricted to distinct brain predilection sites (Thal et al., 2002). Postmortem studies found Aβ deposits in multiple areas of the brain in AD patients (Arnold et al., 1991; Braak and Braak, 1991a; Bancher et al., 1993; The National Institute on Aging, 1997; Thal et al., 2002a; Thal et al., 2006).

In both demented and non-demented cases, the expansion of Aβ deposition throughout the brain follows a hierarchical sequence in which multiple areas of the brain subsequently become affected. Given the differences in the frequency and pattern of the Aβ occurrence in the human brain, five phases of regional Aβ deposition can be distinguished, in which brain regions are hierarchically involved (Thal et al., 2002) (Fig. 3). In the first phase, diffuse Aβ plaques are found exclusively in the neocortex in layers II, III, IV, and V. The

second phase is characterized by additional Aβ deposits in allocortical brain regions, i.e., in the entorhinal region, CA1, and the cingulate cortex.

Subcortical areas become involved in phase 3, i.e., the diencephalic nuclei, the striatum, and the cholinergic nuclei of the basal forebrain. Early prefrontal Aβ deposition is also common in non-demented and preclinical AD cases (Yamaguchi et al., 2001; Bussiere et al., 2002). Further brain regions are usually free of Aβ deposits in non-demented individuals (Thal et al., 2002).

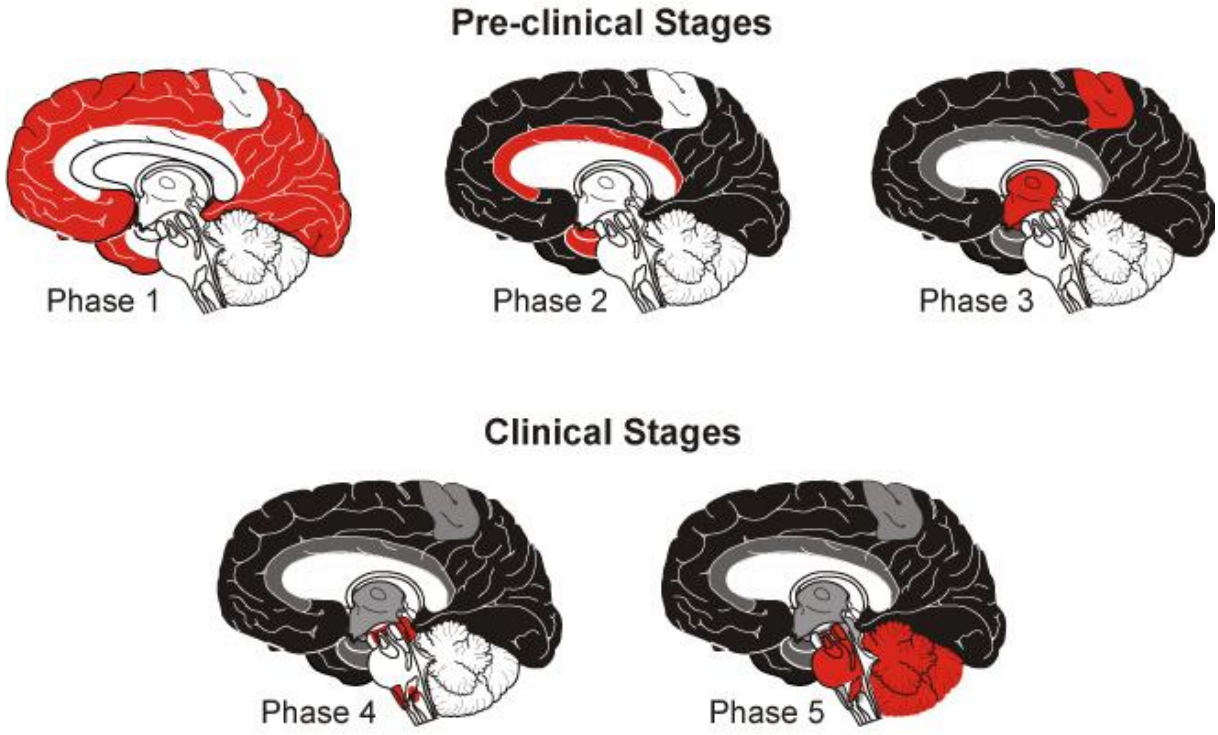

Figure 3: Preclinical and clinical stages of AD-related Aβ plaques. In nondemented elderly persons, Aβ deposits are restricted to the neocortex, allocortex, basal ganglia, and diencephalic nuclei (phases 1 to 3). Phase 1 is characterized by neocortical Aβ deposits and phase 2 shows additional Aβ deposits in the allocortical brain regions (the allocortex is a part of the brain involved in memory processing). Phase 3 exhibits, in addition to neo- and allocortical Aβ deposits, Aβ plaques in the diencephalon and basal ganglia, whereas in AD cases with clinically apparent dementia, Aβ deposits occur in all areas that are already affected in nondemented patients plus in the brain stem and cerebellum (phases 4 and 5). Phase 4 is characterized by Aβ deposits within the neo- and allocortex, diencephalon, basal ganglia, midbrain, and lower brain stem. Phase 5 shows additional Aβ deposits within the pons and the cerebellum. Newly involved brain areas are marked in red. Reproduced with permission from (Thal et al., 2004).

Cognitive deficits usually begin in parallel with the involvement of further brain regions. In phase 4 several midbrain and brain stem regions exhibit plaques, e.g., substantia nigra, red nucleus, central gray, superior and inferior collicle, inferior olivary nucleus, and intermediate reticular zone of the medulla oblongta. Finally, phase 5 is characterized by cerebellar Aβ deposition and involvement of further brain stem nuclei. The five phases of

Aβ deposition resulted from cross-sectional studies of human autopsy brains. Recent studies using PIB-imaging have confirmed the hierarchical expansion of Aβ in the brains of living patients, finally resulting in the development of AD (Klunk et al., 2004; Price et al., 2005; Cairns et al., 2009).

Aβ deposition in AD also occurs in the walls of cerebral blood vessels (Scholz, 1938; Glenner and Wong, 1984) known as CAA. In CAA, the Aβ peptides are mainly located in the walls of cortical and leptomeningeal arteries (Mandybur, 1986; Vinters, 1992; Thal et al., 2008b). CAA can cause cerebral hemorrhage and microhemorrhage in aged individuals (Vinters and Gilbert, 1983; Revesz et al., 2005; Cullen et al., 2006) as well as microinfarction and abnormalities in cerebral blood flow (Mandybur, 1979; Thal et al., 2009).

A major risk factor for capillary CAA is the presence of *APOE* ε4 genotype (Thal et al., 2002b; Thal et al., 2010). Apart from it, the mutations in the *APP* gene can also lead to a familial form CAA with hemorrhage (hereditary CAA with hemorrhage of the Dutch type) (Maat-Schieman et al., 1996).

1.1.4 Neurofibrillary pathology

Neurofibrillary pathology (NFP) is the second major histopathological hallmark of AD and includes pretangles, NFTs, NTs, and dystrophic neurites in neuritic plaques (Fig. 4). Pretangles are phosphorylated tau positive nonfibrillar inclusions inside the cytoplasm of neurons and have been assumed to represent a premature stage of NFT in AD brains (Bancher et al., 1989; Uchihara et al., 2001). NFP consists of the microtubule-associated protein tau which abnormally phosphorylates and aggregates to form these lesions (Grundke-Iqbal et al., 1986; Kosik et al., 1986). Physiologically, tau binds to microtubules in the non-phosphorylated state and regulates axonal transport (Mandelkow and Mandelkow, 1998). In AD, tau undergoes abnormal hyperphosphorylation and begins to aggregate, finally resulting in disassembly of normal microtubules, and formation of NFTs (Hernandez and Avila, 2007).

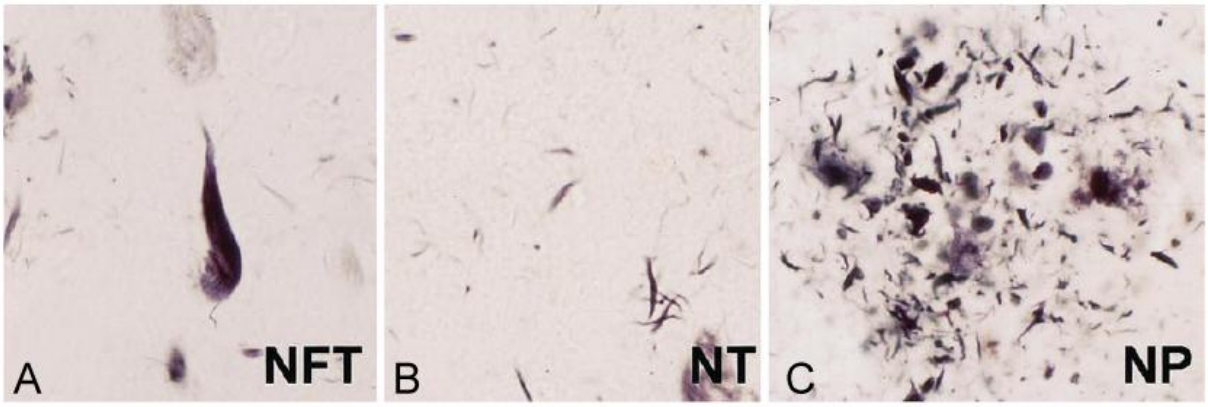

Figure 4 Neurofibrillary pathology in AD using Gallyas-staining to show neurofibrillary tangles (NFT) (A), neuropil threads (NT) (B), and dystrophic neurites (C) of neuritic plaques (NP) (Magnification A-C: 360x Reproduced with permission from (Thal and Braak, 2005).

Owing to the presence of this aggregated abnormal tau protein, AD is classified as a tauopathy. NTs are fibrillary aggregates of abnormal phosphorylated tau within dendrites (Braak and Braak, 1991a). The term neuritic plaque summarizes diffuse and cored plaques, which exhibit dystrophic neurites (Thal and Braak, 2005).

1.1.4.1 Staging of neurofibrillary pathology

Similar to Aβ plaque pathology, NFP is also found in the brains of non-demented individuals. However, in AD patients it affects more brain regions than in non-demented individuals (Braak and Braak, 1991a; Bouras et al., 1994; Braak and Del Tredici, 2011). In particular, the distribution and severity of the NFTs is highly correlated with the progression and severity of the disease (Braak and Braak, 1991). In non-demented elderly individuals, NFP is restricted to the transentorhinal, entorhinal, and limbic areas, whereas in AD brains NFP progresses according to a characteristic sequence into the cortex. The sequential evolution of NFTs can be described in six stages, i.e., Braak-NFT-Stages (Braak and Braak, 1991). Stages I and II are characterized by a mild to severe alteration of the transentorhinal region and the entorhinal cortex (transentorhinal stages I-II). Stages III-IV represent the limbic stages. In addition to the transentorhinal and entorhinal region, there is an involvement of the Ammon's horn and an expansion into the parahippocampal gyrus.

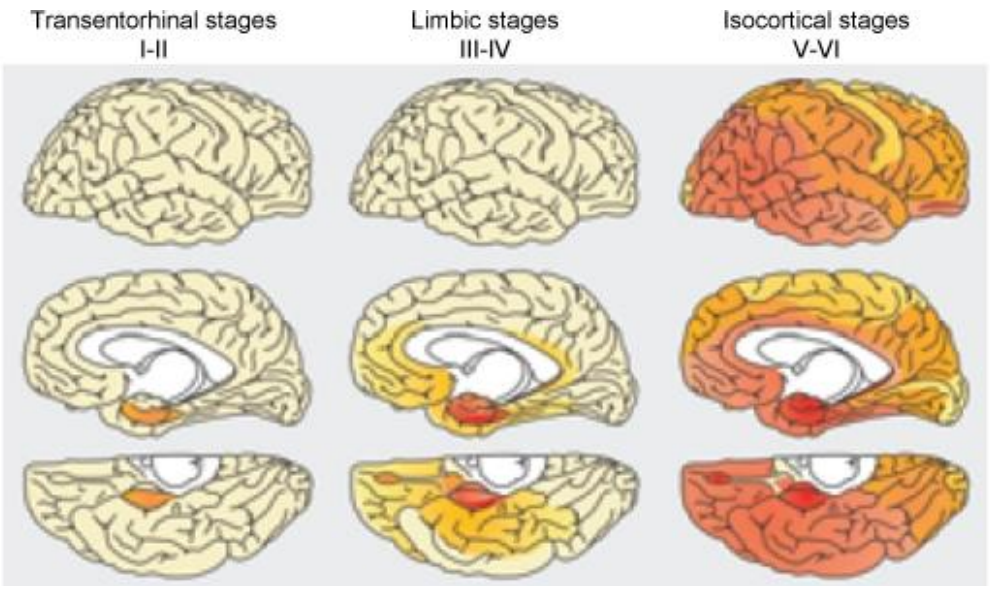

Figure 5: Distribution of the neurofibrillary pathology in human brain is divided in six Braak-NFT stages.

Stage III shows NFP within the transentorhinal and entorhinal regions. Severe involvement of the entorhinal and transentorhinal pre-α layers as well as NFP in the hippocampus and other limbic areas characterize stages III-IV. Finally, additional isocortical NFP characterizes stage V-VI. Reproduced with permission from (Braak and Braak, 1991).

Finally, stages V-VI, show further expansion of NFP in the isocortical parts of the brain. Stages IV-VI are frequently associated with cognitive decline (Thal et al., 2002). It should be noted that similar to the phases of Aβ deposition, the staging studies of NFTs were performed on the cross-sections of human brains autopsied after the death. Since the Braak-NFT stages correlate with the phases of Aβ deposition (Thal et al., 2002) that could be detected by Pittsburgh Compound-B (PIB)-imaging, it is very likely that the development of AD also follows the hierarchical sequence of NFT expansion in vivo. Recently a tau imaging radiotracer has been developed which has a high affinity and selectivity for tau pathology both in vitro and in vivo (Fodero-Tavoletti et al., 2011).

1.1.5 Neuronal and synaptic loss in aging brain and AD

Loss of synapses, dendrite pruning, and cell death are the most significant events that occur in the AD brain and they also provide the morphological correlative of cognitive decline (Ball, 1977; Terry et al., 1987; DeKosky and Scheff, 1990; Masliah et al., 1993; Masliah et al., 1994; Gomez-Isla et al., 1997; Scheff, 2003). Aβ- and NFT-associated lesions in mouse models lead to neuronal injury and synaptic loss, and finally result in neuronal

death (Bancher et al., 1989a; Calhoun et al., 1998; Sassin et al., 2000; Schmitz et al., 2004; Capetillo-Zarate et al., 2006).

There is selective vulnerability among the neuronal populations in the human brain. Although the neocortex and hippocampus are affected in AD, the pathology is not similar in all regions and, additionally, not all neuronal cell types become affected (Morrison and Hof, 1997). With regard to the region-specific neuronal loss, no significant decrease in neuron number in the entorhinal cortex and hippocampus of healthy non-demented individuals was found with age, but in advanced AD patients >46% of neuronal loss in the entorhinal cortex in CA1 was found (West, 1993; West et al., 1994; Price et al., 2001). Between the ages of 13 and 85 there is significant neuronal loss (30-50%) with aging which is limited to the hilus of the dentate gyrus and subiculum (West, 1993). Up to 60% reduction of the pyramidal cells in layer III that are mainly involved in corticocortical connections and of those in layer V have been found in AD patients (Alzheimer, 1907; Terry et al., 1981; Braak and Braak, 1991b; Duyckaerts and Dickson, 2003). In Down-syndrome patients, there is a reduction of number of pyramidal neurons in layer III and V in the frontal neocortex as well (Davidoff, 1928).

1.2 Aβ toxicity

Aβ is capable of inducing dendritic degeneration, neuronal cell loss and synapse loss. This property of Aβ is summarized by the term Aβ toxicity. Various studies have shown that neither Aβ monomers nor insoluble fibrillar Aβ, in the form of amyloid plaque cores, significantly alter synaptic plasticity (Pike et al., 1991; Walsh et al., 2002; Bieschke et al., 2008; Shankar et al., 2008). However, neurotoxicity of Aβ has been attributed to intermediate assemblies of Aβ formed by consecutive aggregation of Aβ monomers (referred to as ADDLs, i.e., Aβ-derived diffusible ligands), which were found to kill mature neurons in organotypic central nervous system cultures at nanomolar concentrations (Lambert et al., 1998). It has now become evident that one of these intermediate aggregates, 56 kDa of $A\beta_{1-42}$ assemblies (Aβ*56), is/may be responsible for memory deficits prior to amyloid deposition in APP-transgenic mice (Lesne et al., 2006). Elevated levels of Aβ oligomers result from increased Aβ concentrations and confer toxicity (Masters and Beyreuther, 2003; Selkoe, 2004). As such, the concentration of soluble Aβ aggregates correlates with disease progression in animal models and in AD cases (Mucke et al., 2000; Naslund et al., 2000; Moolman et al., 2004; Spires et al., 2005; Shankar et al., 2007). There is evidence that oligomeric, protofibrillar, and fibrillar Aβ

aggregates are neurotoxic and may trigger the development of AD-related symptoms in mouse models of AD (Harper and Lansbury, 1997; Kayed et al., 2003; Lesne et al., 2006; Habicht et al., 2007). Fibrillar Aβ in plaques is associated with neuritic alterations (Tsai et al., 2004; Spires et al., 2005). Non-fibrillar oligomers are capable of inducing cognitive changes in mice (Lesne et al., 2006) and alterations of long-term potentiation (Wang et al., 2002). In another study, it has been shown that loMWAβ-oligomers, especially dimers, interact with dendrites and induce alterations of long-term potentiation by impairing synapse structure and function, may represent immediately toxic forms of Aβ.

However, the exact mechanism(s) of Aβ toxicity as well as the minimal toxic form of Aβ are controversely discussed and still require clarification. To study soluble forms of Aβ, the protein lysate is separated by ultracentrifugation; in so doing, the dispersible Aβ is separated out for/ from analysis. Thus, it is unclear whether dispersible Aβ contributes to Aβ toxicity.

1.3 Transgenic mouse models of Alzheimer's disease

Transgenic animals have been generated to investigate disease mechanisms, to identify drug targets, and to test drugs for their efficacy before entering clinical trials. To be useful as an animal model, the transgenic organism must also be able to exhibit the essential pathological, physiological, and/or behavioral features of the human disease. A variety of transgenic mouse models have been generated to study AD pathogenesis (Table 2). Transgenic mouse models of AD overexpress wild-type or mutant APP or PSEN 1/2 with FAD-linked genes or mutant tau protein. Double, triple, as well as 5x transgenic expressing mutant APP, PSEN1 or 2 and tau are also used (Lewis et al., 2000; Lewis et al., 2001; Oddo et al., 2003; Schmitz et al., 2004).

The transgenic mouse models that overexpress mutant human APP with FAD mutations, such as PDAPP mice and Tg2576 mice, display a wide range of parenchymal Aβ lesions, i.e., senile plaques and CAA (Games et al., 1995; Hsiao et al., 1996). These lesions are quite similar to those seen in the AD brain, although biochemical differences in the Aβ deposited e.g., posttranslational modifications, exist between mouse models and AD brain (Radde et al., 2006). Predominantly neuritic plaques, accompanied by dystrophic neurites, reactive astrocytes, hypertrophic microglia, and pronounced synaptic loss near plaques were observed (Dodart et al., 1999). Although both of the aforementioned mouse models showed amyloid deposits, they failed to meet all criteria of the neuropathology of human AD (Irizarry et al., 1997; Wu et al., 2004; Spires et al., 2005). The main limitations were

no significant neuron loss and no formation of NFTs even in aged transgenic mice (Irizarry et al., 1997; Tomidokoro et al., 2001a; Tomidokoro et al., 2001b). A third APP transgenic mouse model is the APP23 mouse (Sturchler-Pierrat et al., 1997). In contrast to Tg2576 and PDAPP mice, which carry hAPP770 and hAPP695 respectively, APP23 mice express the 751 amino acid isoform of hAPP (hAPP751) with the Swedish mutation (K670N, M671LSweAPP) driven by a neuron specific Thy 1 promoter. These mice are characterized by progressive Aβ deposition and dendritic changes [see p. 20] as a result of seven-fold endogenous APP overexpression (Andra et al., 1996; Sturchler-Pierrat et al., 1997). The first Aβ deposits appear at 5-6 months of age (Sturchler-Pierrat et al., 1997; Thal et al., 2006).

Table 2: List of major APP-transgenic mouse lines used in AD research

Transgenic line	Transgene/ Promoter	Behavioural Phenotypes	Neurological characteristic	Pathologies and Deficits	References
PDAPP	human APP/PDGF-β promoter.	Age dependent and non dependent impairment of learning and memory.	Amyloid beta (Aβ) deposits, neuritic plaques, synaptic loss, astrocytosis and microgliosis	Plaques; No neurofibrill-ary tangles (NFT) or neuronal loss	(Games et al., 1995)
APPSWE (Tg2576)	Human AP695 cDNA with KM670/671NL/ hamster prion protein gene promoter	Memory deficits seen in 9-10 month old transgenic mice.	Aβ deposits at 9-12 months. Gliosis, dystrophic neurites containing phosphorylated tau. Localized neurons and synapse loss.	Plaques; No NFTs. Aβ peptide may be modified/proces sed differently to those in AD	(Hsiao et al., 1996)
APP23	APP751Swedish/ murine Thy-1.2 promoter	Learning impairment in Morris water maze and a passive avoidance paradigm	Aβ deposits at 6 months, by 24 months in neocortex and hippocampus. Inflammation, neuritic and synaptic degeneration and tau hyperphosphorylation. Evidence for CAA.	Plaques; No NFTs but dendritic degeneration	(Sturchler-Pierrat et al., 1997; Capetillo-Zarate et al., 2006)
APPLondon V717I	Human APP695 cDNA with V717I/ mouse Thy-1 gene.	Decreased exploration, increased neophobicity, increased male aggressivity.	Amyloid plaques and Cerebrovascular angiopathy - onset 10-12 months, cholinergic fiber distortion.	Plaques; No NFTs.	(Moechars et al., 1999)
PDAPPSwInd (J20)	Transgenic construct: hAPPSwInd Promoter: PDGFB Injected: C57BL/6 x DBA/2F2 embryos	WM spatial memory retention, acquisition, deficits 6-7 months (Palop et al., 2003).	Total Aβ and $A\beta_{42}$ overexpression in neocortical and hippocampus.	Plaques; No NFTs.	(Mucke et al., 2000)
APP/PSEN-1	hAPP (KM670/671NL and V717I, Thy-1 promoter) hPS-1 (M146L, HMG promoter).	Not reported.	High levels of $A\beta_{40}$ and $A\beta_{42}$ before plaque deposition. Hippocampal pyramidal cell loss. Astrocytosis in the surrounding of the plaques.	Plaques; No NFTs.	(Wirths et al., 2001)
APPsw/tau (P301)/PS1 (M146V) 3x transgenic	APPSw (KM670/671NL) tau (P301L)/Thy-1.2 promoter/co-microinjected into pronuclei of embryos of PS1M14VKI mice	Cognitive impairments by 4 months as retention/retrieval deficits occur prior to any plaques or tangle pathology. Early cognitive deficits can be reversed by immunotherapy.	Age related and progressive plaques and tangles. tau and APP expression doubled in homozygous mice in hippocampus and cerebral cortex. Hippocampal neuronal loss.	Plaques and NFTs. Deficits in LTP correlate with accumul- ation of intra-neuronal Aβ.	(Oddo et al., 2003)
APP E693Δ	MoPrP.Xho vector	Memory impairment at 8 months	Age-dependent accumulation of intraneuronal Aβ oligomers from 8 months but no extracellular amyloid deposits even at 24 months.	No plaques. Abnormaly phosphorylated tau, microglail and astrcyte activation Tau positive neurons	(Tomiyama et al., 2010)
APP51/16	Human WT APP/Thy-1.2 promoter	Not reported	Parenchymal amyloidosis, similar to that seen in AD	Plaques; No NFTs; No dendritic degeneration	(Herzig et al., 2004; Thal et al., 2009)
5X FAD APP695/PSEN1	B6SJL-Tg(APPSwFlLon,PSEN1*M146L*L286V)6799Vas/J	Hemizygous mice are viable and fertile.	Aβ42 accumulation (1.5 months), synapse degeneration (4 months), neuron loss, and spatial learning deficit (4-5 months).	Plaques; No NFTs	(Oakley et al., 2006)
APPSwe 2576/Tau JNPL3 Symbol: APP/Tau	P301L 4 repeat Tau (JNPL3) x Appswe (Tg2576)	Developed motor disturbances similar to JNPL3, with identical range in age of onset, including progressive hindlimb weakness, hunched posture, eye irritations, reduced vocalization, and decreased grooming.	Developed motor disturbances similar to JNPL3, with identical range in age of onset, including progressive hindlimb weakness, hunched posture, eye irritations, reduced vocalization, and decreased grooming.	Plaques and NFTs Enhanced NFT in limbic system and Olfactory cortex	(Lewis et al., 2001)

In addition to parenchymal Aβ accumulation, these mice are notable for their prominent vascular amyloid deposition, i.e., CAA, often associated with haemorrhage (Winkler et al., 2001). Activated microglia and astrocytes are associated with Aβ plaques in these mice (Sturchler-Pierrat et al., 1997). Dystrophic neurites and hyperphosphorylated tau protein were also described around plaques (Sturchler-Pierrat et al., 1997), but NFTs were not found. A new feature of APP23 mice not available in Tg2576 and PDAPP mice is the selective neuronal death in the hippocampal sector CA1 (Calhoun et al., 1998). Morevoer, there was selective vulnerability of commissural neurons that were hierarchically affected by Aβ-induced neurodegeneration (Capetillo-Zarate et al., 2006). APP23 mice showed an age-dependent decline of spatial memory capacities. From 3 months of age, these mice displayed major learning and memory deficits (Sturchler-Pierrat et al., 1997). In addition to the cognitive deficits, APP23 mice also show disturbed activity patterns. At 6 months of age lower activity levels and different exploration behaviour were seen in comparison to wild-type mice (Kelly et al., 2003; Van Dam et al., 2003).

Single APP transgenic mouse models have not been able to mimic the full spectrum of AD-related pathologies. As mentioned already, neither PDAPP nor Tg2576 mice, despite the presence of extensive amyloid deposition, exhibit neuronal loss (Irizarry et al., 1997a; Irizarry et al., 1997b). Moderate loss of CA1 pyramidal cells (about 15%) has been reported in APP23 mice (Calhoun et al., 1998), but this was far less than that observed in AD patients. Thus, double and multiple transgenic mice models were developed in an attempt to overcome these limitations. Mutations in the PSEN1 (most models) and PSEN2 can also lead to FAD by shifting the ratio of $A\beta_{42/40}$ towards $A\beta_{42}$, either through a reduction of $A\beta_{40}$ generation or by increasing production of the more fibrillogenic $A\beta_{42}$ (De Strooper, 2007; Selkoe and Wolfe, 2007). However, PSEN1 or PSEN2 single transgenic mice did not develop plaques (Duff et al., 1996), but when crossed with plaque-forming APP mice, the resulting APP/PSEN mice showed earlier and more extensive plaque formation than single APP-transgenic mice (Borchelt et al., 1997; Holcomb et al., 1998). More substantial neuronal loss has only been seen in mice harbouring double or multiple APP and PS mutations at various sites (Casas et al., 2004; Schmitz et al., 2004; Oakley et al., 2006).

The problems associated with APP and/or APP/PSEN overexpressing mouse models have been the general difficulty of inducing the characteristic cytoskeletal pathology of AD in transgenic mice. Combining APP and tau overexpression led to mouse models that mimic the two hallmarks of the AD brain: Aβ plaques and NFTs. Generation of double and triple

transgenic mice by crossing the APP_{SW} mice with human mutant FTD-17 tau transgenic animals showed enhanced amyloid deposition, neuronal loss in selectively vulnerable limbic areas, and the generation of NFTs/NFP (Lewis et al., 2001; Perez et al., 2008). Similary, a triple transgenic mouse model harbouring *PS1-APP* and *TAU* transgenes (Oddo et al., 2003) developed plaques, synaptic loss and NFTs, similarly as seen in AD (Oddo et al., 2004; Billings et al., 2005). Hence, this model was very useful for analyzing the relation between the different pathological proteins involved in AD. However, the upregulation of three mutant proteins at a time does not allow the investigation of the pathological effects of one of these proteins alone. The APP23 mouse is the only transgenic mouse model for AD that overexpresses only a single distinct protein, sweAPP, and exhibits selective neuronal death in a brain region that is affected in AD. Thus, this mouse model permits the investigation of Aβ-induced neurodegeneration in the absence of other contributing factors, such as the expression of mutant PSEN1 or mutant tau-protein. To clarify the toxicity of Aβ, I compared Aβ pathology in APP23 mice exhibiting dendritic degeneration with the pathology in a second mouse model, namely, APP51/16 mice (Herzig et al., 2004) that express human wild-type *APP* gene with Thy-1 promoter and showed Aβ plaque deposition but no Aβ-related neurodegeneration, i.e., dendritic degeneration. Thus, comparing APP23 and APP51/16 mice is a powerful tool in identifying the mechanism of Aβ toxicity.

1.4 Aims of the study

Here, I wanted to identify the toxic forms of Aβ aggregates that distinguish AD cases from non-demented elderly individuals exhibiting AD-related lesions (Aβ deposition, NFP) in the human brains as well as those responsible for dendritic degeneration in APP23 mice not seen in APP51/16 mice. Although high-molecular weight Aβ (hiMWAβ) oligomers, protofibrils, and fibrils, low-molecular weight Aβ (loMWAβ) oligomers, such as dimers, trimers or Aβ*56, have been observed in the human AD brains and in mouse models of AD (Harper and Lansbury, 1997; Walsh et al., 1997; Kayed et al., 2003; Lesne et al., 2006; Habicht et al., 2007; Shankar et al., 2008), it is not entirely clear which of these Aβ species is most relevant for the development of AD and how these Aβ forms are related to one another *in vivo*. To address these questions, I studied two different APP-transgenic mouse models: APP23 and APP51/16. APP23 mice overexpress human mutant APP with the Swedish mutation and show dendritic alterations, whereas APP51/16 mice express high levels of human wild-type APP without any signs of dendritic degeneration. Moreover, I

studied dispersible, i.e., diffusible non-soluble Aβ separately to clarify its role in Aβ toxicity. Since studies by other authors so far did not include native Aβ preparation for western blot analysis it was necessary for me to clarify which Aβ aggregates prevail in native preparations and to determine the role of denaturing conditions used for analysis by SDS-PAGE on the spectrum of Aβ aggregates.

Thus, the specific aims of the study were:

1. to determine the stability of native Aβ aggregates under different experimental/ analytical conditions
2. to characterize soluble Aβ aggregates under native conditions
3. to determine which Aβ aggregates are specifically toxic, i.e., contribute to or cause dendritic degeneration in APP23 mice compared to the APP51/16 mice, and are associated with AD in the human brain.

2 Material and Methods

Table 3: Buffer and Reagents

A. Tris-Buffer Saline (TBS), pH 7.4

Components	**Concentration/Amount**	**Company**
Tris-HCl	20 mM	Merck, Darmstadt, Germany
NaCl	150 mM	Merck, Darmstadt, Germany
ddH_2O	To 1 liter	Millipore GmbH, Schwalbach, Germany

B. Phosphate buffer saline (PBS), pH 7.6

KCl	2.7 Mm	Merck, Darmstadt, Germany
KH_2PO_4	1.46 Mm	Merck, Darmstadt, Germany
NaCl	137 mM	Merck, Darmstadt, Germany
$Na_2HPO_4.2H_2O$	8.1 mM	Merck, Darmstadt, Germany
ddH_2O	To 1 liter	Millipore GmbH, Schwalbach, Germany
Tween (for WB)	0.05 %	Bio-Rad, Hercules, CA, USA

C. 2.6% Phosphate buffer paraformaldehyde solution (PFA), pH 7.6

PFA	2.6%	Sigma, Taufkirchen, Germany
PBS 0.2M, pH 7.6	500 ml	See PBS solution
ddH_2O	500 ml	Millipore GmbH, Schwalbach, Germany

D. Reducing Solution (IHC)

Methanol	10%	Merck, Darmstadt, Germany
H_2O_2	30%	Sigma, Taufkirchen, Germany
in TBS, pH 7.6	0.05 M	See Table 3B

E. Blocking Solution (IHC)

DL-Lysine	0.1 M	Sigma, Taufkirchen, Germany
Triton-X	0.25%	Sigma, Taufkirchen, Germany
in BSA	10%	Sigma, Taufkirchen, Germany

F. Blocking buffer (WB)

Milk powder	5%	Carl Roth GmbH, Karlsruhe
PBS-Tween (0.05 %)	to 1 liter	See Table 3B

G. Anesthetic agents

Ketamine	25%	Bela-pharma GmbH,Vechta, Germany
Xylazine	2%	Riemser Arzneimittel AG, Greifswald, Germany
in PBS		See Table 3B

H. Tracing solution in PFA

DiI crystal	1,1'-dioctadecyl-3,3,3',3'-tetramethylindolcarbocyanine perclorate	Molecular Probes , Eugene, OR, USA

Tracing solution in PFA

Iodocetic acid	8%	Sigma, Taufkirchen, Germany
Sodium periodate	0.8%	Sigma, Taufkirchen, Germany
DL-Lysine	0.1 M	Sigma, Taufkirchen, Germany
In PFA solution	To 1 lit	See Table 3C

I. Perfusion solution

Heparin	0.05%	Roche, Mannheim, Germany
in TBS	To 1 liter	See Table 3A

J. Reagents for IHC and EM

Alcohol	Sigma-Aldrich, Steinheim, Germany
Propanol	Sigma-Aldrich, Steinheim, Germany
Epon	Sigma-Aldrich, Steinheim, Germany
Osmium tetroxide	Chempur, Karlsruhe, Germany
Uranyl acetate	Merck, Darmstadt, Germany
LR-white	London Resins Co. Ltd, Birkshire, England
Pararosaniline	Serva, Heidelberg, Germany
HCl	Applichem, Darmstadt, Germany
Crotonaldehyde	Merck, Darmstadt, Germany
Hydrogenperoxide	Fischar, Saarbrücken, Germany
Formic acid	Applichem, Darmstadt, Germany
Permanent Red	Dako, CA, USA
3,3'-Diaminobenzidine (DAB)	Merck, Darmstadt, Germany
Propylene oxide	Merck, Darmstadt, Germany
Sodium borohydride	Merck, Darmstadt, Germany
Propylene oxide	Merck, Darmstadt, Germany
Glutaraldehyde	Plano, Wetzlar, Germany
Gold Anti-mouse IgG/M 15 nm	Aurion, Wageningen, The Netherlands
Normal Goat Serum	Aurion, Wageningen, The Netherlands
Cold washed fish gelatine (CWFG)	BB International, England, UK

K. Reagents for immunoprecipitation (IP)

µMACS Protein G microbeads	Miltenyi Biotech,Bergisch Gladbach, Germany
µMACS separation columns	Miltenyi Biotech,Bergisch Gladbach, Germany

Table 4: List of Antibodies used for IHC

Primary antibody	Antigen	Species	Dilution (IHC)	Pre-treatment (IHC)	Source of prmary antibody	Source of secondary antibodies
4G8	$A\beta_{17-24}$	MS-Monoclonal	1:5000	Formic acid	Covance, Dedham, USA	ABC kit Linaris, Wertheim, Germany
6E10	$A\beta_{1-17}$	MS-Monoclonal	1:100	Formic acid	„	„
22C11 (Anti-APP)	APP-N-term. 66-81	MS-Monoclonal	1:75	Microwave	Chemicon, Temecula, CA, USA	„
MBC40	$A\beta_{32-40}$	MS-Monoclonal	1:20	Formic acid	Gift of H. Yamaguchi, Gunma, Japan	„
MBC42	$A\beta_{37-42}$	MS-Monoclonal	1:200	Formic acid	“	„
A11	Aβ oligomers	Rb Polyclonal	1:1000	-	Millipore, Temecula, CA, USA	„
Anti-APP C-terminus	APP-C-term. 751-770	Rb Polyclonal	1:10000	-	Merck-Calbiochem, Darmstadt, Germany	„
B10AP	Amyloid Protofibrils	AP conjugate	1:50	Microwave	Gift of M. Fändrich, Halle, Germany	Permanent Red

Table 5: List of Antibodies used for WB

Antibodies	Antigen	Species	Dilution (WB)	Source	Secondary antibodies
6E10	$A\beta_{1-17}$	MS Monoclonal	1:1000	Covance, Dedham, USA	Anti-MS-HRP Bio-Rad
22C11 (Anti-APP)	APP N-terminus 66-81	MS Monoclonal	1:750	Chemicon, Temecula, CA, USA	Anti-MS-HRP Bio-Rad
MBC40	$A\beta_{32-40}$	MS Monoclonal	1:10000	Gift of H. Yamaguchi, Gunma, Japan	Anti-MS-HRP Bio-Rad
MBC42	$A\beta_{37-42}$	MS Monoclonal	1:1000	Gift of H. Yamaguchi, Gunma, Japan	Anti-MS-HRP Bio-Rad
4G8	$A\beta_{17-24}$	MS Monoclonal	1:1000	Covance, Dedham, USA	Anti-MS-HRP Bio-Rad
A11	Aβ oligomers	Rb Polyclonal	1:5000	Millipore, Temecula, CA, USA	Anti-Rb-HRP Bio-Rad
Anti-APP C-terminus	APP-C-term. 751-770	Rb Polyclonal	1:10000	Merck, Darmstadt, Germany	Anti-Rb-HRP Bio-Rad
B10 AP	Amyloid Protofibrils	AP conjugate	-	Gift of M. Fändrich, Halle, Germany	-

Table 6: List of Equipments used

Instruments	Name	Location
Table centrifuge	Mikro 200	Hettich Zentrifugen, Tuttlingen, Germany
Cool centrifuge	Centrifuge 5417R Rotor F-45-30-11	Eppendorf, Hamburg, Germany
Speedvac centrifuge	Concentrator 5301	Eppendorf, Hamburg, Germany
Magnetic Stirrer	MR Hei Standard	Heidolph Instruments, Solingen, Germany
Microscopes	Fluorescence Microscope Leica DMLB	Leica, Bersheim, Germany
	Scanning Confocal Microscope Leica TSC NT	Leica, Bersheim, Germany
	Zeiss EM10	Oberkochen, Germany
	Electron microscope	Philips EM400T 120KV, Eindhoven, The Netherlands
pH Meter	pH-meter 210	Hanna Intruments, Kehl am Rhein, Germany
Thermomixer	Thermomixer 5436	Eppendorf, Hamburg, Germany
Vortex	VM 3000 Mini vortexer	Henry Troemner LLC, NJ, USA
Computer	XPS M1530	Dell, Europe
Vibratome	Leica VT 1000S	Leica, Bersheim, Germany
Progein Gel electrophoresis chamber	XCell4 SureLock™ Midi-Cell	Invitrogen, CA, USA
	Xcell SureLock Mini Cell	Invitrogen, CA, USA
Protein blotting (Transfer)	Criterion Blotter	Bio-Rad, CA, USA
Shaker	SM-30	Edmund Bühler GmbH, Hechingen, Germany
Roller Mixer	Stuart SRT6	Bibby Scientific, Staffordshire, UK
Sonicator	SONOPLUS HD 2070	Bandelin Electronic, Berlin, Germany
Power supply	Minis 150	Kisker-Biotech, Steinfurt, Germany
	Powerpac HC	Bio-Rad, CA, USA
Magnetic stand for IP	µMACS	Miltenyi Biotech,Bergisch Gladbach, Germany
Diamond Knife	Diatomeknives	Hatfield, PA, USA
Distilled water	Millipore	Millipore GmbH, Schwalbach, Germany

Table 7: List of Softwares used

Windows Vista	Microsoft, CA, USA
Axiovision AC 4.2 image analysis software	Carl Zeiss Lichtmikroskopie, Göttingen, Germany
CorelDRAW Graphics Suite 12	CorelDRAW, Unterschleissheim, Germany
EndNote 8.0	Thomson ISI ResearchSoft, Philadelphia, PA, USA
ImageJ, Imaging Processing and Analysis Software	NIH, Bethesda, MD, USA
Leica FireCam Software	Leica, Bersheim, Germany
Leica TCS Software	Leica, Bersheim, Germany
Open Office	www.openoffice.org
SPSS software	Chicago, IL, USA

2.1 Animal models

Heterozygous female APP51/16 mice, APP23 and wild-type littermates were provided as gift by the Novartis Institutes for Biomedical Research (Basel, Switzerland) for

morphological (MOR) and biochemical (BIO) studies. To confirm Aβ specificity and to exclude unspecific reactions APP-knockout mice (APP-KO) (Calhoun et al., 1998; Calhoun et al., 1999) were used. Genotype information of all mice including APP-KO mice was provided.

Table 8: Types of animals used for the morphological (MOR) and biochemical (BIO) experiments.

Study animal	Age (months) Purpose	5 (MOR)	5 (BIO)	7 (MOR)	7 (BIO)	11 (MOR)	12 (BIO)	15 (MOR)
Mice	Wild-type	n = 12	n = 10	-	-	n = 13	n = 9	n = 13
Mice	APP23	n = 9	n = 10	-	-	n = 8	n = 8	n = 8
Mice	APP51/16	n = 8	n = 7	-	-	n = 7	n = 10	n = 5
Mice	APP-KO	-	-	n = 3	n = 4	-	-	-

APP23 and APP51/16 mice were generated as described previously (Sturchler-Pierrat et al., 1997; Herzig et al., 2004) and continuously back-crossed to C57BL/6. An expression construct containing a murine Thy-1 promoter was used to drive neuron-specific expression of a) human mutant APP751 with the Swedish double mutation 670/671 KM→NL in APP23 mice and b) human wild-type APP in APP51/16 mice.

2.2 Morphological Analysis of Traced Neurons

For DiI tracing the brains of APP23, APP51/16 and wild-type mice were studied. Animals were treated in agreement with the German and Swiss laws on the use of laboratory animals. Perfusion fixation and DiI-tracing were performed as previously published (Capetillo-Zarate et al., 2006). After incubation in 2.6% phosphate-buffered PFA for at least 3 months at 37°C, 100 µm thick coronal vibratome sections were cut. Sections were temporarily mounted in TBS for microscopic analysis.

In layer III of the frontocentral cortex of the right hemisphere, contralateral to the implantation site of the tracer, the morphology of traced commissural neurons was examined as reported earlier (Capetillo-Zarate et al., 2006). The traced neurons were assigned to different types according to their morphology (Appendix. Tab. 1). Then the number of traced commissural neurons of each type in wild-type mice was compared with that in APP23 and in APP51/16 mice. For qualitative and quantitative analysis 10 consecutive sections (100 µm thickness each) representing a tissue block of 1 mm thickness were studied for each mouse. Analysis started at the anterior commissure setting the caudal limit of the investigated tissue block. For each coronal section, the medial

boundary of the region investigated was set as the vertical line at the cingulum that separated the cingulate cortex from secondary motor cortex (M2). The horizontal boundary was set as the horizontal line separating the primary somatosensory cortex (S1) from the insular cortex.

For the qualitative analysis a laser scanning confocal microscope (Leica TCS NT, Leica, Bensheim, Germany) was used. Stacks of 2D images were superimposed digitally using the Image J Image Processing and Analysis software (NIH, Bethesda, MD, USA), and 3D data sets were generated for the visualization of neurons with their entire dendritic tree. For quantification, traced neurons in layer III were counted in the region of interest in 10 consecutive sections of the tissue block taken for qualitative and quantitative analysis using a fluorescence microscope (Leica DMLB, Leica). In so doing, we analyzed a cortex volume of 5-6 mm^3 in each mouse. Mean and median values of the number of traced neurons were calculated and compared among wild-type, APP23, and APP51/16 mice.

2.3 Immunohistochemistry for mouse brains

Sections from each traced mouse brain stained for Aβ [4G8, 1/5000, formic acid pretreatment, Sigma-Aldrich, St. Louis, USA; MBC42 (Yamaguchi, et al., 1998), 1/200, formic acid pretreatment; anti-$A\beta_{1-42}$, polyclonal rabbit, (Wild-Bode, et al., 1997), 1/750, formic acid pretreatment)], for Aβ protofibrils and fibrils with B10AP antibody fragments [(Habicht et al., 2007), 1/50, microwave pretreatment] and for Aβ oligomers with A11 [(Kayed et al., 2003), Millipore, Temecula, CA, USA, 1/1000)]. Anti-Aβ and A11 antibodies were detected with a biotinylated anti-mouse IgG secondary antibody and visualized with the ABC-complex (ABC-Kit, Vector Laboratories, Burlingame, CA, USA) and diaminobencidine-HCl (DAB). To avoid a crossreaction of the secondary antibody with intrinsic mouse IgG in mouse brain we blocked intrinsic mouse IgG with a goat-anti-mouse-IgG antibody (Biomeda, Foster City, CA, USA, 1/100) before primary antibody incubation as previously described (Thal et al., 2007). B10AP antibody fragments were coupled with alkaline phosphatase that was visualized with permanent red [(DAKO, Glostrup, Denmark, (Habicht et al., 2007)]. Vibratome sections were viewed without further counterstaining. Sections were mounted in Eukitt (O. Kindler; Freiburg, Germany). Positive and negative controls were performed. PFA-fixed 100 µm thick brain sections from three APP-KO mice were processed in parallel for B10AP- and A11-immunohistochemistry to distinguish B10AP- and A11-positive Aβ-related changes in APP23 and APP51/16 mice from crossreactions with other aggregated proteins also detectable in APP-KO mice.

2.4 Determination of plaque and CAA distribution in the mouse brain

The distributions of Aβ and B10AP-positive plaques as well as that of CAA as stained with anti-Aβ antibodies were determined by assessment of plaques and CAA stained in the cortex, allocortex (hippocampus, cingulate gyrus), basal ganglia, diencepohalon and the mid-brain. The presence of plaques or CAA was assessed dichotomously. According to the anatomical distribution of Aβ and B10AP-positive plaques phases of plaque deposition in the mouse brain were obtained as previously published (Thal et al., 2006). The Aβ phase, thereby, represents the distribution of Aβ plaques, the phase of B10AP plaque distribution that of anti-B10AP-positive plaques. CAA was staged according to its distribution similar as reported for the human brain (Thal et al., 2003). As previously shown the Aβ phase correlates closely with the Aβ load and provides reproducible information about the severity of Aβ plaque pathology (Thal et al., 2008; Alafuzoff et al., 2009).

2.5 Neuropathology and human sample characterization

Autopsy brains from 11 AD, 10 control cases without Aβ pathology and 10 non-demented control cases with Aβ plaques were studied. After autopsy the brains were fixed in a 4 % aqueous solution of formaldehyde. Following fixation the medial temporal lobe (MTL) and a part from the occipital cortex containing the primary visual field were embedded in paraffin. Further parts of the MTL were embedded in polyethylenglycol (PEG). Paraffin sections were cut at 12 µm, PEG sections at 100 µm. Histopathological diagnosis of AD has been performed by analyzing Gallyas, Campbell-Switzer, anti-abnormal phosphorylated tau protein (anti-PHF-τ; AT-8; Innogenetics, Belgium, 1/1000) and anti-Aβ (4G8; 1/5000, formic acid pretreatment, Sigma-Aldrich, St. Louis, USA) stained sections of the MTL and the occipital cortex to determine the distribution of NFTs and the amount of neuritic plaques. Braak-NFT staging and the determination of the CERAD (Consortium to Establish a Registry for Alzheimer's Disease) score for neuritic plaques was performed on the basis of the Gallyas stained sections (Braak and Braak, 1991a; Mirra et al., 1991). The distribution of amyloid plaques in the MTL has been obtained according to previously published criteria (Thal et al., 2000) and represents the distribution of Aβ plaques in the human brain as a semiquantitative parameter for the severity of Aβ plaque pathology (Thal et al., 2002). The clinical dementia rating (CDR) scores were retrospectively obtained by screening the clinical records as previously reported (Thal et al., 2002). Cases with a high and moderate likelihood for AD according to recommended criteria for the post-mortem diagnosis of AD (The National Institute on Aging, 1997) and

lacking evidence of other forms of dementia were classified as AD cases. Controls were defined by the absence of Aβ plaques. They had either no NFTs or not more than Braak-NFT stage II. Non-demented cases with Aβ plaques were studied as a third group of cases (AD-related pathology cases = ADRP-cases). The type of AD as indicated by the presence or absence of capillary cerebral amyloid angiopathy (CAA) was determined as previously published (Thal et al., 2010). The B10AP and A11 IMH was performed on 100 µm PEG section from MTL and occipital cortex. The staining procedure was similar with that used for mouse brain.

2.6 Protein extraction from mouse and human postmortem brain

The flowchart of protein extraction method applied in this study has been described in Fig. 6. Briefly, protein extraction from fresh frozen human occipital and temporal cortex (0.4 g), (Appendix Tab. 3B) and mouse forebrain (0.4 g) was carried out in 2 ml of 0.32 M sucrose dissolved in Tris-buffered saline (TBS) containing a protease and phosphatase inhibitor-cocktail (Complete and PhosSTOP, Roche, Mannheim, Germany). The tissue was homogenized with Micropestle (Eppendorf, Hamburg, Germany) followed by sonication. The homogenate was centrifuged for 30 min at 14.000 x g at 4°C. The supernatant was kept as soluble/dispersible fraction. The pellet was resuspended in 2 % sodium dodecyl sulfate (SDS) (Fig. 6).

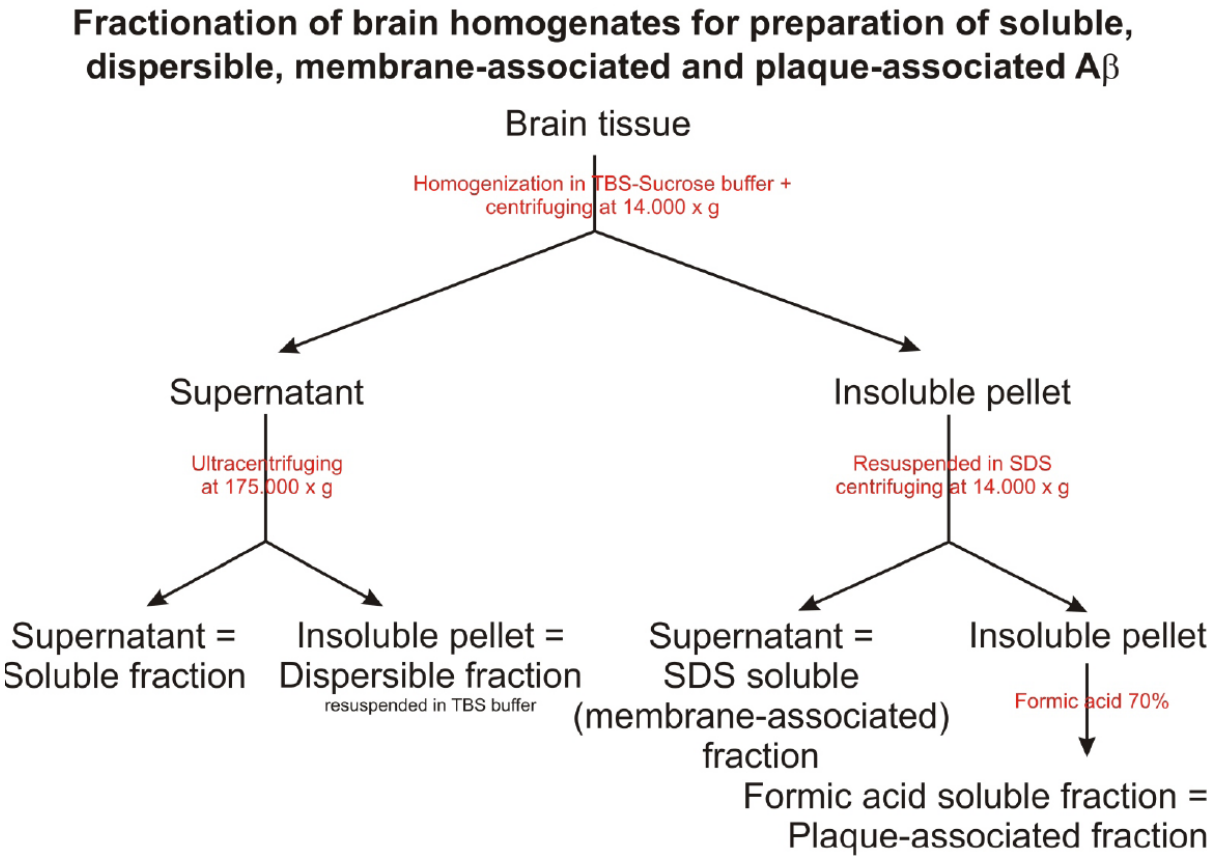

Figure 6: Schematic representation of the biochemical fractionation of brain tissue homogenates into soluble, dispersible, membrane-associated (SDS soluble), and plaque-associated (formic acid soluble) fraction. Reproduced from (Rijal Upadhaya et al., accepted for publication-b)

Ultracentrifuging of the soluble/dispersible fraction at 175.000x g was used to separate the soluble (the supernatant after ultracentrifugation) from the dispersible fraction (the resulting pellet) (Fig. 6).

After the separation of the soluble/dispersible fraction, the SDS-resuspended pellet was centrifuged at 14.000 x g the supernatant was kept as membrane-associated SDS fraction (Fig. 1). The pellet that remained was further dissolved in 70 % formic acid and the homogenate was lyophilized by centrifuging in the vacuum centrifuge (Vacufuge, Eppendorf, Hamburg, Germany) and reconstituted in 100 µl of 2x LDS (lithium dodecyl sulfate) sample buffer (Invitrogen, Carlsbad, CA, USA) followed by heating at 70°C for 5 min. The resultant sample was considered as plaque-associated formic acid-soluble fraction. The total Protein amounts of TBS/Sucrose and SDS fractions were determined using BCA Protein Assay (Bio-Rad, Hercules, CA, USA).

2.7 Measurement of total protein concentration (BCA measurement)

Protein amounts from all the fractions were determined using BCA Protein Assay kit (Thermo scientific, Rockford, IL, USA). To determine the protein concentration of the lysates, bicinchoninic acid (BCA) assays were performed using a BCA Protein Assay Kit (Thermo). An appropriate volume of each sample (2-10 µl) was filled up with lysis buffer to a final volume of 20 µl and two identical mixes of each sample were transferred onto a 96-well plate. Additionally, 20 µl of eight different BSA-solutions (0 µg/µl, 0.125 µg/µl, 0.25 µg/µl, 0.5 µg/µl, 0.75 µg/µl, 1 µg/µl, 1.5 µg/µl, 2.0 µg/µl) were transferred in duplicate to the same plate to calculate a standard curve. Then 200 µl of the BCA assay mix (1:50 ratio of Reagent A to Reagent B) was added to each well and the plate was incubated at 37°C for 30 min. The absorption of each well was measured at 562 nm using the PowerWave 200TM microplate scanning spectrophotometer (Bio-Tek) and analyzed with the software KC4 V3.1 (Bio-Tek Instruments, Inc., Winooski, VT, USA).

2.8 Immunoprecipitation

For immunoprecipitation, 200 µl of soluble and dispersible fraction of brain homogenates was incubated with 1 µl of anti-$A\beta_{1\text{-}17}$ (6E10, Covance, Dedham, USA, 1 mg/ml), A11 antibodies [(Kayed et al., 2003), Millipore, Temecula, CA, USA, 1 mg/ml)] or B10AP antibody fragments [(Habicht et al., 2007), 0.55 mg/ml)] at 4°C for 4 h with gentle agitation. 50 µl of protein G Microbeads (Miltenyi Biotec, Bergisch-Gladbach, Germany) were added to the mixture and incubated overnight at 4°C with gentle agitation. The mixture was then passed through the µColumns which separate the microbeads by retaining them into the column, while the rest of the lysate flows through. After few mild washing steps with 1x TBS, pH 7.4 the microbead-bound-proteins were eluted with 95°C heated 1x LDS sample buffer. Eluates were resolved in SDS-PAGE followed by western blotting.

2.9 Blue native (BN) and SDS Polyacrylamide gel-electrophoresis (SDS-PAGE)

Different protein fractions including immunoprecipitated samples were resolved by BN-PAGE or/and SDS-PAGE followed by western blot antigen detection technique. For BN-PAGE of the TBS fraction, 50 µg of total protein was prepared with 4x NativePAGE sample buffer (Invitrogen) and subjected to native PAGE 4-16% Bis-Tris gel electrophoresis according to the manufacturer's protocol (Invitrogen). Native-Mark unstained protein standards (Invitrogen) were used as molecular weight markers. To avoid

epitope masking due to oligomer structure and to warrant efficient blotting after BN-PAGE gels were incubated in 0.2% SDS containing transfer buffer. After protein transfer onto the nitrocellulose membranes (Bio-Rad, Hercules, CA, USA), membranes were boiled in PBS buffer in microwave oven for 6 min. 3% non-fat dry milk (Roth, Karlsruhe, Germany) diluted in antibody-dilution buffer was used to block unspecific binding for 1 h at room temperature. Blots were developed with an ECL detection system (Supersignal Pico Western system, ThermoScientific-Pierce, Waltham, MA, USA) and illuminated in ECL Hyperfilm (GE Healthcare, Buckinghamshire, UK). Washing and antibody-dilution buffers contained 1 M PBS (pH 7.4) with 0.02% Tween (BioRad).

For SDS-PAGE, soluble and dispersible fractions (50 µg total protein) and IP-products were electrophoretically resolved in a precast NuPAGE 4-12 % Bis-Tris gel system (Invitrogen) with MES buffer (Invitrogen). The protein load was controlled either by Ponceau S staining or β-actin (C4, 1/1000, Santa Cruz Biotechnology, Santa Cruz, CA, USA) immunoblotting. For both BN as well as SDS-PAGE the proteins were transferred to nitrocellulose membranes and the membranes were boiled with PBS for 6 min followed by blocking with 5% non-fat dry milk (Roth, Karlsruhe, Germany; diluted in antibody-dilution buffer) for 1 h at room temperature.

For immunodetection of Aβ the membranes were incubated for 12 h at 4°C with the primary antibodies: anti-$A\beta_{1-17}$ (6E10, 1/1000), anti-$A\beta_{42}$ (MBC42, (Yamaguchi et al., 1998) 1/500), anti-$A\beta_{40}$ (MBC40, (Yamaguchi et al., 1998) 1/1000). For the analysis of full length APP (flAPP), APP N-terminal fragments (sAPPα and sAPPβ) anti-APP (22C11, Chemicon, Temecula, CA, USA, 1/750) was used. The 22C11 antibody is directed against an N-terminal part of the APP molecule outside the Aβ-region (Weidemann et al., 1989). For the detection of APP C-terminal fragments (APP-CTF-α and APP-CTF-β) APP-CT20 (polyclonal rabbit, Merck-Calbiochem, Darmstadt, Germany, 1/10000) was used. After washing steps, the corresponding secondary antibodies (EIA Grade Affinity purified Goat Anti-Mouse/Rabbit IgG-HRP, 1/20000, Bio-Rad, Hercules, CA, USA) were applied for 2 h at room temperature. Blots were developed with an enhanced chemiluminescence (ECL) detection system (Supersignal Pico Western system, Thermo Scientific-Pierce, Waltham, MA, USA) and illuminated in ECL Hyperfilm (GE Healthcare, Buckinghamshire, UK). $A\beta_{42}$ and $A\beta_{40}$ preparations were used as positive and/or negative controls. All BN-PAGE blots were developed with standard chemiluminescence exposure time of 2-5 min up to

maximum exposure times of 2-3 h to detect even minimal amounts of Aβ aggregates. For SDS-PAGE blots, exposure time of 2-5 min was used except when otherwise indicated.

For quantification of the precipitated amounts of SDS-denaturable Aβ, Aβ protofibrils and fibrils and Aβ oligomers we measured the 4 kDa monomer bands densitometrically using the ImageJ software (Institutes of Health, Bethesda, MD, USA) as previously reported (Utter et al., 2008). To document the sensitivity of Aβ quantification by immunoprecipitation we used synthetic $A\beta_{42}$ (Bachem, Switzerland) dissolved in cell culture medium (RPMI1640, GIBCO, Invitrogen, Carlsbad, CA, USA) at concentrations of 2, 6, 8, 10, and 12 µg/ml. The samples were stored at 22°C before analysis allowing aggregation similar as in the soluble fraction of brain lysates as shown recently (Rijal Upadhaya et al., accepted for publication-a). Brain lysates from APP-KO mice were used as negative controls.

2.10 Electron microscopy of immunoprecipitated oligomeric and fibrillar/protofibrillar proteins from human AD and control brains

For electron microscopy, 5 µl of immunoprecipitated and redissolved A11-positive oligomers or B10AP-positive protofibrils/fibrils were placed on formvar coated grids. After 1 min incubation, the excess liquid was wiped off and the grid dried. The grid then was treated with Na-Borhydrite (0.1 % in water for 1 min) followed by blocking with 5 % bovine serum albumin, 5 % normal goat serum, and 0.1 % cold-washed fish gelantine in 1 M PBS. The grids were incubated with anti-$A\beta_{1-17}$ (6E10, 1/50) for 30 min. After washing, the primary antibody was visualized by 15 nm gold-labeled secondary antibodies (1/30, diluted in 1 M PBS, Aurion Immuno Gold Reagents & Accessories, Wageningen, The Netherlands). Then, the grid was post-fixed in 2 % glutaraldehyde and block-stained with a 2 % aqueous solution of uranyl acetate (Merck, Darmstadt, Germany) for 1 min followed by five rinsing steps in H_2O_2. The sections were viewed with a Philips EM400T 120KV (Eindhoven, The Netherlands) and with a Zeiss EM10 (Oberkochen, Germany).

2.11 Analysis of synthetic $A\beta_{42}$ and $A\beta_{40}$ aggregates in native state and after SDS-denaturation

To determine whether synthetic Aβ aggregates primarily form loMWAβ- and hiMWAβ-aggregates, we dissolved 15 µmol synthetic $A\beta_{40}$-peptide (Peptides International, Louisville, KY, USA) in 1 ml cell culture medium (Quantum 263, PAA Laboratories, Pasching, Austria) for 30 min at 4°C [22]. $A\beta_{42}$-peptide (Bachem, Switzerland) was also

dissolved in cell culture medium (RPMI1640, GIBCO, Invitrogen, Carlsbad, CA, USA) [22]. Aggregation was permitted to occur for 4 h at 22°C. To identify oligomers, fibrils, and protofibrils structurally we used electron microscopy. For this purpose, 5 µl of the $A\beta_{40}$- and $A\beta_{42}$ solutions were placed on a formvar coated grid for one minute before wiping off the excess liquid. The protein coated grids were block-stained with a 2 % aqueous solution of uranyl acetate (Merck).

The protein aggregates were also analyzed with BN-PAGE and SDS-PAGE as well as subsequent western blot analysis using the MBC40 and MBC42 antibodies to detect $A\beta_{40}$ and $A\beta_{42}$, respectively. This experiment was repeated 5 times.

2.12 Aβ ELISA

For analysis of Aβ by ELISA, forebrain homogenates from APP23 and APP51/16 mice of each age group (5 months: n = 6 APP23, 6 APP51/16; 11 months: n = 4 APP23, 6 APP51/16; 15 months: n = 7 APP23, 8 APP51/16) were supplemented with concentrated formic acid to a final concentration of 70 %. After 15 min of incubation on ice and mixing every 5 min, the samples were neutralized by addition of 19 volumes 1 M Tris base supplemented with protease inhibitor cocktail. The extracts were cleared by centrifugation (20000 x g for 15 min at 4°C). Supernatants from 5-month-old APP23 mice were directly loaded on sandwich ELISA plates for quantification of Aβ peptides ($A\beta_{1-40}$: ELISA from IBL, Hamburg, Germany; $A\beta_{1-42}$: ELISA from Innogenetics, Ghent, Belgium). Supernatants from 11 and 15 month-old-mice were diluted as necessary in dilution buffers supplied with the ELISAs. Standard curves were prepared with synthetic peptides $A\beta_{1-40}$ and $A\beta_{1-42}$ purchased from Bachem and diluted in extracts of non-transgenic mouse forebrain prepared in parallel as described above. Each sample was analyzed in duplicate.

2.13 Electron Microscopy and Analysis of Synaptic Density and Dystrophic Dendrites

100 µm thick vibratome sections of the frontocentral cortex from six 15-18-month-old wild-type, 15-month-old APP23, and APP51/16 mice were flat-embedded in Epon (Fluka-Sigma, Taufkirchen, Germany). A part of the frontocentral cortex covering all six cortical layers was dissected under microscopic control and pasted on Epon blocks with a drop of Epon. Ultrathin sections were cut at 70 nm, block stained with uranyl acetate and lead citrate, and viewed with a Philips EM400T 120KV (Eindhoven, The Netherlands). Digital pictures were taken from 20 soma-free neuropil areas located in layers II-VI at 4600-times magnification. Twenty pictures of the soma free cortical neuropil were taken randomly.

The numbers of the symmetric and asymmetric synapses were counted and the length of the synapses was determined using the ImageJ software (NIH, Bethesda, USA). The synaptic density was determined separately for symmetric and asymmetric synapses according to DeFelipe et al. (DeFelipe, et al., 1999) (synaptic density = Number of synapse-profiles in a given area/length of synaptic profiles). These semiquantitative data were used to compare the synaptic densities between the different mouse lines. Asymmetric and symmetric synapses were distinguished according to published criteria (Colonnier, 1968, Miranda, et al., 2009).

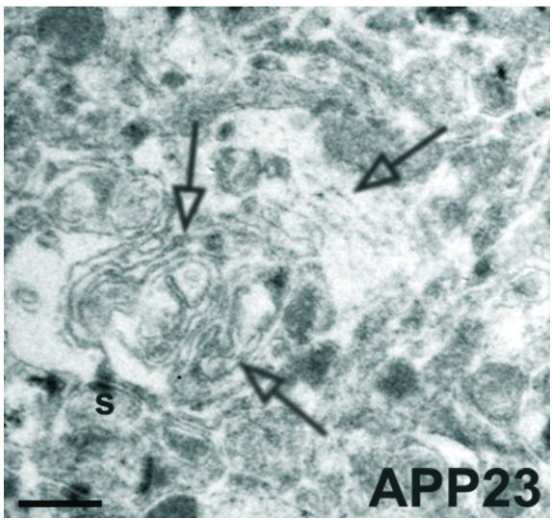

Figure 7: Electron microscopy picture showing dystrophic dendrites. Accumulations of membranous structures (arrows) within a swollen dendrite as observed at the electron microscopic level were referred to as dystrophic dendrites. The association of the neurite with presynaptic terminals from other neurons (s) indicates the dendritic nature of these dystrophic neurites. This photograph was taken from the frontocentral cortex of a 15-month-old APP23 mouse. Calibration bar: 570 nm. Reproduced from (Rijal Upadhaya et al., accepted for publication-b).

The frequency of dystrophic dendrites was observed by counting the number of dystrophic neurites in the 20 pictures taken for the determination of the synapse densities. The criteria for the identification of dystrophic dendrites at the ultrastructural level were: neurite profiles with a disorganized cytoplasm, occurrence of multilamellar, whirl-like structures in the absence of ultrastructurally intact cell organelles in the area of the lesion, and an enlarged sized compared with neighbouring neuritic profiles (Fig. 7). This number was determined in 6 of each mouse model: APP23, APP51/16 and wild-type mice and used as a semiquantitative score for structural dendritic alterations.

2.14 Stereological assessment of the number of hippocampal neurons

APP23 (n=6), APP51/16 (n=6), and wild-type (n=6) mice at the age of 15 months were chosen randomly for stereology. One brain section of the hippocampal formation was selected by chance and stained with aldehyde fuchsin-Darrow red. Quantification of neurons was performed according to the principles of unbiased stereology (Schmitz and Hof, 2000). The CA1 volume was measured in serial 100 µm thick sections of the entire mouse brain at 5x magnification. Neurons were counted in three different, randomly chosen microscopic fields (40x magnification) of an aldehyde fuchsin – Darrow red stained section of CA1. For optical dissection, stacks of 10 images in 2 µm focus distance were generated for each microscopic field. Only those neurons having nuclei with dark and round nucleoli visible in the center of soma in one of the stack-images were considered for quantification using the ImageJ software (NIH, Bethesda, USA). The number of neurons in the frontocentral cortex and CA1 was calculated on the basis of the respective reference volumes and neuron densities.

2.15 Photoconversion of DiI-traced neurons and subsequent immunoelectron microscopy

To clarify whether dendritic changes in traced commissural neurons are related to Aβ, the tracer signal was converted into electron dense material by incubating sections from 5-month-old APP23 mice containing traced type 1 commissural neurons with dendritic degeneration and from 5-month-old APP51/16 mice with healthy-appearing type 1 commissural neurons and 3-5-month-old wildtype mice in phosphate buffered 0.05% DAB solution (pH: 7.6) at 27°C under fluorescence light excitation at 460-490 nm as long as photoconversion of the target neuron took place. For photoconversion a Leica DMLB fluorescence microscope was used. The section with the photoconverted neuron was embedded in LR-white (Hard-grade Acrylic Resin; London Resin Company, Berkshire, UK) between two plastic membranes that allowed microscopic analysis of the section (Fig. 4). The photoconverted neuron was cut and pasted on an epon block for preparing semithin and ultrathin sections. Ultrathin sections were immunostained with anti-$A\beta_{42}$ (MBC42, (Yamaguchi et al., 1998), 1/20), anti-$A\beta_{1\text{-}42}$ (polyclonal rabbit, (Wild-Bode et al., 1997), 1/75) or with anti-$A\beta_{1\text{-}17}$ (6E10, Covance, Dedham, USA, 1/100). The primary antibody was visualized with gold-labeled secondary antibodies (Aurion Immuno Gold Reagents & Accessories, Wageningen, The Netherlands). Ultrathin sections were viewed with a Philips EM400T 120KV.

Immunoelectron microscopy with anti-Aβ1-17 (6E10) was also performed without prior photoconversion in 15-month-old APP23, APP51/16, and wildtype mice to validate the findings in the photoconverted dendrites with better morphological resolution.

2.16 Statistical analysis

SPSS-Statistics 19.0 (SPSS, Chicago, IL, USA) software was used to calculate statistical tests. Non-parametric tests were used to compare variables among wild-type, APP23, and APP51/16 mice. p-values were corrected for multiple testing by Bonferoni correction in the event that multiple tests were performed to compare two mouse lines with one another in a sample of three mouse lines. Statistical analysis of quantitative Aβ measurements was performed using one-way ANOVA. The Games-Howell post-hoc test was used to correct for multiple testing.

3 Results

Signs of neurodegeneration mice such as alterations of type 1 commissural neurons as previously published (Capetillo-Zarate et al., 2006), reduction of asymmetric synapses, increased frequency of dystrophic dendrites and neuron loss were seen in APP23 mice whereas APP51/16 mice did not exhibit such signs of neurodegeneration. At the biochemical level neurodegeneration in APP23 mice was associated with increased levels of dispersible, SDS-denaturable Aβ aggregates in comparison to APP51/16 mice rather than with a distinct, toxic type of Aβ aggregates. Similar results were obtained when comparing AD patients with non-demented individuals that have cerebral Aβ plaques.

3.1 Neurodegeneration in APP23 mice but not in APP51/16 mice

Tracing of commissural neurons in the frontocentral cortex revealed a degeneration of the dendritic tree in type 1 commissural neurons of APP23 mice (Fig. 8A-C, Appendix Tab. 1) beginning at 5 months of age, which is neither seen in wild-type nor in APP51/16 mice. The dendritic degeneration of type 1 commissural neurons in APP23 mice was accompanied by a reduction of the number of detectable type 1 neurons in 5-15-month-old APP23 mice but not in wild-type and APP51/16 mice (Fig. 8D, Appendix Tab. 2A) (Capetillo-Zarate, et al., 2006). Type II commissural neurons were reduced only in 15 month-old APP23 mice but not in younger mice or in APP51/16 mice when compared with the respective wild-type littermates (Fig. 8E). There were no significant differences in the number of type III commissural neurons (Fig. 8F). A second hallmark of neurodegeneration in APP23 mice is the neuron loss in CA1 (Calhoun, et al., 1998) that was not seen in 15-month-old APP51/16 mice (Fig. 9A). At the electron microscopic level, 15-month-old APP23 mice showed more frequently dystrophic changes in dendrites distant from plaques than 15-month-old APP51/16 mice and wild-type animals that do not contain plaques (Fig. 9B, Appendix Tab. 2A).

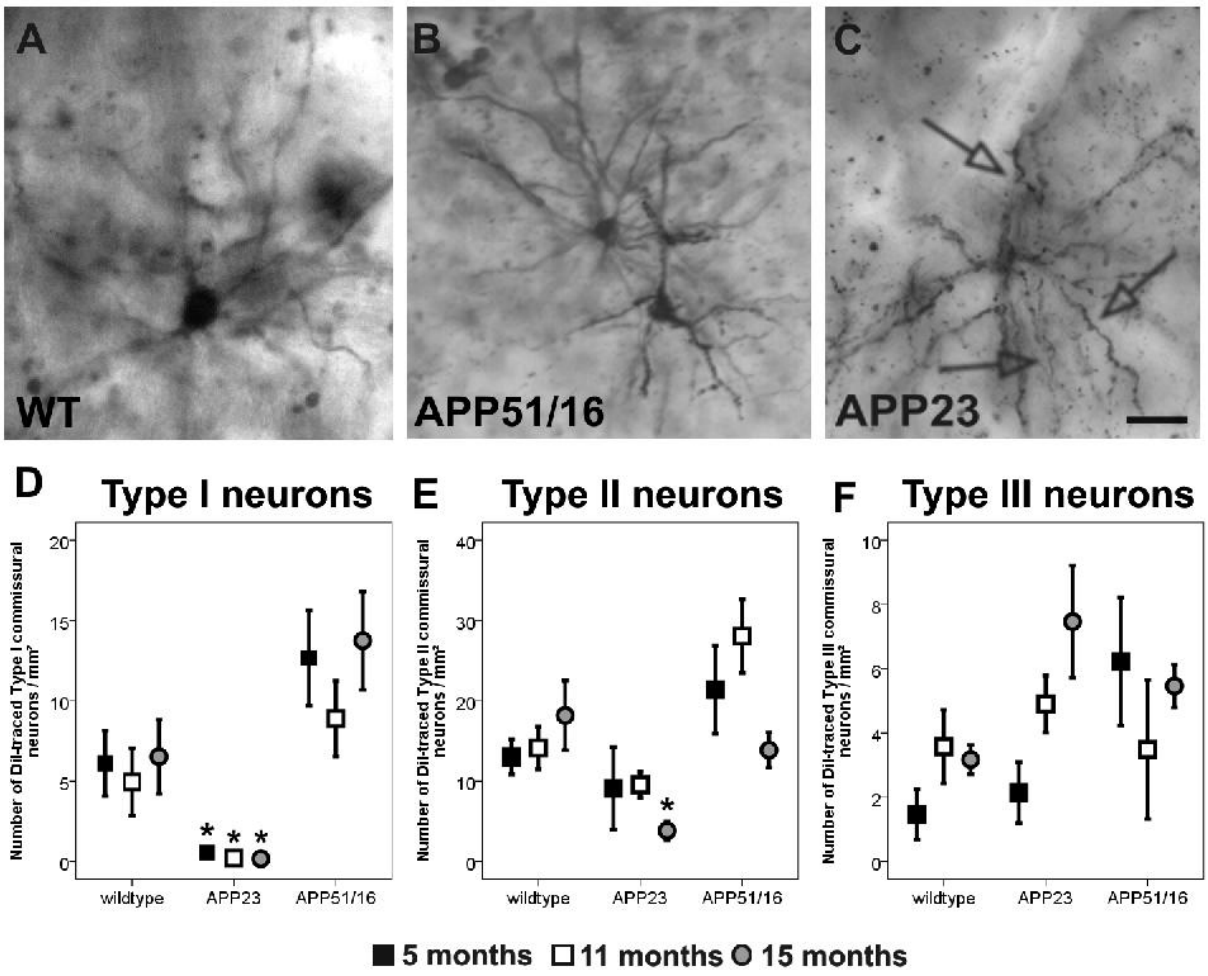

Figure 8: The quantification of DiI-traced commissural neurons in the frontocentral cortex. **A**: Photoconverted layer III type I commissural neuron in a 3-month-old wild-type mouse exhibits a symmetric dendritic tree with regularly shaped dendrites without abnormal kinking. **B**: A DiI-traced and photoconverted type 1 commissural neuron in layer III of the frontocentral cortex of a 5-month-old APP51/16 mouse similarly shows a symmetric dendritic tree without abnormal kinking and caliber reduction. **C**: A photoconverted type 1 commissural neuron in a 5-month-old APP23 mouse exhibits abnormal kinking as well as caliber reduction of the dendrites (arrows) indicative for dendritic degeneration. **D-F**: The quantification of DiI-traced commissural neurons in the frontocentral cortex of 5, 11 and 15-month-old mice revealed a significant reduction of the number of type I commissural neurons in APP23 mice in comparison to wild-type mice (**D**). At 15 months of age there was also a decrease in the number of traced type II commissural neurons in APP23 mice (**E**). Such a decrease in the number of type I or type II commissural neurons was not observed in APP51/16 mice (**D**, **E**). No differences were observed for the number of type III commissural neurons (**F**). The diagrams indicate mean and standard error. All DiI-traced mice were included. *$p < 0.05$. For detailed statistical analysis see Appendix Tab. 2A. Calibration barin **A**: 50 µm for all figures. Reproduced from (Rijal Upadhaya et al., accepted for publication-b).

An example of a dystrophic dendrite has been shown in Fig. 7. A decreased number of asymmetric synapses in 15-month-old APP23 mice compared to wild-type mice was observed as well (Fig. 9C, Appendix Tab. 2A).

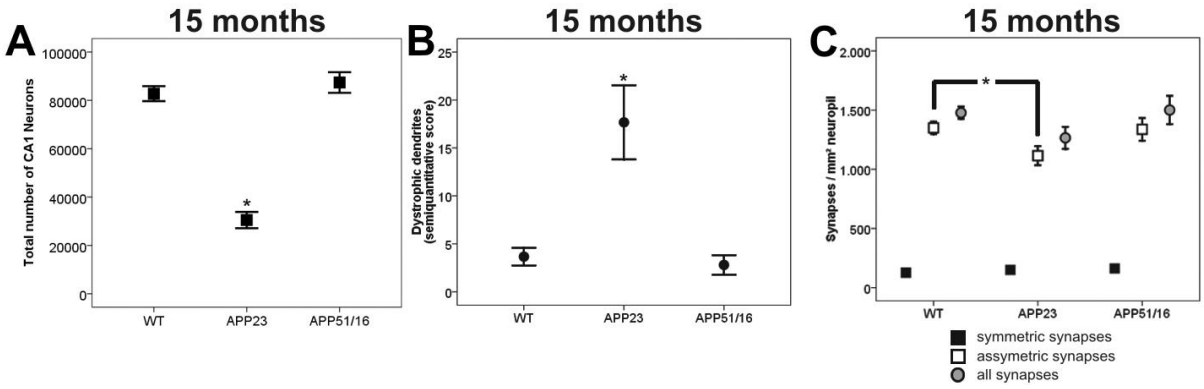

Figure 9: **Amyloid beta (Aβ) induced neuron loss, dendritic degeneration and synaptic loss in APP23 mice. A**: Unbiased stereology of Cornus Ammonis 1 (CA1) hippocampal neurons revealed a lower number of neurons in the CA1 sector of APP23 mice when compared with that of APP51/16 and wild-type mice. APP51/16 mice showed similar numbers of CA1 neurons as wild-type animals. **B**: The semiquantitative assessment of the frequency of dystrophic dendrites shows more dystrophic dendrites in the frontal cortex neuropil of 15-month-old APP23 mice than in age-matched APP51/16 and wild-type mice. **C**: Quantification of synapses at the electron microscopic level revealed a decrease of asymmetric synapses in 15-month-old APP23 mice in comparison to wild-type mice. Such a decrease was not observed in APP51/16 mice. *$p < 0.05$. For detailed statistical analysis see Appendix Tab. 2A. Reproduced from (Rijal Upadhaya et al., accepted for publication-b)

15-month-old APP51/16 mice did not show such a decrease in the synaptic density. Photoconversion of DiI-traced altered type 1 commissural neurons from 5-month-old APP23 mice and subsequent immunoelectron microscopy revealed numerous gold particles within the dendrites of these neurons indicating the presence of Aβ (Fig. 10D-F). Here, no fibrillar or protofibrillar material was observed.

There was only an accumulation of spherical- amorphous electron dense material associated with the gold particles as seen after precipitation with the A11 antibody against non-fibrillar oligomers (see also Fig. 19) indicating the presence of non-fibrillar Aβ oligomers in altered dendrites. Aβ fibrils or protofibrils were not observed within dendrites. Non-altered dendrites in 5- and 15-month-old APP23 and 15-month-old APP51/16 mice did not exhibit more than single gold particles labeling very small amounts of Aβ-positive material at the immunoelectron microscopic level. No Aβ-positive material was detected in wild-type animals.

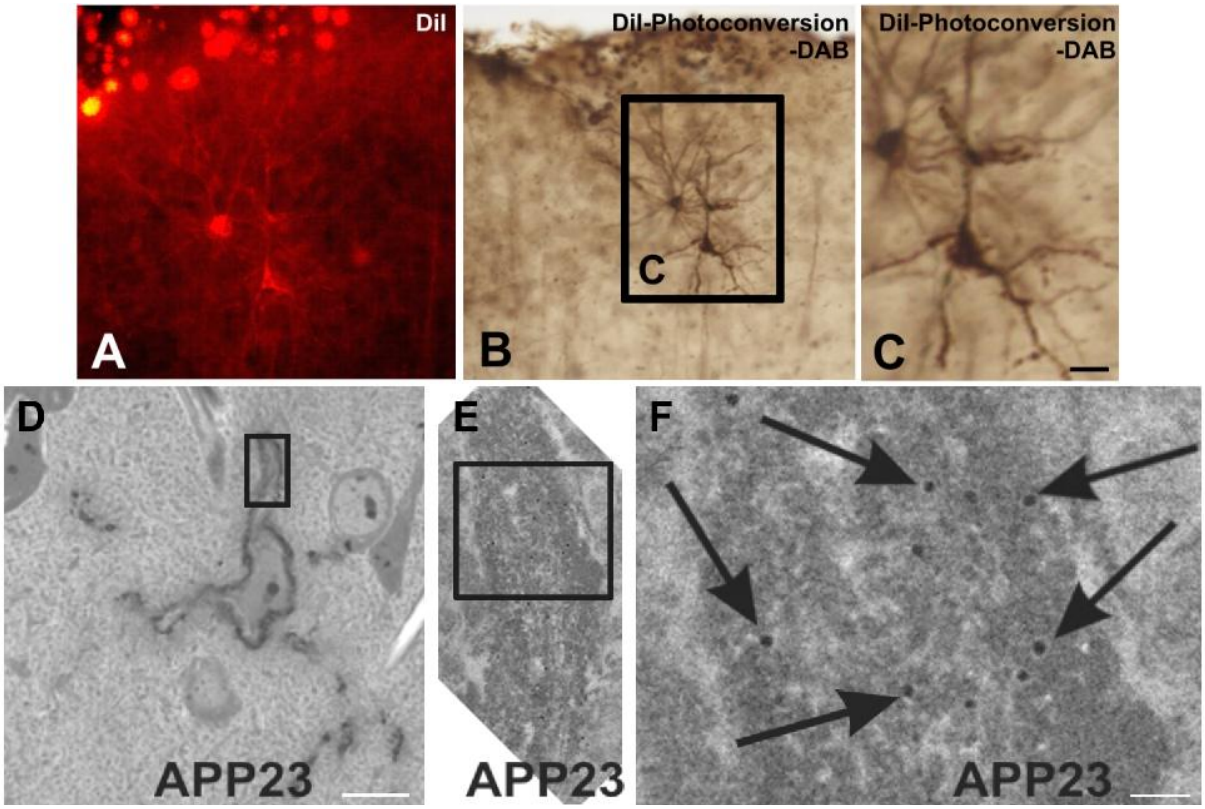

Figure 10: Photoconversion of DiI-labeled neurons with 3.3-diaminobencidine (DAB)-HCl for detection under normal light microscopy. A: A type I commissural neuron of a 5-month-old APP51/16 mouse with a highly ramified dendritic tree exhibits fluorescence after DiI-labeling. **B**: After photoconversion with DAB the same cell is visible under light microscopy. **C**: The higher magnification shows that all dendrites are similarly labeled as with DiI under fluorescence microscopy. The dendritic tree of this mouse exhibits no obvious alterations. **D**: The photoconverted neuron in **C** was embedded in LR-white and prepared at the semi-thin section level. The photoconverted neuron and its dendrites are labeled with DAB. The boxed area indicates the part of the apical dendrite observed at the immunoelectron microscopic level in **E**. **E**: Immunogold labeling with anti-$A\beta_{1-42}$ (Wild-Bode, et al., 1997) exhibited a specific accumulation of Aβ in the dendrite of this degenerated neuron of the 5-month-old APP23 mouse at the electron microscopic level (EM). Due to photoconversion with DAB the dendrite is marked as an electron dense structure. The boxed area is shown in higher magnification in **F**. **F**: Aβ (marked with gold particles (arrows) was localized in electron dense particles in the photoconverted degenerated dendrite. The Aβ-positive material did not show a fibrillar or protofibrillar pattern but roundish particles, thus, suggesting that the Aβ-positive material represents non-fibrillar, presumably oligomeric Aβ-aggregates. For detailed statistical analysis see Appendix Tab. 2A. Calibration bar in **D** valid for: **D** = 12 µm, **E** = 1.2 µm; calibration bar in **F** = 225 nm. Calibration bar in **C** valid for: **A** = 40 µm, **B, C**: 20 µm. Reproduced from (Rijal Upadhaya et al., accepted for publication-b).

3.2 Aβ-aggregates and deposits in APP23 and APP51/16 mice

In comparison to wild-type mice, APP23 mice showed amyloid plaques detected with antibodies against $A\beta_{17-24}$ (4G8) or against $A\beta_{1-42}$ at 5, 11, and 15 months of age increasing in number and distribution with age (Capetillo-Zarate et al., 2006) (Fig. 11A, C, D). APP51/16 mice showed the first plaques at 11 months of age located in the neocortex (Fig. 11B). With 15 months the number of plaques increased and allocortical areas were affected as well but APP23 mice showed more and more widely distributed plaques in a given age (Fig. 11B, C, D). There were similar amounts of Aβ-plaques in 5-month-old APP23 mice

with neurodegeneration and in 11-month-old APP51/16 mice without neurodegeneration (Fig. 11B). CAA was absent in 5-month-old APP23 and APP51/16 mice. At the age of 11 months and higher, CAA was seen in most APP23 and APP51/16 mice. CAA was more widely distributed in APP23 than in APP51/16 mice as previously shown (Thal et al., 2009). Capillary CAA was observed in the thalamus of 15-month-old APP23 mice but not in APP51/16 mice as previously described in 25-26-month-old animals (Thal et al., 2009).

Quantification of $A\beta_{1-42}$ and $A\beta_{1-40}$ by ELISA at 5, 11, and 15 months of age confirmed the increase of total $A\beta_{1-42}$ and $A\beta_{1-40}$ with age in the brains of APP23 and APP51/16 mice as well as higher total Aβ levels in APP23 mice than in APP51/16 mice (Fig. 12C, Appendix Tab. 2B). Comparing 15-month-old APP51/16 mice with 5-month-old APP23 mice the total $A\beta_{42}$ and $A\beta_{40}$ was higher in APP51/16 mice without neurodegeneration than in APP23 mice with neurodegeneration (Fig. 12C). The $A\beta_{42}/A\beta_{40}$-ratio did not vary significantly when comparing the ELISA data from APP23 and APP51/16 mice (Mann-Whitney U-test (two-sided): exact $p = 0.633$).

B10AP-positive plaques were found in the neocortex of APP23 mice beginning at 5 months of age and in APP51/16 mice at 15 months of age. In APP23 mice B10AP-positive plaques expanded into the cingulate gyrus and the hippocampus in 11- and 15-month-old animals (Fig. 11G, H). Younger APP51/16 mice did not exhibit histologically detectable B10AP-positive aggregates (Fig. 12D, Appendix Tab. 2B).

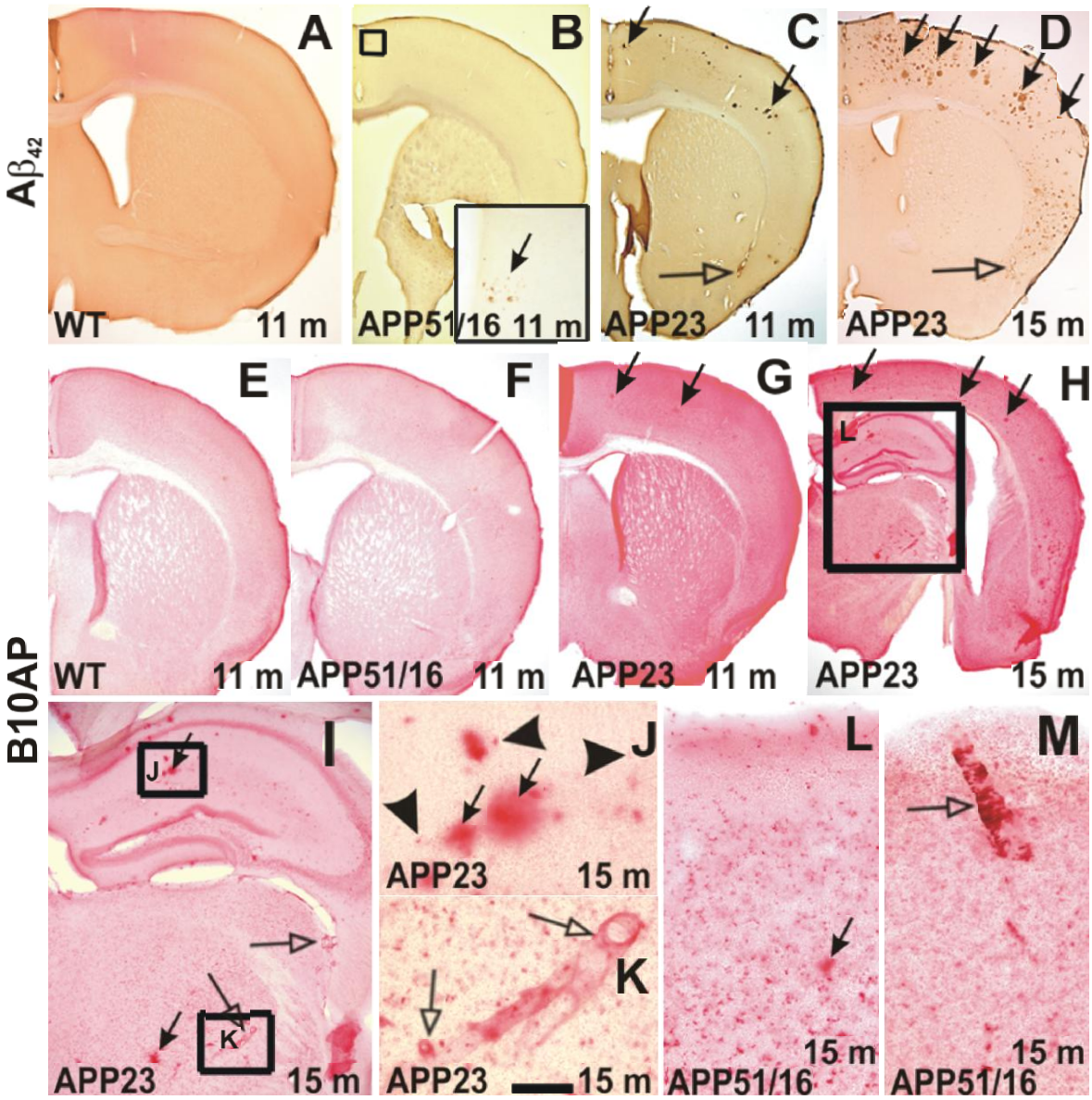

Figure 11: Deposition of amyloid beta (Aβ) and B10AP positive material in APP-transgenic mice and wild-type littermates.

A-D: Aβ-plaques as detected with antibodies against $A\beta_{1-42}$ were not found in wild-type animals (**A**). Only single plaques were seen in the neocortex of 11-month-old APP51/16 mice (**B**). These plaques could only be identified at the high magnification level (arrow in inset **B**). In APP23 mice of the same age neo- and allocortical plaques (arrows in **C**) and cerebrovascular Aβ-deposits, i.e. cerebral amyloid angiopathy (CAA; lucent arrow in **C**) were visible even at the low power magnification level. At 15 months of age the number of plaques in the APP23 mouse has been increased (arrows in **D**). CAA-affected vessels were observed at this age as well (lucent arrow in **D**). **E**: B10AP-positive plaques were not found in wild-type (**E**) and in APP51/16 mice at 11 months of age (**F**). In APP23 mice single plaques were strongly marked with B10AP in the neocortex of 11-month-old animals (arrows in **G**). 15-month-old APP23 mice showed more B10AP-positive plaques in the cortex (arrows in **H**) and additional ones in the hippocampal formation and the thalamus (black arrows in **I**, **J**). In the neighborhood of B10AP-positive plaques dot-like B10AP-positive granules are observed (arrowheads in **J**). In addition CAA-affected vessels exhibited strongly B10AP-positive material (lucent arrows in (**I**, **K**). **L**, **M**: In 15-month-old APP51/16 mice single B10AP-positive plaques (arrow in **L**) and CAA-affected vessels (lucent arrow in **M**) were observed in the frontocentral and cingulate cortex. Calibration bar in **K** valid for: **A-H** = 230 µm, **I** = 66 µm, **J, K =** 12.5 µm, **L**, **M** = 77 µm. Reproduced from(Rijal Upadhaya et al., accepted for publication-b).

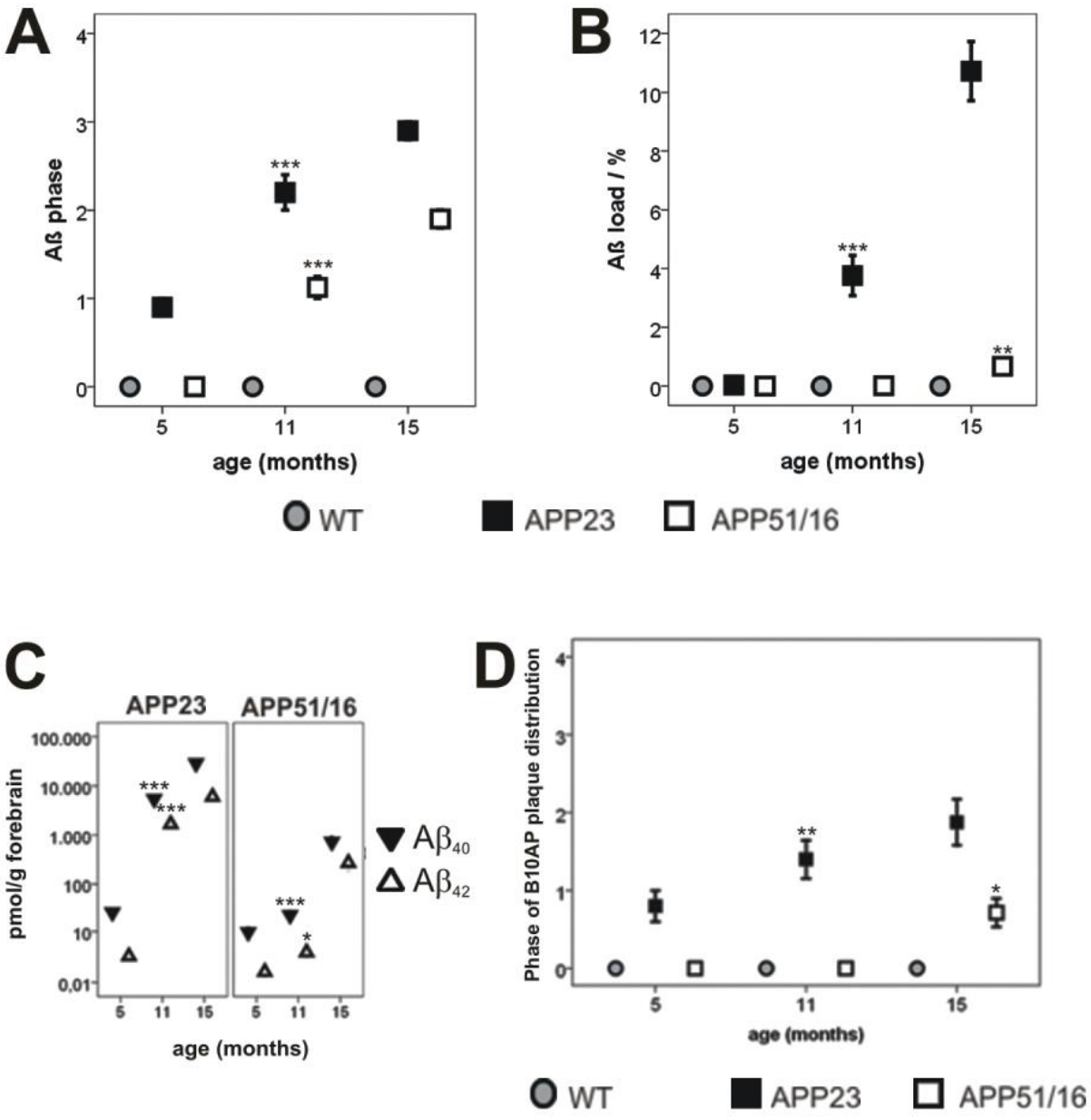

Figure 12: Graphical representation of quantified amyloid beta (Aβ) and B10AP-positive material in APP-transgenic and wild-type mice. **A**: The expansion of Aβ-plaques throughout the different brain regions (Aβ-phase) increases with age in APP23 mice and APP51/16 mice. APP51/16 mice, thereby, develop Aβ-plaques later than APP23 mice and its expansion at a given age is less than in APP23 mice. **B**: The Aβ load increases significantly in APP23 mice with 11 months of age and rises strikingly up to 15 months of age whereas only a moderate increase in the Aβ load is seen in 15-month-old APP51/16 mice. **C**: ELISA measurements of the total $A\beta_{1\text{-}40}$ and $A\beta_{1\text{-}42}$-content in 5, 11, and 15-month-old animals confirmed the increase of total $A\beta_{1\text{-}40}$ and $A\beta_{1\text{-}42}$ with age in APP23 and APP51/16 mice. At 5 months of age APP51/16 mice contained lower levels of $A\beta_{42}$ and $A\beta_{40}$ in the brain than APP23 mice. **D**: The expansion of B10AP-positive plaque pathology representing fibrillar and protofibrillar material increased with age as well. Mean and standard errors are presented. *$p < 0.05$; ** $p < 0.01$; ***$p < 0.001$. **A**, **B**, **D**: All DiI-traced mice were included in the diagrams. **C**: All animals used for ELISA measurements were included. For detailed statistical analysis see Appendix Tab. 2B. Reproduced from (Rijal Upadhaya et al., 2011).

Only a minority of the amyloid plaques detected by anti-$A\beta_{17-24}$ or anti-$A\beta_{1-42}$ exhibited strongly stained B10AP-positive material (Fig. 11B-I). Near B10AP-positive plaques small dot-like granules were stained as well (Fig. 11J arrowhead).

3.3 Oligomeric, protofibrillar and fibrillar Aβ-aggregates in human AD, ADRP, and control brain

Histologically, we found in AD cases only a small number of B10AP-positive plaques in contrast to a high number of senile plaques that were detected with an antibody against the $A\beta_{17-24}$ (4G8) (Fig. 13A, B) and with the Campbell-Switzer silver staining (Fig. 13D). Dot-like B10AP-positive material was observed in the neuropil of AD cases (Fig. 13C) but not in control cases without Aβ deposits (Fig. 13E-G). All AD cases as well as 40% of the non-demented ADRP cases, with Braak-NFT stages ranging between II and III and Aβ phases between 3 and 4, exhibited B10AP-positive plaques and B10AP-positive dot like material (Fig. 13A). Dot-like structures were also marked in A11-stained sections from AD brain (Fig. 13H, I) as already seen by other authors (Kayed et al., 2003). A11-dots in the neuropil were observed in all AD cases, in 50% of the non-demented cases with AD-related pathology, and in 11.1% of the controls without Aβ deposits whereas A11-positive material near plaques was seen in none of the non-demented cases and in only 72.7% of the AD cases.

The distribution of the A11-dots appeared as neurite-associated deposits in stack reconstructions from AD cases but not in control cases (Fig. 13H,I) as already reported for oligomers (Lacor et al., 2004). The B10AP- and A11-dots were not stained with antibodies against Aβ [4G8 (Fig. 13A), MBC42] and with the Campbell-Switzer method (Fig. 13D), a marker for amyloid fibrils (Iqbal et al., 1993; Thal et al., 1999). Statistical analysis revealed that B10AP- and A11-positive material was more frequently observed in AD than in non-demented ADRP and control cases (Fig. 14A, B, Appendix Tab. 2D).

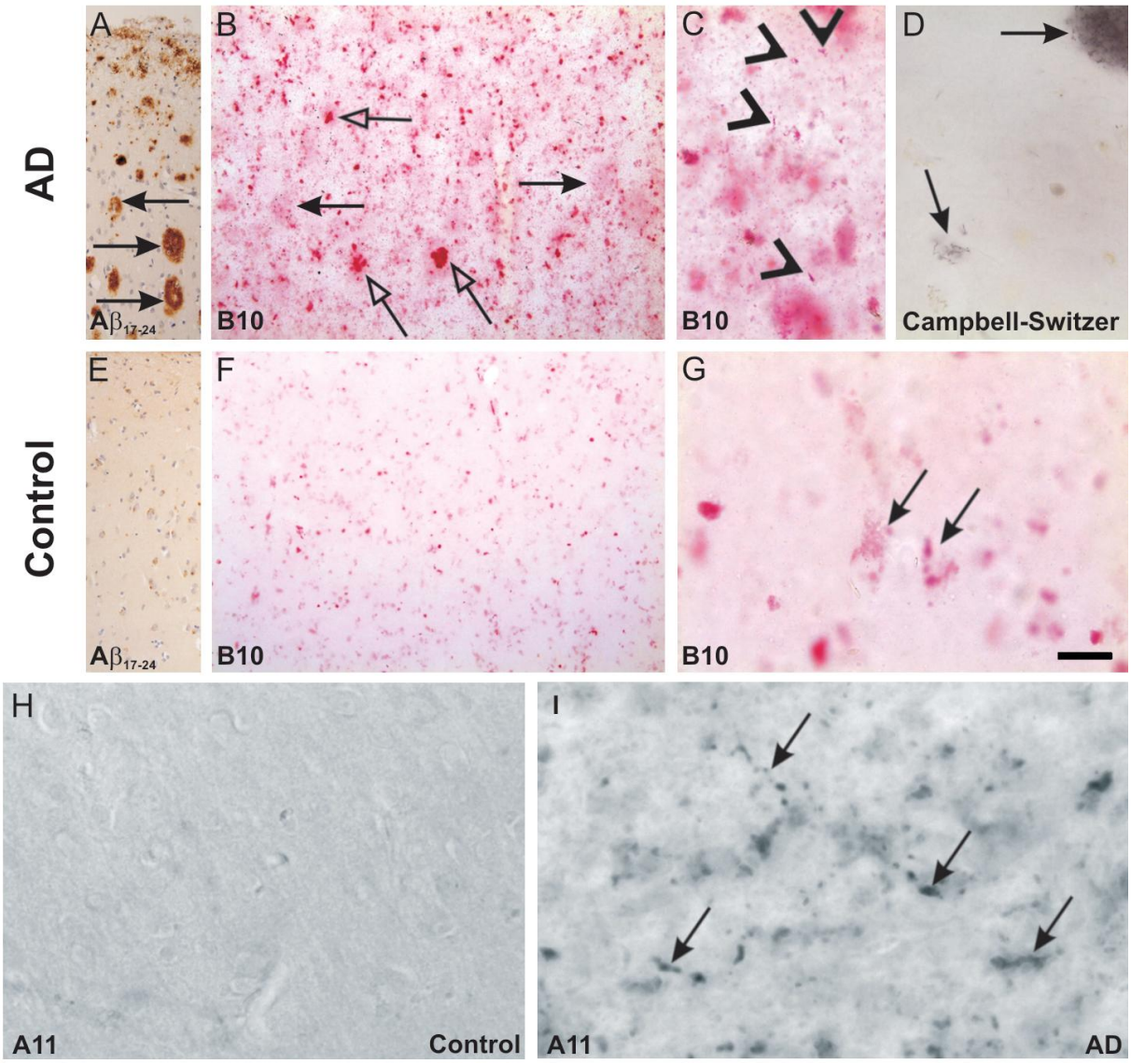

Figure 13: Physiological and abnormal B10AP- and A11-positive material in the human Alzheimer's disease (AD) and control brains. A: In AD, Aβ was detected in a high number of senile plaques (arrows) with an antibody raised against $A\beta_{17-24}$. **B**: Using B10AP a small number of senile plaques was strongly B10AP-positive (lucent arrows) whereas other plaques were moderately labeled (arrows). **C**: At high magnification strongly B10AP-positive dot-like and thread-like material was observed in the neuropil (arrowheads). **D**: This material did not show properties of amyloid fibrils because it did not stain with the Campbell-Switzer silver technique. Here, only fibrillar amyloid in plaques, including diffuse plaque-forms is marked (arrows). **E**: In a control case the anti-$A\beta_{17-24}$ staining documents the absence of senile plaques. **F**, **G**: With B10AP-labelling there are no plaques (**F**) and no B10AP-positive dots in the neuropil (**G**) as well. Only a moderate homogeneous neuropil staining is seen in the cortex indicating that B10AP also marked proteins that did not contain Aβ as previously shown [12; 29]. **H**, **I**: A11-positive Aβ-oligomers are not detectable in control cases (H) but in AD cases (I) showing an accumulation of these oligomers along neurites (arrows in I). Calibration bar in **G** valid for: **A**, **E**, **F** = 100 µm, **B** = 75 µm, **C**, **D**, **G** = 15 µm, **H** = 25 µm, **I** = 20 µm.

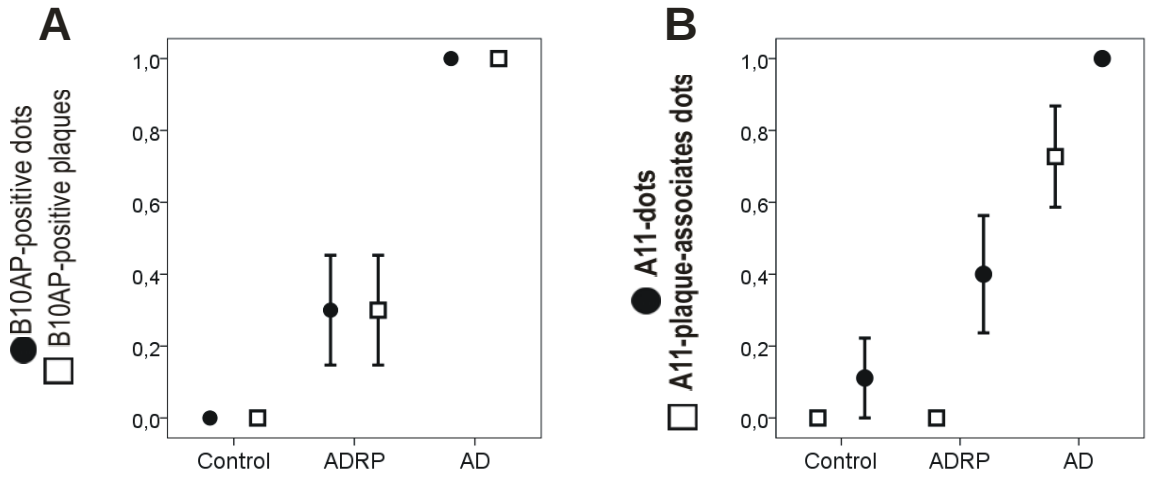

Figure 14: Quantification of B10AP and A11 positive materials in human brains. A: The statistical analysis revealed significant differences in the occurrence of B10AP-positive plaques and B10AP-positive dots between Alzheimer's disease (AD) cases and controls (Fisher's exact test: $p<0.001$). All AD cases showed such plaques and B10AP-positive dots whereas none of the control cases without senile plaques showed this kind of pathology. 30% of the non-demented cases with AD-related Aβ-pathology (ADRP) exhibited B10AP-positive plaques and dots. **B**: In single control cases as well as in 40% of the ADRP cases single A11-positive dots were observed but no plaque-associated staining of A11-positive dots. Plaque-associated A11-positive material was observed in 72.7 % of the AD cases. All AD cases exhibited A11-positive dot-like material. Statistical analysis confirmed that the occurrence of A11-positive plaques and dot-like aggregates in the neuropil increased in AD cases in comparison with control cases and ADRP-cases (Statistical analysis is provided in Appendix Tab. 2D, all cases listed in Appendix are included. Mean and standard errors are given).

3.4 High-molecular weight $A\beta_{42}$ aggregates predominate in the soluble/dispersible fraction of native brain homogenates from human and APP23 and APP51/16 mice

The soluble/dispersible fraction of human brain lysate was analyzed in the native form without any denaturating agent via BN-PAGE and subsequent western blot analysis. This revealed a high-molecular weight anti-$A\beta_{42}$-positive smear >1000 kDa in AD cases (Fig. 15A) that was not found in controls. Non-demented ADRP cases showed moderate levels of this hiMWAβ_{42}. Aβ-monomers, dimers, or other loMWAβ-species were not observed in AD cases or in controls (Fig. 15A).

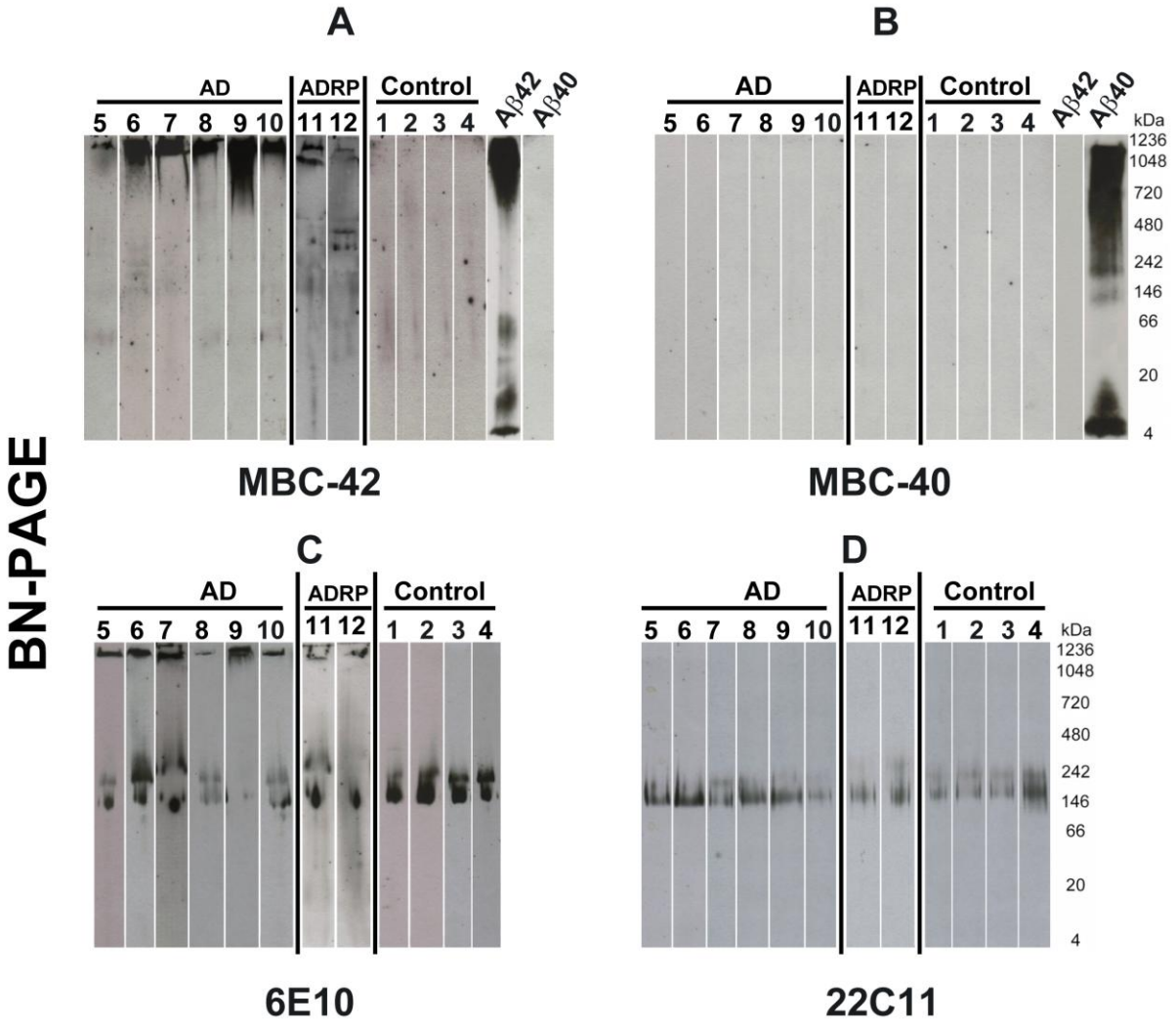

Figure 15: Western blot analysis of Tris Buffer Saline (TBS) soluble proteins from Alzheimer's disease (AD) and control brains after Blue native polyacrylamide gel electrophoresis (BN-PAGE) All BN-PAGE blots were developed 2-3 h for chemiluminescence exposure. **A:** The protein lysates from AD brains (cases No. 5-10) in BN-PAGE showed a high-molecular weight amyloid beta ($A\beta_{42}$) positive smear >1000 kDa when detected with anti-$A\beta_{40}$ antibodies (MBC42). Such smears were not observed in controls (cases No. 1-4), however, in non demented cases with AD related pathology (ADRP) such smears were detected in lower intensity compared to AD. Synthetic $A\beta_{42}$ and $A\beta_{40}$ were loaded as positive and negative controls respectively. In $A\beta_{42}$ preparations, long chemiluminescence exposure led to the detection of additional dimer and ~50kDa bands that were not observed after 2-5 min exposures, as shown in Fig. 24 C. **B:** The $A\beta_{42}$-positive material seen in **A** was not detectable in AD (cases No. 5-10) or in the controls (cases No. 1-4) in the native gel blotted with anti-$A\beta_{40}$ antibodies (MBC40). Synthetic $A\beta_{42}$ and $A\beta_{40}$ were loaded as positive and negative controls respectively. After 3 h of chemiluminescence exposure, synthetic $A\beta_{40}$ blots display a dimer band at ~10 kDa in addition to the monomer band and the hiMWAβ smear already detected with shorter exposure times as depicted in Fig. 24 C. **C:** The anti-$A\beta_{1\text{-}17}$ (6E10) antibody also detected the high molecular weight protein aggregates >1000 kDa in the area of stacking gel in the protein lysate from AD brains (cases No. 5-10), which was not detectable in control brains (cases No. 1-4) and very less in ADRP (cases 11-12). In addition, anti-$A\beta_{1\text{-}17}$ also showed APP bands in all cases (140-240 kDa). **D**: The APP-positive bands were re-confirmed with an antibody directed against N-terminal epitope of APP (22C11) in control (cases No. 1-4) and AD cases (cases No. 5-10). Reproduced from (Rijal Upadhaya et al., accepted for publication-a).

The high-molecular weight smear was also seen with anti-$A\beta_{1\text{-}17}$ at the level of stacking gel in AD cases (Fig. 15C) but not with anti-$A\beta_{40}$ (Fig. 15B). The detection of synthetic $A\beta_{40}$

but not $A\beta_{42}$ indicated specific antibody function (Fig. 15B). Anti-$A\beta_{1-17}$ stained an additional 150-250 kDa band (Fig. 15C) that was also observable with anti-APP antibodies (Fig. 15D), thereby indicating that this band represents APP-containing material. The APP-related band was also present in control cases, whereas the high-molecular weight anti-$A\beta_{1-17}$ smear was not seen. The BN-PAGE blots from brain samples were developed with a chemiluminescence exposure time of 2-3 h to detect even very minimal amounts of proteins.LoMWAβ as well as an Aβ-monomer band were neither detected in BN-PAGE analysis of AD nor of ADRP cases (Fig. 15A-C). $A\beta_{40}$ was not detectable in BN-PAGE of the soluble/ dispersible fraction of AD brains (Fig. 15B).

In case of APP23 and APP51/16 mouse models the soluble and dispersible fraction was analyzed separately under native conditions by BN-PAGE which revealed no detectable soluble $A\beta_{42}$ and $A\beta_{40}$ in 5-month-old animals (Fig. 16A). In 12-month-old APP23 and APP51/16 mice, we observed a smear of high-molecular weight Aβ oligomers (hiMWAβ) with a molecular-weight above 240 kDa. This material was detectable with anti-$A\beta_{42}$, while anti-$A\beta_{40}$ showed only a very weak staining (Fig. 16B) similarly as reported for native hiMWAβ aggregates in the human brain (Fig. 15). In wild-type and knockout mice this material was not seen. The amount of soluble native hiMWAβ_{42} appeared nearly similar in 12-month-old APP23 and APP51/16 mice. BN-PAGE of the dispersible fraction revealed anti-$A\beta_{42}$-positive material at the protein application site indicating that the native dispersible Aβ was unable to enter the blue native gel in significant amounts (Fig. 16B).

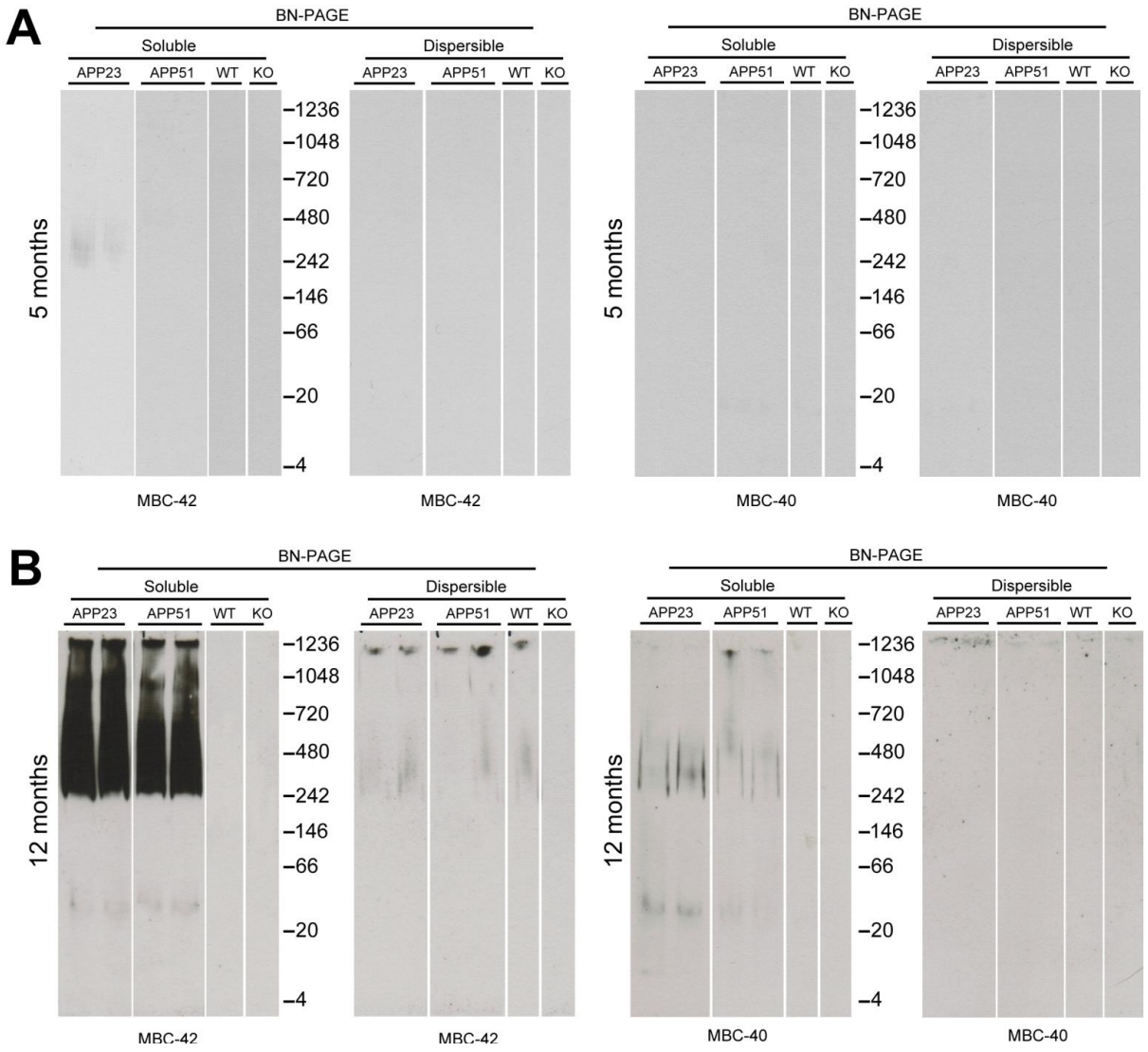

Figure 16: Blue native polyacrylamide gel electrophoresis (BN-PAGE) and Western blot analysis of amyloid beta 42 ($A\beta_{42}$) and 40 ($A\beta_{40}$) in the soluble and dispersible fraction of mouse brain homogenates. **A**: In 5-month-old APP23 and APP51/16 mice significant amounts of Aβ were not observed in the soluble and in the dispersible fraction. **B**: 12-month-old APP23 and APP51/16 mice exhibited high molecular weight amyloid beta 42 (hiMWAβ_{42}) with a molecular weight of 240 kDa and higher in the soluble fraction. With anti-$A\beta_{40}$ this material was only very weakly labeled. In the dispersible fraction anti-$A\beta_{42}$-positive material was detected in the pouches of the gel but significant amounts of Aβ aggregates were not observed within the gel. In the pouches of the gel also a weak signal with anti-$A\beta_{40}$ was observed when analyzing the dispersible fraction. Reproduced from (Rijal Upadhaya et al., accepted for publication-b).

3.5 SDS-treatment destroys native high-molecular weight $A\beta_{42}$ and $A\beta_{40}$ aggregates

Since the spectrum of Aβ aggregates observed after BN-PAGE was different from that of Aβ aggregates after SDS-PAGE (Lesne et al., 2006; Rijal Upadhaya et al., accepted for publication-a) I addressed the question whether the changes in the pattern of Aβ aggregates is due to the different methods of sample preparation applied in SDS-PAGE and BN-PAGE. For this purpose I used synthetic synthetic $A\beta_{42}$ and $A\beta_{40}$ to form oligomeric,

protofibrillar and fibrillar aggregates detectable by electron microscopy (Fig. 17A, B). To confirm the SDS induced denaturation the synthetic Aβ aggregates were prepared protein samples with SDS buffer and native buffer for SDS-PAGE and BN-PAGE analysis respectively. With 2-5 min chemiluminescence exposure time, BN-PAGE blots revealed a monomer band and an additional prominent smear of $A\beta_{42}$- and $A\beta_{40}$-aggregates with a molecular weight >700 kDa and 240 kDa respectively (Fig. 17C). However, after longer exposure time of 2-3 h smeary bands at ~10 kDa and ~50 kDa in $A\beta_{42}$ preparations was observed, whereas $A\beta_{40}$ preparations exhibited an additional dimer band (~ 8 kDa) that was not detectable in short chemiluminescence exposure blots (Fig. 15A,B).

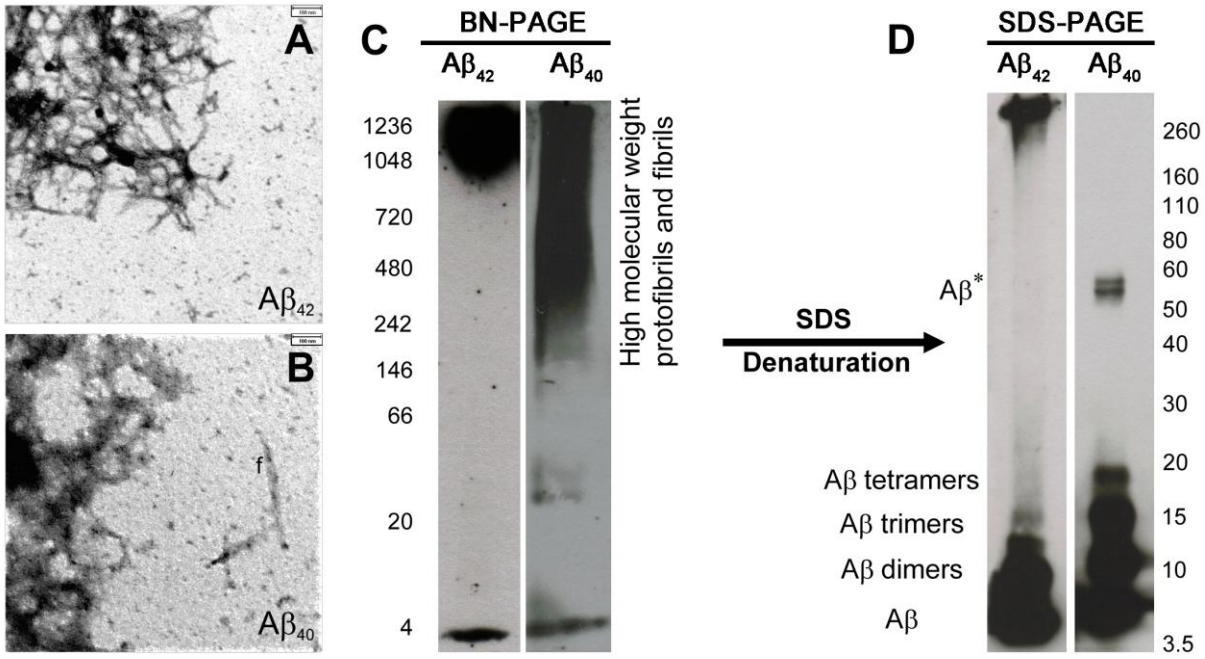

Figure 17: Analysis of synthetic amyloid beta 42 ($A\beta_{42}$) and 40 ($A\beta_{40}$) by electron microscopy, blue native polyacrylamide gel electrophoresis (BN-PAGE) and Sodium dodecyl sulfate PAGE (SDS-PAGE). A and B: Synthetic $A\beta_{42}$ (**A**) and $A\beta_{40}$ (**B**) aggregates were dissolved in cell culture medium aggregated to amorphous oligomers, protofibrils, and fibrils (f), as detectable by electron microscopy. **C:** In BN-PAGE, a high-molecular weight smear occurred mainly above 700 kDa in $A\beta_{42}$ preparations in addition to a distinct monomeric band at ~4 kDa. $A\beta_{40}$ preparations produced a smear of Aβ-aggregates with a molecular weight above 242 kDa in addition to a clear monomeric band at ~4 kDa. The BN-PAGE blots were developed with standard chemiluminescence exposure time of 2-5 min. Longer chemiluminescence exposure for 3 hrs resulted in additional low molecular weight amyloid beta (loMWAβ) bands depicted in Fig. 21A,B, thereby indicating that these preparations contain low levels of these Aβ species as well. **D:** In SDS-PAGE, high molecular weight amyloid beta ($hiMWA\beta_{42}$) aggregates were strikingly reduced. Instead, the monomer, dimer, and trimer bands displayed strong staining. Other $loMWA\beta_{42}$-oligomers were not evident. No $hiMWA\beta_{40}$ aggregates were seen after denaturing SDS-PAGE, but $A\beta_{40}$ monomer, dimer, trimer, and tetramer bands as well as an Aβ*56 band were detectable at 56 kDa. Reproduced from (Rijal Upadhaya et al., accepted for publication-a).

Following SDS-PAGE of the same sample I observed only few high-molecular weight aggregates above 240 kDa in Aβ42 preparations and no hiMW Aβ aggregates in Aβ40 preparations, whereas very prominent Aβ-monomer, dimer, and trimer bands were observed for both synthetic $A\beta_{42}$ and $A\beta_{40}$ preparations. In SDS-treated $A\beta_{40}$ preparations, tetramer and Aβ*56 bands were present that were not seen in SDS-treated $A\beta_{42}$ preparations (Fig. 17D).

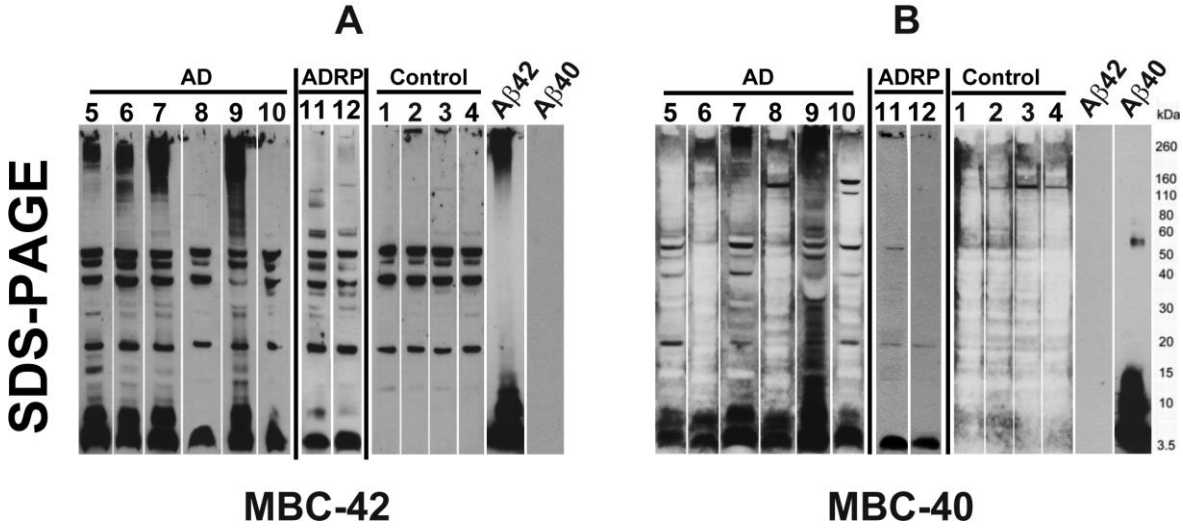

Figure 18: Sodium dodecyl sulphate PAGE (SDS-PAGE) analysis of Alzheimer's disease (AD) brains protein lysates. Cases No. 5-10 exhibited amyloid beta (Aβ) monomer and dimer bands with anti-$A\beta_{42}$ antibodies (MBC42) (**A**) and anti-$A\beta_{40}$ antibodies MBC40 (**B**) that were not detected in control brains (cases No. 1-4). The anti-$A\beta_{42}$ positive dimer bands (**A**) were not seen in all AD cases, whereas anti-$A\beta_{40}$ consistently detected dimer bands in all AD cases (**B**). A high-molecular smear was found in most AD cases with both antibodies directed against Aβ. The detection of the low molecular weight Aβ (loMWAβ) oligomers required chemiluminescence exposure for 3 h (i.e., long exposure times). Reproduced from (Rijal Upadhaya et al., accepted for publication-a).

SDS-PAGE with subsequent anti-$A\beta_{42}$ and anti-$A\beta_{40}$ western blot analysis showed Aβ-monomers and dimers in AD cases (Fig. 18A-B). Aβ aggregates with a molecular weight of >160 kDa were observed in 4/6 cases with anti-$A\beta_{42}$ and at least 3 cases with anti-$A\beta_{40}$.

3.6 A11-antibody and B10AP-antibody fragments specifically precipitate oligomeric and protofibrillar/fibrillar proteins including Aβ oligomers, Aβ protofibrils and Aβ fibrils in AD cases

To further analyze the hiMW Aβ protofibrils/fibrils and oligomers, B10AP and A11 antibodies that specifically bind to protofibrillar/fibrillar and oligomeric confirmations respectively were used. Immunoprecipitation with these antibodies was performed in TBS-soluble brain homogenates of AD and normal individuals and the precipitated material was analyzed by electron microscopy. In non-AD control brains, immunoelectron microscopy of A11- and B10AP-precipitated proteins revealed a high number of precipitated and

aggregated proteins that did not contain Aβ-positive material (Fig. 19A-D). There was no unspecific labeling with anti-$A\beta_{1-17}$ in controls.

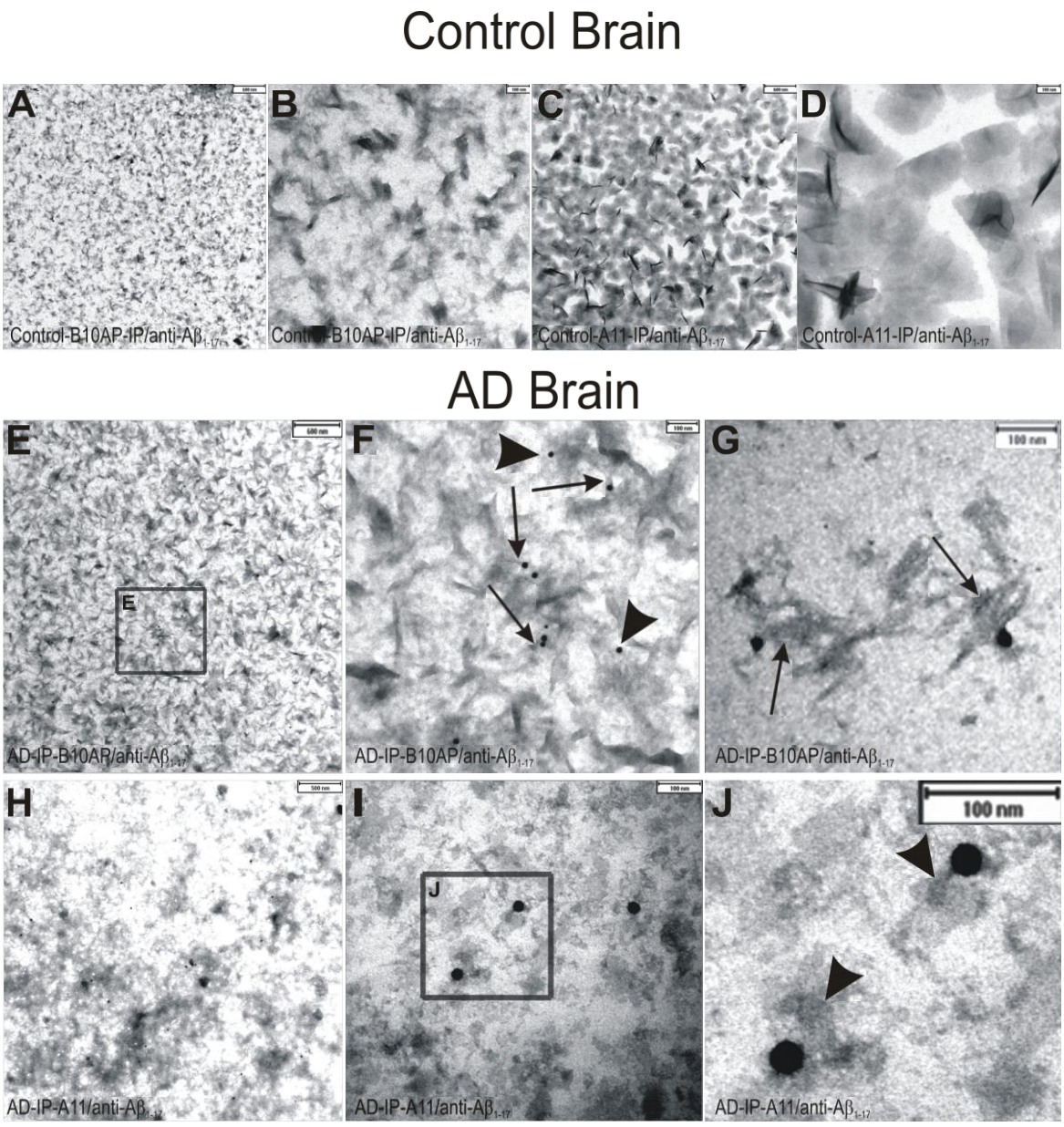

Figure 19: Electron microscopic analysis of immunoprecipitated protein-aggregates from Alzheimer's disease (AD) and control brain as precipitated with B10AP-antibody fragments (B10AP-IP) and A11 antibodies (A11-IP). A, B: B10AP-IP protein aggregates in control cases did not show amyloid beta (Aβ) positive material. The protein aggregates exhibited protofibril-aggregate-like architecture that is more evident at higher magnification (**B**). **C, D**: A11-IP from control cases resulted in detection of amorphous to spherical presumably oligomeric protein aggregates, but did not exhibit Aβ as a component of these protein aggregates. The high magnification demonstrates the spherical shape of the precipitated proteins (**D**). **E, F**: B10AP-IP from AD brain lysate showed protein aggregates of protofibril-like morphology. Immunogold labeling indicated $A\beta_{1-17}$-positive proteins. The frame in **E** indicates the areas enlarged in **F**. At higher magnification, $A\beta_{1-17}$-positive material following B10AP-IP exhibited protofibril-like morphology (arrows in **F**) and less frequently amorphous structures (arrowheads in **F**). These types of Aβ aggregates prevailed in B10AP-precipitates. **G**: Only a few precipitated Aβ-positive protein-aggregates exhibited fibrillar architecture resembling synthetic Aβ fibrils (Fig. 17A, B). **H**, **I**, **J**: A11-precipitated protein aggregates from AD exhibited spherical to amorphous morphology. Immunogold particles indicate the presence of anti-$A\beta_{1-17}$-positive aggregates. Reproduced from (Rijal Upadhaya et al., accepted for publication-a). Calibration Bar:

B10AP-precipitated material exhibited a pattern that showed fibril/protofibril-like architectures (Fig. 19A, B) whereas the proteins precipitated by A11 displayed a spherical pattern (Fig. 19C, D).

In B10AP-precipitates of the soluble fraction of AD brain homogenates, protein aggregates with a fibril/protofibril-like pattern similar to that seen in controls were observed.

However, in AD brains a high number of Aβ-positive protein aggregates was detected with anti-$A\beta_{1-17}$ (Fig. 19E-G). High magnification analysis of anti-$A\beta_{1-17}$-labeled protein aggregates revealed a protofibril-like pattern (Fig. 19F, arrows). However, a few amorphous protein-aggregates (Fig. 19F, arrowheads) as well as fibrillar aggregates (Fig. 19G) were seen. Spherical Aβ-oligomers were not observed following B10AP-immunoprecipitation. Amorphous and spherical protein aggregates were observed after A11-immunoprecipitation from AD brain lysates. Anti-$A\beta_{1-17}$ antibodies detected protein aggregates of spherical and amorphous morphology (Fig. 19H-J). Protofibril-like structures as seen in B10AP-precipitates were not observed in A11-precipitates.

To verify the efficiency of immunoprecipitation with B10AP and A11 dot blot analysis of the sample-antibody cocktail subjected to immunoprecipitation before incubation with the beads and the flow through of these lysates after incubation with the beads was measured (Fig. 20). A decrease in signal intensity of flow through compared to the sample-antibody cocktail indicated a successful precipitation of the respective antigens through IP.

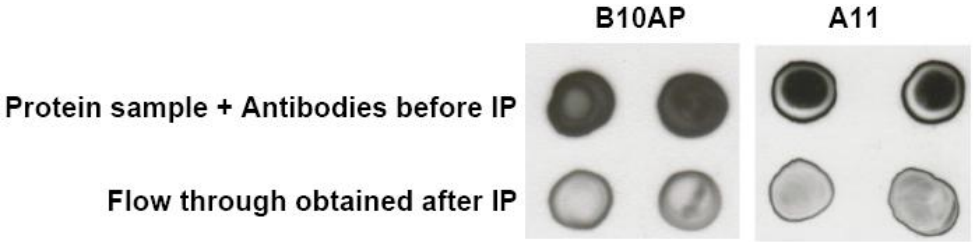

Figure 20: Dot blot assay to verify efficiency of immunoprecipitation (IP). The upper panel shows the signal of the mixture of protein sample and antibodies was blotted on the nitrocellulose membrane and the lower panel shows the signal of flow through obtained after IP-filtration.

Furthermore to document the sensitivity of Aβ quantification by immunoprecipitation we used synthetic $A\beta_{42}$ (Bachem, Switzerland) dispersed in cell culture medium (RPMI1640, GIBCO, Invitrogen, Carlsbad, CA, USA) at concentrations of 2, 6, 8, 10, and 12 µg/ml (Fig. 21). The Aβ samples were incubated for 4 h at 22°C before analysis allowing aggregation similar as in the soluble/dispersible fraction of brain lysates as shown recently (Rijal Upadhaya et al., accepted for publication-a). Immunoprecipitation of only medium used as negative controls. Immunoprecipitation with anti-$A\beta_{1-17}$ (6E10), subsequent

western blot analysis and quantification was performed as described previously.

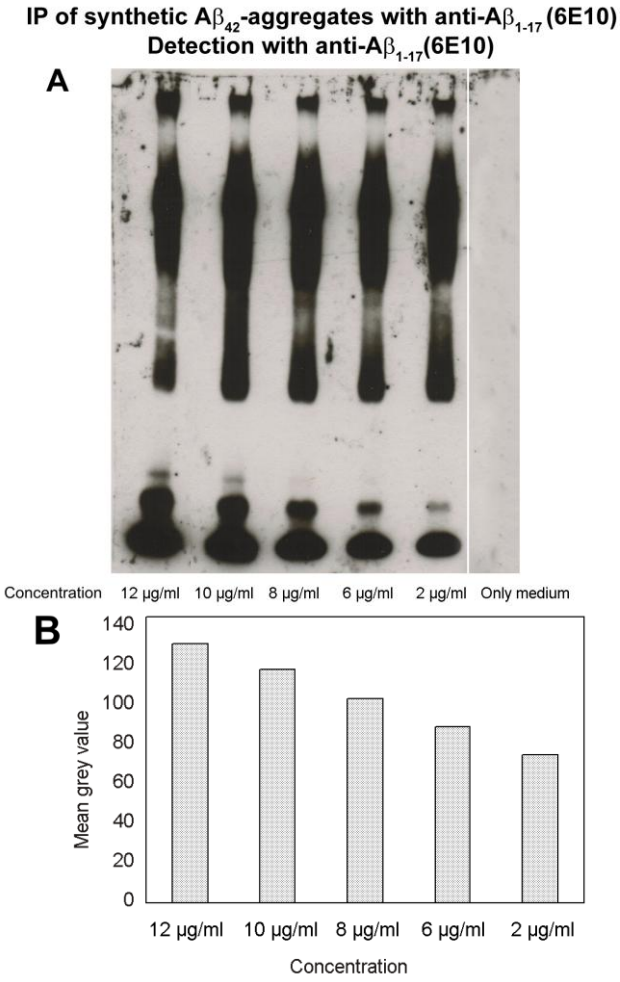

Figure 21: Quantification of synthetic amyloid beta 42 ($A\beta_{42}$) preparations using immunoprecipitation (IP) with subsequent quantification of the monomer bands. A: Five different concentrations (2 µg/ml, 6 µg/ml, 8 µg/ml, 10 µg/ml and 12 µg/ml) of the $A\beta_{42}$ aggregates were immunoprecipitated in the similar way as for the protein samples with 6E10 antibody and analyzed by western blotting by using 6E10 as detecting antibody. **B**: The diagram showed the quantification data of the monomeric bands in the Western blot. As the concentration decreased the mean gray value also decreased accordingly. This confirmed the validity of Aβ-quantification by immunoprecipitation with subsequent sodium dodecyl sulphate- polyacrylamide gele electrophoresis (SDS-PAGE) and western blot analysis. Reproduced from (Rijal Upadhaya et al., accepted for publication-b).

3.7 Quantitative differences in dispersible Aβ oligomer, protofibril and fibril levels distinguish APP23 from APP51/16 mice and AD from control/ADRP brain

Immunoprecipitation and subsequent SDS-PAGE-induced protein denaturation was used to analyze non-fibrillar Aβ oligomers precipitated by A11 and Aβ protofibrils and fibrils precipitated by B10AP in the soluble and dispersible fraction of brain lysates. In BN-PAGE the hiMWAβ-aggregates remain as smeary band on the upper part of the gel, however in case of SDS-PAGE the hiMWAβ-aggregates dissociate in SDS-containing

buffers (Rijal Upadhaya, et al., 2011) so, I focused my analysis on differences among the monomer bands detected after SDS-PAGE of Aβ oligomers, protofibrils and fibrils that is indicative for changes in the protein levels of Aβ aggregates as demonstrated in Fig. 22. Only 12-month-old APP23 mice showed a weak monomer band after precipitation with A11 and B10AP from the soluble fraction (Fig. 22A, B). In contrast, the dispersible fraction exhibited Aβ monomer bands after SDS denaturation of A11- and B10AP-precipitated aggregates in APP23 and APP51/16 mice at 5 and 12 months of age (Fig. 22A, B). 12-month-old APP23 mice also exhibited a significant dimer band at 8 kDa. We observed no detectable amounts of Aβ in APP-KO and wild-type mice after precipitation with B10AP or A11 (Fig. 22A, B). Quantitatively APP23 mice exhibited more Aβ-positive material in the monomer band, representing SDS-denaturable Aβ oligomers (precipitated with A11), protofibrils and fibrils (precipitated with B10AP) than APP51/16 mice even when comparing 5-month-old APP23 mice with 12-month-old APP51/16 mice (Fig. 22C; one way ANOVA with Games-Howell post-hoc test: $p \leq 0.036$, Appendix Tab. 2C).

The 12 kDa band in the dispersible fraction represents APP C-terminal fragments (APP-CTF) as well as Aβ trimers. The presence of APP-CTFα and APP-CTFβ in precipitated Aβ oligomers, protofibrils and fibrils from the dispersible fraction was confirmed by anti-APP-CTF immunoblotting of the precipitates (Fig. 22D). APP-CTFα prevailed in APP51/16 mice whereas APP-CTFβ was more prominent in APP23 mice. In the soluble fraction APP-CTFs were not observed in association with precipitated Aβ aggregates (Fig. 22D).

SDS-PAGE protein analysis with subsequent western blotting showed a significant 4kDa band of monomeric Aβ as well as a second band representing Aβ dimers in the membrane-associated (SDS soluble) and plaque-associated (formic acid soluble) fractions from 5- and 12-month-old APP23 mouse brain homogenates (Fig. 23A). APP51/16 mice at the same age showed less Aβ in both fractions although both monomer and dimer bands were observed (Fig. 23A). APP and C-terminal fragments of APP were overexpressed in the membrane-associated (SDS soluble) fraction of 5- and 12-month-old APP23 and APP51/16 mouse brain homogenates (Fig. 23B).

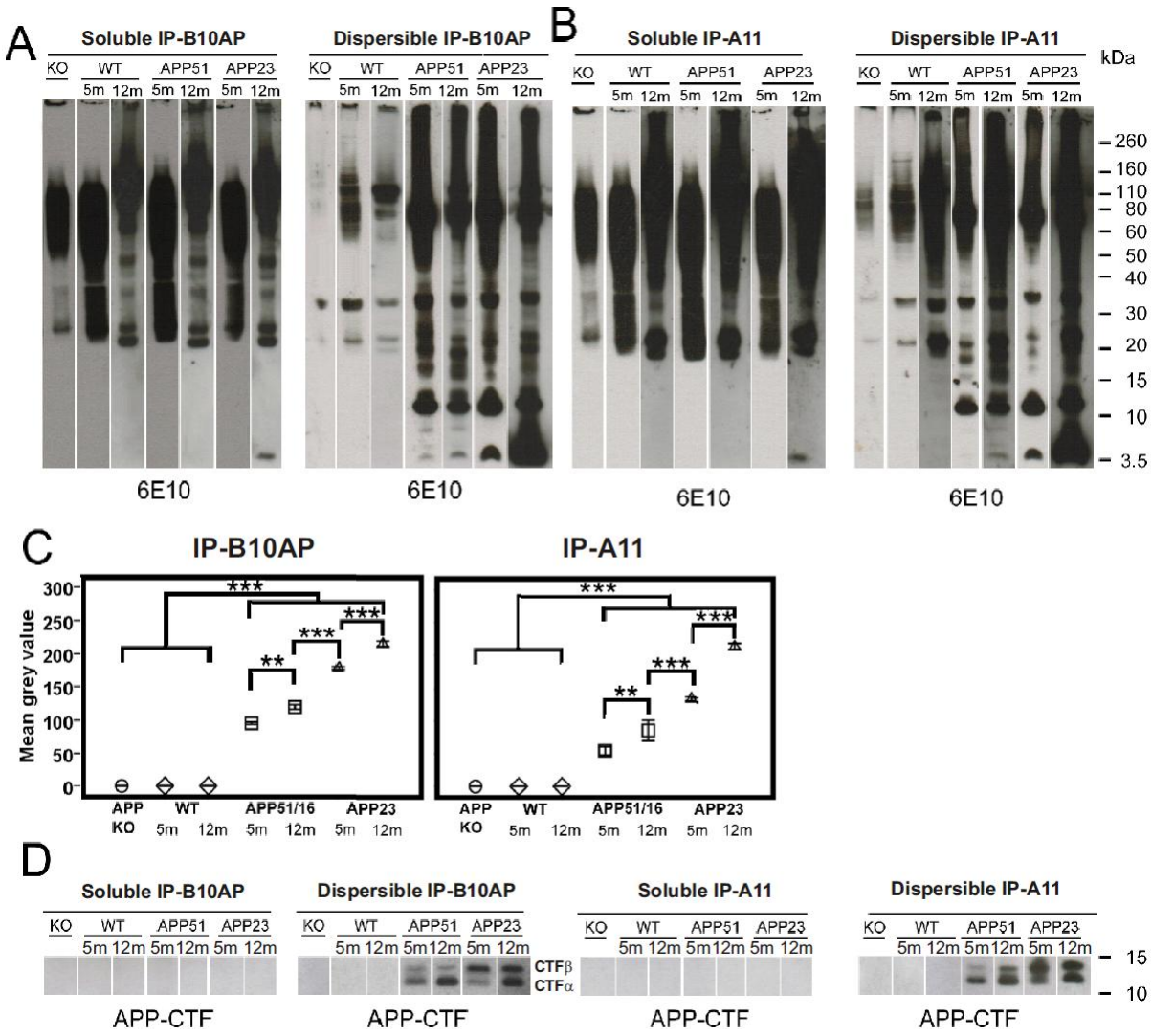

Figure 22: Immunoprecipitation (IP) from the soluble and the dispersible fraction with B10AP and A11 and subsequent denaturing western blot analysis with anti-amyloid beta 1-17 ($A\beta_{1-17}$) antibodies (6E10). **A**: A 4 kDa Aβ-monomer band in the soluble fraction only in 12-month-old APP23 mice was detected after immunoprecipittion with B10AP. In contrast, B10AP-immunoprecipitation of protofibrils and fibrils from the dispersible fraction lead to the detection of monomer bands in 5- and 12-month-old APP23 and APP51/16 mice after SDS-induced denaturation. An ~8 kDa dimer band was observed in 12-month-old APP23 mice. Wild-type and APP-KO mice were used as negative controls and indicate unspecific antibody interactions with proteins mainly between 60 and 160 kDa. The ~12 kDa band detected in all APP-transgenic animals represents β-secretase cleaved C-terminal APP-fragments (APP-CTFβ). α-secretase cleaved APP-CTFα was not detectable with the 6E10 antibody. **B**: Similarly, after immunoprecipitation with A11 only 12-month-old APP23 mice exhibited a 4 kDa Aβ monomer band in the soluble fraction. In the dispersible fraction of precipitated non-fibrillar oligomers monomer bands were obse100rved in APP23 and APP51/16 mice at 5 and 12 months of age after SDS-induced denaturation. Aβ dimers were found only in 12-month-old APP23 mice. APP-CTFβ was also observed in the A11-precipitated oligomers. **C**: Quantification of immunoprecipitated SDS-denaturated Aβ protofibrils, fibrils (IPB10AP), and oligomers (IPA11) in the soluble/dispersible fraction showed more intensely stained Aβ monomer bands in APP23 than in APP51/16 mice. APP23 mice of 5 months of age exhibited more intense Aβ monomer bands after SDS denaturation of the oligomers, protofibrils and fibrils than 12-month-old APP51/16 mice (one way analysis of variance (ANOVA) with Games-Howell post-hoc test: ** $p < 0.01$; *** $p < 0.001$; $n = 6$ for each group except APP-KO mice $n = 3$). Mean and standard errors are presented (for details see Appendix Tab. 2C). **D**: APP-CTFs were not detected in the soluble fraction precipitated with B10AP and A11 but in the dispersible fraction containing B10AP-precipitated protofibrils and fibrils and A11-precipitated oligomers. Both APP-CTFα and APP-CTFβ were found in the precipitated with APP-CTFα predominating in APP51/16 mice and APP-CTFβ being more prevalent in APP23 mice. Reproduced from (Rijal Upadhaya et al., accepted for publication-b).

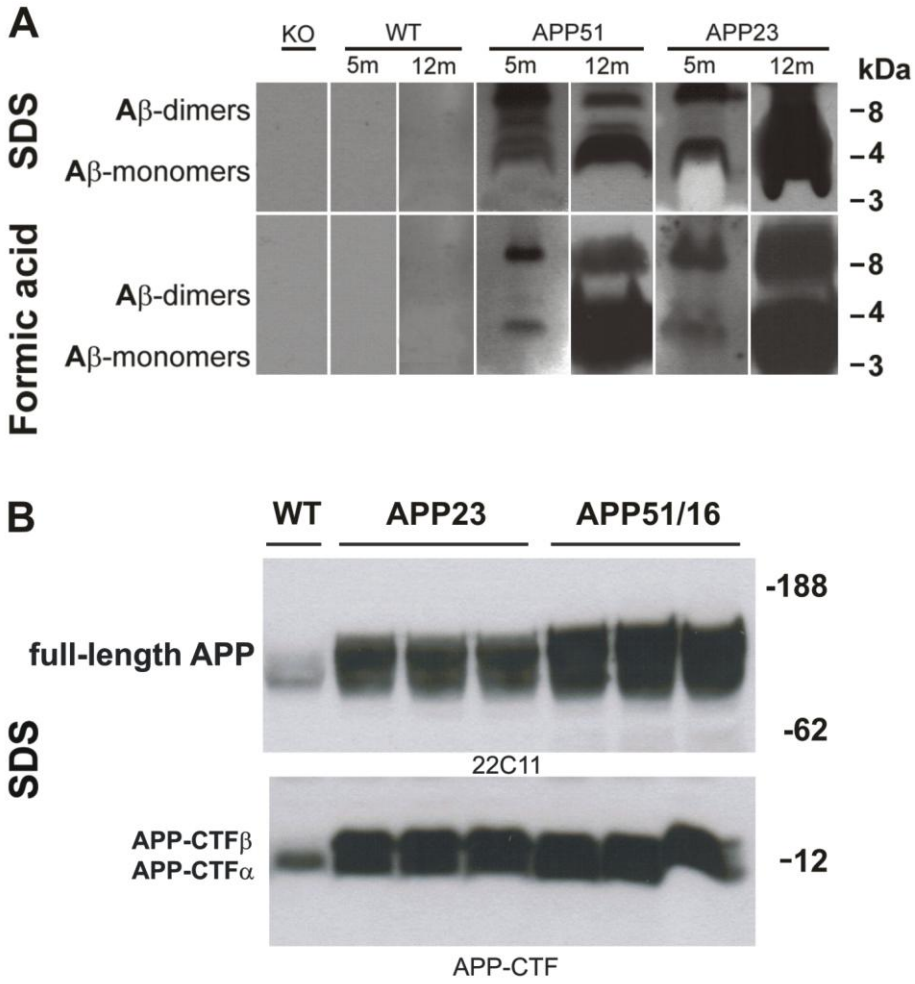

Figure 23 Denaturing western blot analysis of the sodium dodecyl sulphate (SDS) solube (membrane-associated) and formic acid soluble (plaque-associated) fraction. **A**: With anti- amyloid beta 1-17($A\beta_{1-17}$) (6E10) detected no 4 and 8 kDa bands in 5- and 12-month-old wild-type mice and in APP-KO mice. In 5- and 12-month-old APP23 and APP51/16 mice Aβ monomer and dimer bands were detected in the SDS and formic acid fraction with stronger intesities in APP23 mice indicating that these animals contained higher levels of these proteins than APP51/16 mice and that the amount of membrane-associated Aβ increases with age in both APP-trangenic mouse lines. **B**: Expression of APP, and the C-terminal fragments of 12-month-old APP (APP-CTF) in APP23, APP51/16, and wild-type mice in the membrane-associated SDS fraction. Full-length APP detectable with the 22C11 antibody against an N-terminal epitope of APP was overexpressed in APP23 and APP51/16 compared to wild-type mice. APP-CTFα and APP-CTFβ were both overexpressed in APP23 and APP51/16 mice as well. Reproduced from (Rijal Upadhaya et al., accepted for publication-b).

Immunoprecipitation of human brain lysates with B10AP, and A11 and subsequent western blot analysis (Fig. 24) revealed similar pattern as observed in APP23 and APP51/16 mice (Fig. 22). Highest amounts of Aβ aggregates and most prominent monomer bands of SDS-induced denaturation of protofibrils/fibrils (Fig. 24A) and oligomers (Fig. 24B) were seen in AD cases. ADRP cases also exhibited lower levels of these aggregates showing no significant differences in the spectrum of aggregates precipitated. Because of SDS-denaturation the Aβ monomer band distinguishes Aβ-concentrations between AD, ADRP, and control cases. Quantification (Fig. 24 C)

confirmed higher levels of Aβ precipitated with B10AP and A11 in AD cases than in ADRP and control cases (one way ANOVA with Games-Howell post-hoc test: p = 0.004).

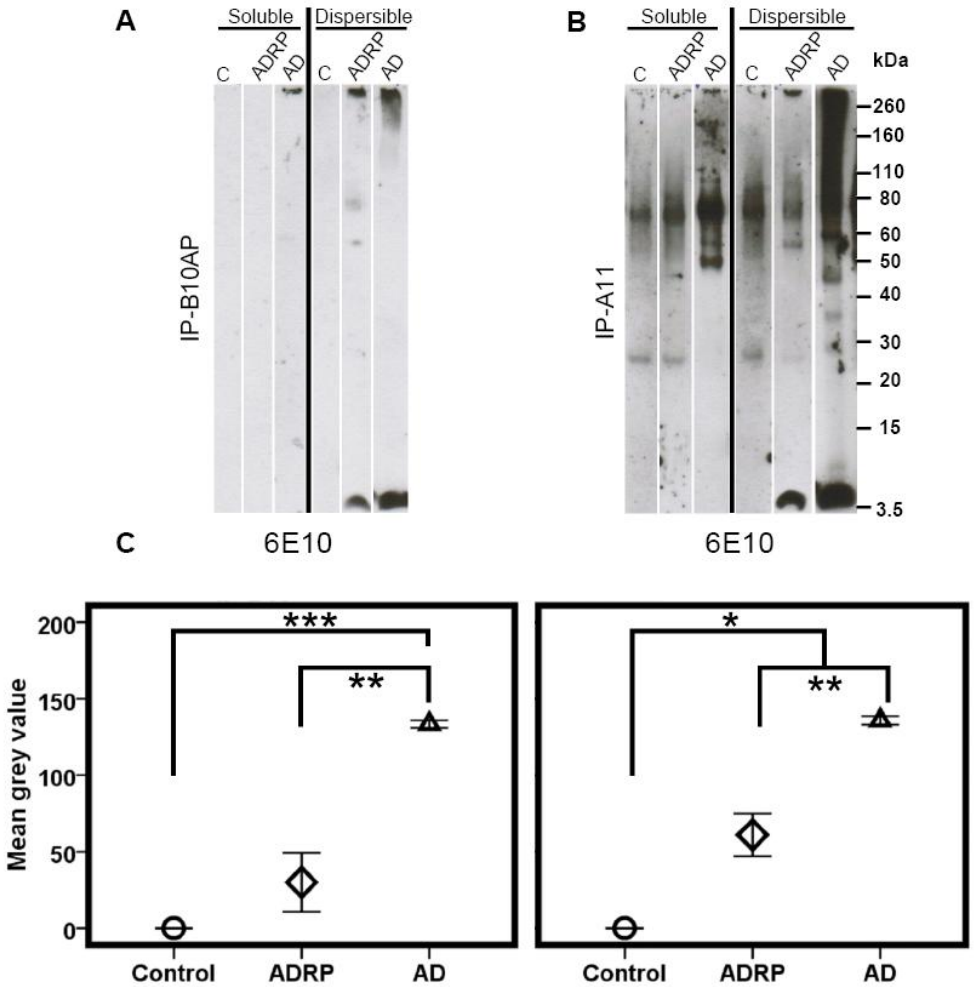

Figure 24 Immunoprecipitation (IP) of soluble and dispersible fraction of human brain. A: Immunoprecipitation of amyloid beta (Aβ) protofibrils and fibrils (with B10AP antibodies) and Aβ oligomers (with A11 antibodies) **(B)** from the soluble and dispersible fraction of control, Alzheimer's disease related pathology (ADRP) and AD brain lysates. Subsequent denaturing western blotting with anti-$A\beta_{1\text{-}17}$ (6E10) demonstrated the presence of remarkable monomer and dimer bands only in the dispersible fraction of AD and ADRP but not in controls. ADRP cases displayed less intense monomer bands than AD cases. **C:** Quantification of sodium dodecyl sulfate (SDS) denaturable Aβ-positive material precipitated with 6E10, Aβ oligomers precipitated with A11, Aβ protofibrils and fibrils precipitated with B10AP as represented by the resulting monomer bands showed higher amounts of Aβ in AD than in ADRP and control cases. ADRP cases, thereby, exhibited more Aβ oligomers than controls whereas a significant difference in the amounts of B10AP precipitated Aβ protofibrils and fibrils was not observed (one way analysis of variance (ANOVA) with Games-Howell post-hoc test: * p <0.05; ** p < 0.01; ***p < 0.001). See Appendix Tab. 2E for further details.

The major difference between AD and ADRP cases was the content of denaturable Aβ oligomers, protofibrils, and fibrils as precipitated with A11 and B10AP in the dispersible fraction (Fig. 24 A, B). The levels of SDS-denaturable Aβ aggregates precipitated with B10AP, and A11 correlated with Braak-NFT stage, phase of Aβ-deposition in the MTL, CERAD neuritic plaque score, and with the CDR score (Appendix Tab. 3) (Spearman correlation coefficient 7.12 – 9.43; $p \leq 0.004$, Appendix Tab. 2E).

4 Discussion

In this study, I showed that, under native conditions, hiMWAβ-oligomers and protofibrils with a molecular weight >1000 kDa predominate in the dispersible fraction of APP23 mice and in human AD brain homogenates. It is evident from the results presented here that dispersible Aβ oligomers, protofibrils, and fibrils are pathogenetically relevant forms of Aβ aggregates that interact with membrane-associated APP-CTFs and are associated with neurodegeneration in APP23 mice in high concentration. There are quantitative but no qualitative differences in the pattern of dispersible Aβ aggregates between APP23 mice with and APP51/16 mice without neurodegeneration. Likewise, Aβ occurring in the SDS and formic acid fraction showed quantitative but no qualitative differences between APP23 and APP51/16 mice. A potential relevance of these findings for AD was confirmed by similar quantitative differences in dispersible fraction between demented AD cases and non-demented cases with and without AD-related pathology.

After immunoprecipitation with the protofibril and fibril specific antibody fragments, B10AP, as well as with the oligomer specific antibody, A11, these hiMWAβ aggregates readily dissociated in SDS containing buffers into loMW forms, especially into monomers and dimers. Hence, for the purpose of analysis, the monomeric bands were best indicative for the changes in the protein levels of Aβ aggregates (Fig. 17).

4.1 High-molecular weight Aβ-oligomers and protofibrils are the predominant Aβ-species in the native soluble/dispersible protein fraction of the AD brain.

HiMWAβ_{42}-oligomers and protofibrils with a molecular weight >1000 kDa predominated in the soluble fraction of AD brain homogenates when these samples were analyzed under native BN-PAGE conditions. Aβ_{40}-aggregates were not detected following BN-PAGE. Immunoelectron microscopy of immunoprecipitated oligomeric, fibrillar, and protofibrillar proteins confirmed the presence of fibrillar, protofibrillar, and spherical hiMWAβ-aggregates in the soluble/dispersible fraction of AD brain homogenates. These hiMWAβ-aggregates were not seen in controls, whereas analysis of control cases revealed that the A11 and B10AP antibodies/antibody fragments precipitate other proteins of similar morphology, and that only a portion of the precipitated proteins from AD cases were Aβ aggregates. Denaturation of the hiMWAβ-aggregates by SDS resulted in the detection of Aβ monomers, dimers, and hiMWAβ with a molecular weight >160 kDa in SDS-PAGE analysis of AD cases but not in controls. When using immunoprecipitation with anti-Aβ_{1-}

$_{17}$, a smear of loMWAβ and hiMWAβ was consistently seen following SDS-PAGE and subsequent western blot analysis, thus indicating that dimers, trimers, tetramers, and Aβ*56 are not the only Aβ oligomers that can be detected with SDS-PAGE, as shown previously also by other groups (Rosen et al., 2010b; Rosen et al., 2010a). The finding of this study led to the conclusion that, under native conditions, Aβ monomers and loMWAβ aggregates, such as dimers, trimers, and Aβ*56, do not represent the major pool of Aβ-aggregates in the human AD brain. More than likely, loMWAβ aggregates may occur transiently during aggregation or after denaturation of hiMWAβ. The strongest argument in favor of this hypothesis is the finding that hiMWAβ oligomer preparations and Aβ protofibril/fibril preparations of synthetic $Aβ_{42}$ and $Aβ_{40}$ peptides did not exhibit high levels of loMWAβ oligomers after BN-PAGE but did so after SDS-PAGE. Moreover, subsequent to SDS-induced protein denaturation, synthetic hiMWA$β_{40}$ aggregates were no longer seen and synthetic hiMWA$β_{42}$ aggregates were remarkably reduced. A possible argument against the predominance of hiMWAβ in the soluble fraction is that Aβ monomers tend to aggregate in the presence of oligomers (Nguyen et al., 2007) and that this occurs during protein preparation. Nevertheless, in synthetic Aβ preparations with high amounts of aggregated Aβ, a significant monomer band was detected after BN-PAGE. This may indicate that Aβ monomers in the soluble brain lysates remained stable during the process of native protein preparation. As such, it is likely that the hiMWA$β_{42}$ aggregates observed in the native soluble fraction indeed represent the major form of soluble Aβ in the human AD brain.

The finding that $Aβ_{40}$ was detected in AD cases in SDS-PAGE but not in BN-PAGE could be attributable either to a lower resolution of native gels in comparison to that of denaturing gels or to the fact that a potential smear of $Aβ_{40}$ aggregates falls below detectable levels. Presumably, SDS treatment denatures all kinds of $Aβ_{40}$-oligomers and, in so doing, leads to the accumulation of $Aβ_{40}$ monomers in a single band. Thus, a non detectable $Aβ_{40}$ smear in BN-PAGE might be converted into a detectable well-defined band in the SDS-PAGE. This hypothesis is supported by the finding of a detectable hiMWA$β_{40}$ smear in synthetic $Aβ_{40}$ preparation that disappeared after SDS treatment and converted into strongly stained monomer and loMWAβ oligomer bands. In BN-PAGE, the spectrum of synthetic hiMWA$β_{40}$ oligomers was greater (>240 kDa) than that of synthetic hiMWA$β_{42}$ oligomers (>700 kDa). This suggests that the concentrations of distinct hiMWA$β_{40}$ oligomers are lower than those of distinct hiMWA$β_{42}$-oligomers owing to the more widespread distribution of hiMWA$β_{40}$ aggregates in the gel. As a result, hiMWA$β_{40}$-

oligomers may be less easily detected in native brain lysates. An alternative explanation, on the other hand, could be that $A\beta_{40}$ interacts with other proteins that hide its C-terminus. In addition, the predominance of hiMWAβ_{42} in the native soluble fraction of the AD brains investigated here confirmed previous reports of a predominant occurrence of $A\beta_{42}$ in parenchymal soluble and insoluble Aβ-aggregates in AD (Roher et al., 1993; Murphy et al., 2007).

At first, the results reported here appear to contradict the findings of other authors, who argue that distinct loMWAβ oligomers, such as dimers and Aβ*56, are critical for the development of AD (Lesne et al., 2006; Shankar et al., 2008; Reed et al., 2009). These authors provide evidence that loMWAβ oligomer preparations received by size-exclusion chromatography are detectable in human as well as transgenic mouse brains, and are capable of inducing cognitive deficits in the rat (Lesne et al., 2006) or altering long-term potentiation (Shankar et al., 2008). Given in vitro and in vivo findings of this study, however, one could also speculate that small amounts of loMWAβ oligomers (possibly resulting from the denaturation of hiMWAβ oligomers, protofibrils, and fibrils) either are critical for the development of AD or that, upon their administration, loMWAβ oligomers may spontaneously aggregate and form hiMWAβ oligomers, as appears to be the case based upon our native gel analysis of $A\beta_{40}$ and $A\beta_{42}$ preparations and the results of Nguyen et al. (Nguyen et al., 2007), who showed that Aβ oligomers accommodate added Aβ monomers. Thus, hiMWAβ aggregates contribute to the pathogenesis of AD either on its own or do so indirectly by providing the reservoir of hiMWAβ aggregates that denature and, in so doing, release loMWAβ oligomers.

That Aβ aggregates, including Aβ plaques, dissociate during the pathogenesis of AD is corroborated by the finding that in late-stage AD cases, plaque frequency is lower than in earlier stages (Thal et al., 1998). The relevance of soluble hiMWAβ for the pathogenesis of AD may be further supported by the finding of neuritic degeneration near Aβ plaques, i.e., in areas with high levels of hiMWAβ presumably dissolved from Aβ plaques, in the amyloid precursor protein (APP) transgenic mouse brain (Tsai et al., 2004; Spires et al., 2005; Meyer-Luehmann et al., 2008), in aged rhesus monkeys (Shah et al., 2010) and in the AD brain (Serrano-Pozo et al., 2010), and also by the finding that dendritic degeneration in another APP-transgenic mouse model begins at the same time as the deposition of initial diffuse Aβ plaques, i.e., when hiMWAβ aggregates begin to predominate in the cortex (Capetillo-Zarate et al., 2006).

Here, the stability of hiMWAβ_{42} aggregates was greater than that of Aβ_{40} aggregates in *in vitro* experiments, thus confirming previous reports that soluble Aβ_{42} aggregates are more stable than Aβ_{40} aggregates (Levine, 1995; Lambert et al., 1998). Taken together with the finding that hiMWAβ_{42} aggregates predominate in the native soluble fraction of the brain, it may be speculated that it is the stability of soluble Aβ_{42}-aggregates in the soluble compartment of the brain that accounts for its predominance in parenchymal Aβ plaque deposition (Roher et al., 1993).

As such, it can also be argued that hiMWAβ oligomers, protofibrils, and fibrils are the predominant soluble Aβ aggregates in the AD brain. LoMWAβ oligomers in high concentrations are detectable only after denaturation of hiMWAβ aggregates. In view of the denaturation of hiMWAβ aggregates and fibrils into loMWAβ oligomers, I propose that Aβ plaques consisting of both fibrillar Aβ as well as soluble hiMWAβ aggregates may serve as reservoirs for the release of loMWAβ oligomers.

4.2 Dispersible, SDS-denaturable high-molecular weight Aβ aggregates are associated with dendritic degeneration in amyloid precursor protein transgenic mouse models and with Alzheimer's disease

Here I showed that dispersible Aβ oligomers, protofibrils and fibrils are pathogenetically relevant forms of Aβ aggregates that interact with membrane-associated APP-CTFs and are associated with neurodegeneration in APP23 mice in high concentration. Dispersible, diffusible non-soluble Aβ aggregates are different from insoluble, plaque-associated Aβ aggregates that become soluble only after formic acid treatment and from membrane-associated Aβ usually seen in the SDS-fraction. In contrast to plaque-associated and membrane-associated Aβ, dispersible Aβ is considered to represent Aβ aggregates in mixture with the extra- or intracellular fluid that are not fully dissolved but dispersed. They can be separated from soluble Aβ by ultracentrifugation. Thus, for the preparation of the soluble and dispersible fractions, in contrast to other authors, brain lysates were centrifuged first at 14.000 x g to separate dispersible and soluble Aβ from cells, microsomes, synaptosomes, and plaque-associated material (Sanchez-Varo et al., 2011). In a second step the soluble portion was separated from the dispersible fraction by ultracentrifuging at 175.000 x g (Roher et al., 1996; Lue et al., 1999; McLean et al., 1999) (Fig. 6). Centrifugation at 100.000 x g and more clears high-molecular weight proteins and dispersed protein aggregates from supernatant and excludes these dispersed proteins from the soluble fraction (Alumot, et al., 1971, Robinson, et al., 1938, Svedberg, 1966). Given the detection of hiMWAβ aggregates in the dispersible fraction, I think it is very likely that

dispersed Aβ aggregates occur in the extracellular and intracellular fluid. Dispersible, non-soluble Aβ aggregates differ from insoluble, plaque-associated Aβ aggregates that become soluble only after formic acid treatment and from membrane-associated Aβ usually seen in the SDS-fraction.

The second major finding of this study pertains to quantitative differences in dispersible Aβ aggregates between APP transgenic mouse models with and without neurodegeneration. The high amount of dispersible Aβ oligomers, protofibrils and fibrils found in APP23 mice seems to explain neurodegeneration. Qualitative changes in the composition of distinct Aβ oligomers, protofibrils, and fibrils have not been observed. Similarly, Aβ occurring in the SDS and formic acid fraction showed quantitative but not qualitative differences between APP23 and APP51/16 mice. Dispersible hiMWAβ aggregates (B10AP-precipitated protofibrils and fibrils and A11-precipitated oligomers) that readily dissociated under denaturing conditions, thereby, appeared to be most critical for neurodegeneration in APP23 mice.

That soluble Aβ aggregates alter dendrites in APP transgenic mice (Bittner, et al., 2010, Capetillo-Zarate, et al., 2006, Spires, et al., 2005, Tsai, et al., 2004, Wu, et al., 2004) and that they interact with N-methyl-D-aspartate (NMDA) receptors has already been shown (Decker, et al., 2010, Lacor, et al., 2004, Li, et al., 2011, Shankar, et al., 2007, Shankar, et al., 2008 Wang, et al., 2002). The presence of Aβ in degenerating dendrites in mouse, as shown here, may reflect the interaction of Aβ aggregates with the dendrites as well as the uptake of Aβ into the dendrites. Since fibrillar or protofibrillar Aβ within the dendrites was not observed at the electron microscopic level, it can be speculated that the critical interaction between the dendritic membrane and Aβ aggregates is restricted to oligomers. This interpretation supports the finding of Shankar et al. (Shankar, et al., 2008) that especially loMWAβ oligomers interact with dendrites and, thereby, may represent immediately toxic forms of Aβ. Since hiMWAβ aggregates predominate in the native soluble fraction of the human brain it is likely that dissociation of hiMWAβ into loMWAβ oligomers plays an important role in Aβ-induced neurotoxicity. However, the A11- and B10AP-precipitated dispersible Aβ oligomers, protofibrils, and fibrils contained APP-CTFs. A possible explanation for this finding is the interaction of Aβ oligomers, protofibrils, and fibrils with membrane-associated APP-CTFs. Such an interaction might result in a mechanical alteration of neighboring receptors and membrane domains by hiMWAβ aggregates finally leading to dendrite degeneration. Alterntively, the uptake and endosomal/lysosomal degradation of dispersible Aβ aggregates could account for the

presence of non-fibrillar Aβ aggregates in degenerating dendrites observable by immunoelectron microscopy. Such an interaction of hiMWAβ with membrane proteins is supported by the occurrence of other membrane-associated proteins, such as the β-subunit of the $\alpha_2$macroglobulin receptor/low density lipoprotein receptor-related protein (LRP1), in plaque cores (Thal, et al., 1997). Another alternative is that APP-CTFs might simply represent membrane particles that contaminated the dispersible fraction after homogenizing the brain. However, to prevent accidental detection of such contaminations, immunoprecipitation of oligomers, protofibrils, and fibrils was performed before biochemical analysis. In so doing, membrane proteins were excluded from analysis when they were not components of oligomeric, protofibrillar, or fibrillar aggregates. Therefore, it appears very likely that there are critical interactions between dispersible Aβ aggregates and APP-CTFs in the cell membrane.

5-month-old APP23 mice were compared with 11-12-month-old APP51/16 mice to exclude Aβ plaque pathology, total Aβ content, $A\beta_{1-42}/A\beta_{1-40}$ ratio, CAA, occurence of protofibrils and fibrils in the brain, and APP expression as potential causes for neurodegeneration in APP23 mice. In contrast to 3-month-old APP23 mice, 5-month-old APP23 mice exhibited degeneration of type 1 commissural neurons (Capetillo-Zarate, et al., 2006) but had similar amounts of plaques and total Aβ as 11-12-month-old APP51/16 animals that did not exhibit such a degeneration of type 1 commissural neurons. CAA was absent in 5-month-old APP23 mice. The $A\beta_{1-42}/A\beta_{1-40}$-ratio, detected by ELISA did not show notable differences when comparing APP23 with APP51/16 mice. B10AP-positive plaques were observed in 5-month-old APP23 mice and in 15-month-old APP51/16 mice without signs of neurodegeneration. In so doing, neither the amount of Aβ plaques nor total Aβ levels nor CAA nor the $A\beta_{1-42}/A\beta_{1-40}$-ratio nor the presence of Aβ protofibrils or fibrils explained neurodegeneration in APP23 but not in APP51/16 mice.

Despite differences in the predominance of α- and β-secretase cleaved APP fragments, APP23 and APP51/16 mice overexpress APP and produce increased amounts of APP-CTFα and APP-CTFβ in comparison to wild-type mice. As such, the expression of APP and its C- and N-terminal fragments alone did not explain the presence of dendritic degeneration in APP23 mice in contrast to APP51/16 mice. Moreover, neurodegeneration in the AD cases takes place in the absence of increased APP, APP-CTFα, and APP-CTFβ levels as reported earlier (Neve, et al., 1988).

Thus, the parameter that best distinguished 5-month-old APP23 mice with neurodegeneration from 11-12-month-old APP51/16 mice without neuronal alterations was

the amount of dispersible Aβ oligomers, protofibrils, and fibrils that dissociated after immunoprecipitation in the SDS-gel into monomers. Therefore, it is indeed likely that the concentration of dispersible Aβ oligomers, protofibrils, and fibrils plays a much more important role in Aβ toxicity than soluble oligomeric forms. These results further point to a critical interaction between dispersible Aβ oligomers, protofibrils, and fibrils with membrane-associated APP-CTFs presumably involved in the mechanism of Aβ-induced neurodegeneration.

To confirm that the changes found in mice are relevant for the pathogenesis of AD, I determined the levels of soluble and dispersible Aβ-aggregates in human AD, ADRP, and control brains. Higher levels of easily denaturable dispersible Aβ-oligomers, protofibrils, and fibrils, as precipitated with A11 and B10AP in AD cases than those in controls with and without Aβ-plaque pathology indicated that, indeed, the concentration of these Aβ-aggregates was related to neurodegeneration in AD. The important role of increasing concentrations of soluble and dispersible Aβ oligomers, protofibrils, and fibrils was highlighted by the detection of dot-like B10-positive material in the neuropil of all AD cases studied but not in controls without Aβ pathology. The existence of these aggregates correlated in a concentration dependent manner with the anatomical distribution pattern of Aβ plaque pathology as represented by the phase of Aβ-deposition in the MTL, Braak-NFT stages, and CERAD score for neuritic plaques and cognitive decline as represented by the CDR-score as shown here. Thus, Aβ toxicity depends on the concentration of soluble and dispersible, SDS-denaturable hiMWAβ aggregates that exceed a critical threshold when entering the clinically symptomatic phase of AD. Overstepping this threshold is accompanied by an increasing distribution of Aβ plaque and CAA pathology (Thal et al., 2002; Thal et al., 2003). The hypothesis that there are thresholds in Aβ concentration for the induction of neurodegeneration is supported by the selective vulnerability against Aβ and hierarchical affection of distinct types of neurons (Capetillo-Zarate et al., 2006). Thereby, highly susceptible neurons with a highly ramified dendritic tree are the first to exhibit pathology in response to Aβ in APP23 mice, whereas less susceptible ones become inolved later, when higher concentrations of soluble/dispersible Aβ aggregates prevail, as shown for dendritic alterations in layer III commissural neurons in the frontocentral cortex of APP23 mice (Capetillo-Zarate et al., 2006).

4.3 Conclusion and Future perspective

It can be concluded from this study that there are no specific Aβ aggregates that distinguish AD or dendritic degeneration in APP23 mice from non-AD cases or mice without neurodegeneration, i.e, APP51/16 mice. However, dispersible, SDS-denaturable Aβ oligomers, protofibrils, and fibrils appear to contribute to AD-related dendrite and synapse degeneration in a concentration dependent manner. Dispersible Aβ aggregates are thereby found in the TBS-soluble homogenates from the brain along with smaller soluble oligomers. Dispersible Aβ aggregates are separated bio-physically from soluble oligomers by high-speed ultracentrifugation and are very likely to occur in mixture with the extracellular or intracellular fluid of the brain.

Under physiological conditions the generation of dispersible and soluble Aβ aggregates in the brain is presumably influenced by pH and metal ion concentrations that effect protein stability. For example, I found that under native conditions TBS-soluble protein lysates consist of large amounts of hiMW Aβ aggregates. These hiMWAβ aggregates readily dissociated into smaller loMWAβ oligomers under denaturing conditions as shown here *in vitro.* In the light of my finding that only Aβ oligomers but not protofibrils and fibrils occur in degenerating dendrites it is tempting to speculate that loMWAβ oligomers might be the immediate toxic Aβ species after release from dispersible Aβ. Another possible mechanism for the toxicity of dispersible Aβ aggregates is the interaction with membrane-associated APP-CTFs presumably involved in the mechanism of Aβ-induced neurodegeneration.

On the basis of these results I want to further clarify the toxicity mechanism of dispersible Aβ oligomers, protofibrils and fibrils. The association of membrane-associated APP-CTFs with dispersible Aβ oligomers, protofibrils and fibrils presumably indicates an interaction between Aβ aggregates and the plasma membrane and may interfere with the complex system of receptor and/or channel proteins and downstream signalling pathways that are required for synaptic plasticity. Thus, it is important to further clarify specific receptors and oligomers binding interactions in selectively vulnerable neurons leading to a wide range of adverse signalling effects. An elevated level of metal ions, particularly zinc and copper has been found in and around the Aβ plaques (Lovell et al., 1998). This clearly means dyshomeostasis and miscompartmentalization of these ions in the brain. These ions are believed to modulate Aβ aggregation (Bush et al., 1994; Atwood et al., 1998). Hence a potential therapeutic approach that blocks such interactions modulating the spectrum of Aβ

aggregates would be predicted to be beneficial in delaying, preventing, or treating AD. As such I plan to further investigate Aβ aggregation properties *in vitro* and its relation to metal ions and interacting proteins *in vitro* and *in vivo*.

5 Summary

Soluble amyloid β-protein (Aβ) aggregates have been identified in Alzheimer's disease (AD) brain. The role of dispersed Aβ aggregates in the brain parenchyma has not been studied carefully until today. To address the roles of soluble and dispersible Aβ aggregates for neurodegeneration we analyzed two different amyloid precursor protein (APP)-transgenic mouse models. APP23 mice overexpress human mutant APP with the Swedish mutation. APP51/16 mice express high levels of human wild-type APP. Both mice develop Aβ plaques. Dendritic degeneration, neuron loss, and loss of asymmetric synapses were seen in APP23 but not in APP51/16 mice. High levels of high-molecular weight Aβ-oligomers, protofibrils, and fibrils (hiMWAβ) were observed in the dispersible fraction of forebrain lysates from APP23 and APP51/16 mice as well as in human AD brains. The soluble/dispersible fraction was, thereby, received after centrifugation of native forebrain homogenates at 14.000 x g. Subsequent high-speed ultracentrifugation of this fraction separated the soluble, i.e. the supernatant, from the dispersible fraction, i.e. the resuspended pellet. The major difference between APP23 and APP51/16 mice was that APP23 mice exhibited higher levels of SDS-denaturable dispersible Aβ oligomers, protofibrils and fibrils precipitated with oligomer (A11) and protofibril/ fibril (B10AP) specific antibodies than APP51/16 mice. Dispersible Aβ oligomers, protofibrils, and fibrils were found associated with APP-C-terminal fragments (APP-CTFs).

A potential relevance of these findings for AD was confirmed by similar quantitative differences between AD cases and non-demented cases with Aβ pathology. HiMWAβ_{42}-oligomers and protofibrils with a molecular weight >1000 kDa predominated in the soluble fraction of AD brain homogenates when these samples were analyzed under native BN-PAGE conditions. Denaturation of the hiMWAβ-aggregates by SDS resulted in the detection of Aβ monomers, dimers, and hiMWAβ with a molecular weight >160 kDa in SDS-PAGE analysis of AD cases but not in controls. Hence, under native conditions Aβ monomers and loMWAβ, such as, dimers and trimers, do not represent the major pool of Aβ aggregates in the human AD brain. These loMWAβ may occur transiently during aggregation or after dissociation of hiMWAβ. This result was further confirmed by synthetic Aβ preparations which did not exhibit hight levels of loMWAB oligomers after BN-PAGE but did so after SDS-PAGE. Likewise, AD cases exhibited higher brain levels of denaturable, soluble hiMWAβ aggregates than controls with and without Aβ plaques.

This strongly indicates that the hiMWAβ_{42} aggregates observed in the native soluble fraction indeed represent the major form of soluble Aβ in the human AD brain.

In conclusion, hiMWAβ aggregates prevail in the native human AD brain and dispersible Aβ oligomers, protofibrils, and fibrils, represent an important pool of Aβ aggregates in the brain that interact with membrane-associated APP-CTFs. Thus, the concentration of dispersible SDS-denaturable Aβ oligomers, protofibrils, and fibrils is related to its toxicity and distinguishes AD cases from non-demented elderly individuals even if they already exhibit AD-related pathology in the brain as well as APP-transgenic mouse lines with and without signs of dendritic degeneration.

6 References

1. Arnaiz E, Almkvist O (2003) Neuropsychological features of mild cognitive impairment and preclinical Alzheimer's disease. Acta Neurol Scand Suppl 179:34-41.
2. Atwood CS, Moir RD, Huang X, Scarpa RC, Bacarra NM, Romano DM, Hartshorn MA, Tanzi RE, Bush AI (1998) Dramatic aggregation of Alzheimer abeta by Cu(II) is induced by conditions representing physiological acidosis. J Biol Chem 273:12817-12826.
3. Bancher C, Brunner C, Lassmann H, Budka H, Jellinger K, Wiche G, Seitelberger F, Grundke-Iqbal I, Iqbal K, Wisniewski HM (1989) Accumulation of abnormally phosphorylated tau precedes the formation of neurofibrillary tangles in Alzheimer's disease. Brain Res 477:90-99.
4. Bennhold H (1992) Eine spezifische amyloidfärbung mit Kongorot [Specific staining of amyloid with Congo red]. Münch MedWochenschr:1537–1538.
5. Billings LM, Oddo S, Green KN, McGaugh JL, Laferla FM (2005) Intraneuronal abeta causes the onset of early Alzheimer's disease-related cognitive deficits in transgenic mice. Neuron 45:675-688.
6. Blennow K, de Leon MJ, Zetterberg H (2006) Alzheimer's disease. Lancet 368:387-403.
7. Braak H, Braak E (1991) Neuropathological stageing of Alzheimer-related changes. Acta Neuropathol 82:239-259.
8. Braak H, Braak E, Ohm T, Bohl J (1989) Alzheimer's disease: mismatch between amyloid plaques and neuritic plaques. Neurosci Lett 103:24-28.

9. Brookmeyer R, Gray S, Kawas C (1998) Projections of Alzheimer's disease in the United States and the public health impact of delaying disease onset. Am J Public Health 88:1337-1342.

10. Bush AI, Pettingell WH, Multhaup G, d Paradis M, Vonsattel JP, Gusella JF, Beyreuther K, Masters CL, Tanzi RE (1994) Rapid induction of Alzheimer A beta amyloid formation by zinc. Science 265:1464-1467.

11. Calhoun ME, Wiederhold KH, Abramowski D, Phinney AL, Probst A, Sturchler-Pierrat C, Staufenbiel M, Sommer B, Jucker M (1998) Neuron loss in APP transgenic mice. Nature 395:755-756.

12. Calhoun ME, Burgermeister P, Phinney AL, Stalder M, Tolnay M, Wiederhold KH, Abramowski D, Sturchler-Pierrat C, Sommer B, Staufenbiel M, Jucker M (1999) Neuronal overexpression of mutant amyloid precursor protein results in prominent deposition of cerebrovascular amyloid. Proc Natl Acad Sci U S A 96:14088-14093.

13. Capetillo-Zarate E, Staufenbiel M, Abramowski D, Haass C, Escher A, Stadelmann C, Yamaguchi H, Wiestler OD, Thal DR (2006) Selective vulnerability of different types of commissural neurons for amyloid beta-protein induced neurodegeneration in APP23 mice correlates with dendritic tree morphology. Brain 129:2992-3005.

14. Casas C, Sergeant N, Itier JM, Blanchard V, Wirths O, van der Kolk N, Vingtdeux V, van de Steeg E, Ret G, Canton T, Drobecq H, Clark A, Bonici B, Delacourte A, Benavides J, Schmitz C, Tremp G, Bayer TA, Benoit P, Pradier L (2004) Massive CA1/2 neuronal loss with intraneuronal and N-terminal truncated Abeta42 accumulation in a novel Alzheimer transgenic model. Am J Pathol 165:1289-1300.

15. Davidoff LM (1928) The Brain in mongolian idiocy: A report of ten cases. Arch Neurol Psychiatry 20:1229-1257.

16. De Strooper B (2007) Loss-of-function presenilin mutations in Alzheimer disease. Talking Point on the role of presenilin mutations in Alzheimer disease. EMBO Rep 8:141-146.

17. Duff K, Eckman C, Zehr C, Yu X, Prada CM, Perez-tur J, Hutton M, Buee L, Harigaya Y, Yager D, Morgan D, Gordon MN, Holcomb L, Refolo L, Zenk B, Hardy J, Younkin S (1996) Increased amyloid-beta42(43) in brains of mice expressing mutant presenilin 1. Nature 383:710-713.

18. Duyckaerts C, Dickson DW (2003) Neuropathology of Alzheimer's disease. In: Neurodegeneration: The molecular pathology of dementia and movement disorders (Dickson D, ed), pp 47-65. Basel: ISN Neuropath Press.

19. Games D, Adams D, Alessandrini R, Barbour R, Berthelette P, Blackwell C, Carr T, Clemens J, Donaldson T, Gillespie F, et al. (1995) Alzheimer-type neuropathology in transgenic mice overexpressing V717F beta-amyloid precursor protein. Nature 373:523-527.

20. Geula C, Nagykery N, Nicholas A, Wu CK (2008) Cholinergic neuronal and axonal abnormalities are present early in aging and in Alzheimer disease. J Neuropathol Exp Neurol 67:309-318.

21. Glenner GG (1980) Amyloid deposits and amyloidosis. The beta-fibrilloses (first of two parts). N Engl J Med 302:1283-1292.

22. Glenner GG, Wong CW (1984) Alzheimer's disease: initial report of the purification and characterization of a novel cerebrovascular amyloid protein. Biochem Biophys Res Commun 120:885-890.

23. Glenner GG, Terry WD, Isersky C (1973) Amyloidosis: its nature and pathogenesis. Semin Hematol 10:65-86.

24. Haass C, Schlossmacher MG, Hung AY, Vigo-Pelfrey C, Mellon A, Ostaszewski BL, Lieberburg I, Koo EH, Schenk D, Teplow DB, Selkoe DJ (1992) Amyloid

beta-peptide is produced by cultured cells during normal metabolism. Nature 359:322-325.

25. Habicht G, Haupt C, Friedrich RP, Hortschansky P, Sachse C, Meinhardt J, Wieligmann K, Gellermann GP, Brodhun M, Gotz J, Halbhuber KJ, Rocken C, Horn U, Fandrich M (2007) Directed selection of a conformational antibody domain that prevents mature amyloid fibril formation by stabilizing Abeta protofibrils. Proc Natl Acad Sci U S A 104:19232-19237.
26. Hardy J, Selkoe DJ (2002) The amyloid hypothesis of Alzheimer's disease: progress and problems on the road to therapeutics. Science 297:353-356.
27. Harper JD, Lansbury PT, Jr. (1997) Models of amyloid seeding in Alzheimer's disease and scrapie: mechanistic truths and physiological consequences of the time-dependent solubility of amyloid proteins. Annu Rev Biochem 66:385-407.
28. Hartley DM, Walsh DM, Ye CP, Diehl T, Vasquez S, Vassilev PM, Teplow DB, Selkoe DJ (1999) Protofibrillar intermediates of amyloid beta-protein induce acute electrophysiological changes and progressive neurotoxicity in cortical neurons. J Neurosci 19:8876-8884.
29. Hernandez F, Avila J (2007) Tauopathies. Cell Mol Life Sci 64:2219-2233.
30. Herzig MC, Winkler DT, Burgermeister P, Pfeifer M, Kohler E, Schmidt SD, Danner S, Abramowski D, Sturchler-Pierrat C, Burki K, van Duinen SG, Maat-Schieman ML, Staufenbiel M, Mathews PM, Jucker M (2004) Abeta is targeted to the vasculature in a mouse model of hereditary cerebral hemorrhage with amyloidosis. Nat Neurosci 7:954-960.
31. Hsiao K, Chapman P, Nilsen S, Eckman C, Harigaya Y, Younkin S, Yang F, Cole G (1996) Correlative memory deficits, Abeta elevation, and amyloid plaques in transgenic mice. Science 274:99-102.

32. Jarrett JT, Berger EP, Lansbury PT, Jr. (1993) The carboxy terminus of the beta amyloid protein is critical for the seeding of amyloid formation: implications for the pathogenesis of Alzheimer's disease. Biochemistry 32:4693-4697.

33. Kang J, Lemaire HG, Unterbeck A, Salbaum JM, Masters CL, Grzeschik KH, Multhaup G, Beyreuther K, Muller-Hill B (1987) The precursor of Alzheimer's disease amyloid A4 protein resembles a cell-surface receptor. Nature 325:733-736.

34. Kayed R, Head E, Thompson JL, McIntire TM, Milton SC, Cotman CW, Glabe CG (2003) Common structure of soluble amyloid oligomers implies common mechanism of pathogenesis. Science 300:486-489.

35. Kelly JW (1996) Alternative conformations of amyloidogenic proteins govern their behavior. Curr Opin Struct Biol 6:11-17.

36. Kumar S, Walter J (2011) Phosphorylation of amyloid beta (Abeta) peptides - a trigger for formation of toxic aggregates in Alzheimer's disease. Aging (Albany NY) 3:803-812.

37. Lacor PN, Buniel MC, Chang L, Fernandez SJ, Gong Y, Viola KL, Lambert MP, Velasco PT, Bigio EH, Finch CE, Krafft GA, Klein WL (2004) Synaptic targeting by Alzheimer's-related amyloid beta oligomers. J Neurosci 24:10191-10200.

38. Lambert MP, Barlow AK, Chromy BA, Edwards C, Freed R, Liosatos M, Morgan TE, Rozovsky I, Trommer B, Viola KL, Wals P, Zhang C, Finch CE, Krafft GA, Klein WL (1998) Diffusible, nonfibrillar ligands derived from Abeta1-42 are potent central nervous system neurotoxins. Proc Natl Acad Sci U S A 95:6448-6453.

39. Lamy C, Duyckaerts C, Delaere P, Payan C, Fermanian J, Poulain V, Hauw JJ (1989) Comparison of seven staining methods for senile plaques and neurofibrillary tangles in a prospective series of 15 elderly patients. Neuropathol Appl Neurobiol 15:563-578.

40. Lansbury PT, Jr. (1999) Evolution of amyloid: what normal protein folding may tell us about fibrillogenesis and disease. Proc Natl Acad Sci U S A 96:3342-3344.

41. Lejeune J, Turpin R, Gautier M (1959) [Mongolism; a chromosomal disease (trisomy)]. Bull Acad Natl Med 143:256-265.

42. Lesne S, Koh MT, Kotilinek L, Kayed R, Glabe CG, Yang A, Gallagher M, Ashe KH (2006) A specific amyloid-beta protein assembly in the brain impairs memory. Nature 440:352-357.

43. Levine H, 3rd (1995) Soluble multimeric Alzheimer beta(1-40) pre-amyloid complexes in dilute solution. Neurobiol Aging 16:755-764.

44. Lewis J, Dickson DW, Lin WL, Chisholm L, Corral A, Jones G, Yen SH, Sahara N, Skipper L, Yager D, Eckman C, Hardy J, Hutton M, McGowan E (2001) Enhanced neurofibrillary degeneration in transgenic mice expressing mutant tau and APP. Science 293:1487-1491.

45. Lovell MA, Robertson JD, Teesdale WJ, Campbell JL, Markesbery WR (1998) Copper, iron and zinc in Alzheimer's disease senile plaques. J Neurol Sci 158:47-52.

46. Lue LF, Kuo YM, Roher AE, Brachova L, Shen Y, Sue L, Beach T, Kurth JH, Rydel RE, Rogers J (1999) Soluble amyloid beta peptide concentration as a predictor of synaptic change in Alzheimer's disease. Am J Pathol 155:853-862.

47. Maat-Schieman ML, van Duinen SG, Bornebroek M, Haan J, Roos RA (1996) Hereditary cerebral hemorrhage with amyloidosis-Dutch type (HCHWA-D): II--A review of histopathological aspects. Brain Pathol 6:115-120.

48. Mandelkow EM, Mandelkow E (1998) Tau in Alzheimer's disease. Trends Cell Biol 8:425-427.

49. Masters CL, Beyreuther K (2003) Molecular Pathogenesis of Alzheimer's disease. In: Neurodegeneration: The Molecular Pathology of Dementia and Movement Disorders (Dickson D, ed), pp 69-73. Basel: ISN Neuropath Press.

50. Masters CL, Multhaup G, Simms G, Pottgiesser J, Martins RN, Beyreuther K (1985) Neuronal origin of a cerebral amyloid: neurofibrillary tangles of Alzheimer's disease contain the same protein as the amyloid of plaque cores and blood vessels. Embo J 4:2757-2763.

51. McLean CA, Cherny RA, Fraser FW, Fuller SJ, Smith MJ, Beyreuther K, Bush AI, Masters CL (1999) Soluble pool of Abeta amyloid as a determinant of severity of neurodegeneration in Alzheimer's disease. Ann Neurol 46:860-866.

52. Meyer-Luehmann M, Spires-Jones TL, Prada C, Garcia-Alloza M, de Calignon A, Rozkalne A, Koenigsknecht-Talboo J, Holtzman DM, Bacskai BJ, Hyman BT (2008) Rapid appearance and local toxicity of amyloid-beta plaques in a mouse model of Alzheimer's disease. Nature 451:720-724.

53. Meyer-Luehmann M, Coomaraswamy J, Bolmont T, Kaeser S, Schaefer C, Kilger E, Neuenschwander A, Abramowski D, Frey P, Jaton AL, Vigouret JM, Paganetti P, Walsh DM, Mathews PM, Ghiso J, Staufenbiel M, Walker LC, Jucker M (2006) Exogenous induction of cerebral beta-amyloidogenesis is governed by agent and host. Science 313:1781-1784.

54. Moechars D, Dewachter I, Lorent K, Reverse D, Baekelandt V, Naidu A, Tesseur I, Spittaels K, Haute CV, Checler F, Godaux E, Cordell B, Van Leuven F (1999) Early phenotypic changes in transgenic mice that overexpress different mutants of amyloid precursor protein in brain. J Biol Chem 274:6483-6492.

55. Morrison JH, Hof PR (1997) Life and death of neurons in the aging brain. Science 278:412-419.

56. Mouton PR, Martin LJ, Calhoun ME, Dal Forno G, Price DL (1998) Cognitive decline strongly correlates with cortical atrophy in Alzheimer's dementia. Neurobiol Aging 19:371-377.

57. Nguyen PH, Li MS, Stock G, Straub JE, Thirumalai D (2007) Monomer adds to preformed structured oligomers of Abeta-peptides by a two-stage dock-lock mechanism. Proc Natl Acad Sci U S A 104:111-116.

58. Ni CL, Shi HP, Yu HM, Chang YC, Chen YR (2011) Folding stability of amyloid-beta 40 monomer is an important determinant of the nucleation kinetics in fibrillization. FASEB J 25:1390-1401.

59. Oakley H, Cole SL, Logan S, Maus E, Shao P, Craft J, Guillozet-Bongaarts A, Ohno M, Disterhoft J, Van Eldik L, Berry R, Vassar R (2006) Intraneuronal beta-amyloid aggregates, neurodegeneration, and neuron loss in transgenic mice with five familial Alzheimer's disease mutations: potential factors in amyloid plaque formation. J Neurosci 26:10129-10140.

60. Oddo S, Billings L, Kesslak JP, Cribbs DH, LaFerla FM (2004) Abeta immunotherapy leads to clearance of early, but not late, hyperphosphorylated tau aggregates via the proteasome. Neuron 43:321-332.

61. Oddo S, Caccamo A, Shepherd JD, Murphy MP, Golde TE, Kayed R, Metherate R, Mattson MP, Akbari Y, LaFerla FM (2003) Triple-transgenic model of Alzheimer's disease with plaques and tangles: intracellular Abeta and synaptic dysfunction. Neuron 39:409-421.

62. Perez M, Moran MA, Ferrer I, Avila J, Gomez-Ramos P (2008) Phosphorylated tau in neuritic plaques of APP(sw)/Tau (vlw) transgenic mice and Alzheimer disease. Acta Neuropathol 116:409-418.

63. Petersen RC, Doody R, Kurz A, Mohs RC, Morris JC, Rabins PV, Ritchie K, Rossor M, Thal L, Winblad B (2001) Current concepts in mild cognitive impairment. Arch Neurol 58:1985-1992.

64. Plassman BL, Havlik RJ, Steffens DC, Helms MJ, Newman TN, Drosdick D, Phillips C, Gau BA, Welsh-Bohmer KA, Burke JR, Guralnik JM, Breitner JC (2000) Documented head injury in early adulthood and risk of Alzheimer's disease and other dementias. Neurology 55:1158-1166.

65. Reed MN, Hofmeister JJ, Jungbauer L, Welzel AT, Yu C, Sherman MA, Lesne S, Ladu MJ, Walsh DM, Ashe KH, Cleary JP (2009) Cognitive effects of cell-derived and synthetically derived Abeta oligomers. Neurobiol Aging:doi:10.1016/j.neurobiolaging.2009.1011.1007.

66. Rijal Upadhaya A, Lungrin I, Yamaguchi H, Fändrich M, Thal DR (accepted for publication-a) High-molecular weight Aβ-oligomers and protofibrils are the predominant Aβ-species in the native soluble protein fraction of the AD brain. J Cell Mol Med. doi:10.1111/j.1582-4934.2011.01306.x.

67. Rijal Upadhaya A, Capetillo-Zarate E, Kosterin I, Abramowski D, Kumar S, Yamaguchi H, Walter J, Fändrich M, Staufenbiel M, Thal DR (accepted for publication-b) Dispersible amyloid β-protein oligomers, protofibrils, and fibrils represent diffusible but not soluble aggregates: Their role in neurodegeneration in amyloid precursor protein (APP) transgenic mice. Neurobiology of Aging.

68. Roher AE, Lowenson JD, Clarke S, Woods AS, Cotter RJ, Gowing E, Ball MJ (1993) beta-Amyloid-(1-42) is a major component of cerebrovascular amyloid deposits: implications for the pathology of Alzheimer disease. Proc Natl Acad Sci U S A 90:10836-10840.

69. Roher AE, Chaney MO, Kuo YM, Webster SD, Stine WB, Haverkamp LJ, Woods AS, Cotter RJ, Tuohy JM, Krafft GA, Bonnell BS, Emmerling MR (1996)

Morphology and toxicity of Abeta-(1-42) dimer derived from neuritic and vascular amyloid deposits of Alzheimer's disease. J Biol Chem 271:20631-20635.

70. Rosen RF, Tomidokoro Y, Ghiso JA, Walker LC (2010a) SDS-PAGE/immunoblot detection of Abeta multimers in human cortical tissue homogenates using antigen-epitope retrieval. J Vis Exp 38:doi: 10.3791/1916.

71. Rosen RF, Ciliax BJ, Wingo TS, Gearing M, Dooyema J, Lah JJ, Ghiso JA, LeVine H, 3rd, Walker LC (2010b) Deficient high-affinity binding of Pittsburgh compound B in a case of Alzheimer's disease. Acta Neuropathol 119:221-233.

72. Roses AD (1996) Apolipoprotein E alleles as risk factors in Alzheimer's disease. Annu Rev Med 47:387-400.

73. Salmon DP, Bondi MW (2009) Neuropsychological assessment of dementia. Annu Rev Psychol 60:257-282.

74. Sanchez-Varo R, Trujillo-Estrada L, Sanchez-Mejias E, Torres M, Baglietto-Vargas D, Moreno-Gonzalez I, De Castro V, Jimenez S, Ruano D, Vizuete M, Davila JC, Garcia-Verdugo JM, Jimenez AJ, Vitorica J, Gutierrez A (2011) Abnormal accumulation of autophagic vesicles correlates with axonal and synaptic pathology in young Alzheimer's mice hippocampus. Acta Neuropathol 123:53-70.

75. Schmitz C, Rutten BP, Pielen A, Schafer S, Wirths O, Tremp G, Czech C, Blanchard V, Multhaup G, Rezaie P, Korr H, Steinbusch HW, Pradier L, Bayer TA (2004) Hippocampal neuron loss exceeds amyloid plaque load in a transgenic mouse model of Alzheimer's disease. Am J Pathol 164:1495-1502.

76. Scholz W (1938) Studien zur Pathologie der Hirngefäße. II. Die drusige Entartung der Hirnarterien und -capillaren. (Eine Form seniler Gefäßerkrankung). Z ges Neurol Psychiatr 4:694-715.

77. Selkoe DJ, Wolfe MS (2007) Presenilin: running with scissors in the membrane. Cell 131:215-221.

78. Serrano-Pozo A, William CM, Ferrer I, Uro-Coste E, Delisle MB, Maurage CA, Hock C, Nitsch RM, Masliah E, Growdon JH, Frosch MP, Hyman BT (2010) Beneficial effect of human anti-amyloid-beta active immunization on neurite morphology and tau pathology. Brain 133:1312-1327.

79. Shah P, Lal N, Leung E, Traul DE, Gonzalo-Ruiz A, Geula C (2010) Neuronal and Axonal Loss Are Selectively Linked to Fibrillar Amyloid-{beta} within Plaques of the Aged Primate Cerebral Cortex. Am J Pathol 177:325-333.

80. Shankar GM, Li S, Mehta TH, Garcia-Munoz A, Shepardson NE, Smith I, Brett FM, Farrell MA, Rowan MJ, Lemere CA, Regan CM, Walsh DM, Sabatini BL, Selkoe DJ (2008) Amyloid-beta protein dimers isolated directly from Alzheimer's brains impair synaptic plasticity and memory. Nat Med 14:837-842.

81. Sherrington R, Rogaev EI, Liang Y, Rogaeva EA, Levesque G, Ikeda M, Chi H, Lin C, Li G, Holman K, et al. (1995) Cloning of a gene bearing missense mutations in early-onset familial Alzheimer's disease. Nature 375:754-760.

82. Spires TL, Meyer-Luehmann M, Stern EA, McLean PJ, Skoch J, Nguyen PT, Bacskai BJ, Hyman BT (2005) Dendritic spine abnormalities in amyloid precursor protein transgenic mice demonstrated by gene transfer and intravital multiphoton microscopy. J Neurosci 25:7278-7287.

83. Sturchler-Pierrat C, Abramowski D, Duke M, Wiederhold KH, Mistl C, Rothacher S, Ledermann B, Burki K, Frey P, Paganetti PA, Waridel C, Calhoun ME, Jucker M, Probst A, Staufenbiel M, Sommer B (1997) Two amyloid precursor protein transgenic mouse models with Alzheimer disease-like pathology. Proc Natl Acad Sci U S A 94:13287-13292.

84. Thal DR, Braak H (2005) [Post-mortem diagnosis of Alzheimer's disease.]. Pathologe 26:201-213.

85. Thal DR, Del Tredici K, Braak H (2004) Neurodegeneration in normal brain aging and disease. Sci Aging Knowledge Environ 2004:PE26.

86. Thal DR, Rüb U, Orantes M, Braak H (2002) Phases of Abeta-deposition in the human brain and its relevance for the development of AD. Neurology 58:1791-1800.

87. Thal DR, Ghebremedhin E, Orantes M, Wiestler OD (2003) Vascular pathology in Alzheimer's disease: Correlation of cerebral amyloid angiopathy and arteriosclerosis / lipohyalinosis with cognitive decline. J Neuropathol Exp Neurol 62:1287-1301.

88. Thal DR, Capetillo-Zarate E, Del Tredici K, Braak H (2006) The development of amyloid beta protein deposits in the aged brain. Sci Aging Knowledge Environ 2006:re1.

89. Thal DR, Capetillo-Zarate E, Larionov S, Staufenbiel M, Zurbruegg S, Beckmann N (2009) Capillary cerebral amyloid angiopathy is associated with vessel occlusion and cerebral blood flow disturbances. Neurobiol Aging 30:1936-1948.

90. Thal DR, Arendt T, Waldmann G, Holzer M, Zedlick D, Rüb U, Schober R (1998) Progression of neurofibrillary changes and PHF-tau in end-stage Alzheimer's disease is different from plaque and cortical microglial pathology. Neurobiol Aging 19:517-525.

91. Thal DR, Rüb U, Schultz C, Sassin I, Ghebremedhin E, Del Tredici K, Braak E, Braak H (2000) Sequence of Abeta-protein deposition in the human medial temporal lobe. J Neuropathol Exp Neurol 59:733-748.

92. Thal DR, Papassotiropoulos A, Saido TC, Griffin WS, Mrak RE, Kölsch H, Del Tredici K, Attems J, Ghebremedhin E (2010) Capillary cerebral amyloid angiopathy identifies a distinct APOE epsilon4-associated subtype of sporadic Alzheimer's disease. Acta Neuropathol 120:169-183.

93. Thal DR, Larionov S, Abramowski D, Wiederhold KH, Van Dooren T, Yamaguchi H, Haass C, Van Leuven F, Staufenbiel M, Capetillo-Zarate E (2007) Occurrence and co-localization of amyloid beta-protein and apolipoprotein E in perivascular drainage channels of wild-type and APP-transgenic mice Neurobiol Aging 28:1221-1230.

94. The National Institute on Aging aRIWGoDCftNAoAsD (1997) Consensus recommendations for the postmortem diagnosis of Alzheimer's disease. The National Institute on Aging, and Reagan Institute Working Group on Diagnostic Criteria for the Neuropathological Assessment of Alzheimer's Disease. Neurobiol Aging 18:S1-2.

95. Tsai J, Grutzendler J, Duff K, Gan WB (2004) Fibrillar amyloid deposition leads to local synaptic abnormalities and breakage of neuronal branches. Nat Neurosci 7:1181-1183.

96. Uchihara T, Nakamura A, Yamazaki M, Mori O (2001) Evolution from pretangle neurons to neurofibrillary tangles monitored by thiazin red combined with Gallyas method and double immunofluorescence. Acta Neuropathol 101:535-539.

97. Utter S, Tamboli IY, Walter J, Rijal Upadhaya A, Birkenmeier G, Pietrzik CU, Ghebremedhin E, Thal DR (2008) Cerebral small vessel disease-induced apolipoprotein E leakage is associated with Alzheimer disease and the accumulation of amyloid beta-protein in perivascular astrocytes. J Neuropathol Exp Neurol 67:842-856.

98. Virchow R (1854) Zur Cellulose-Frage. Virchows Arch Path Anat 6:416-426.

99. Virchow R (1855) Über den Gang der amyloiden Degeneration. Virchows Arch Path Anat 8:364-368.

100. Walker LC, Bian F, Callahan MJ, Lipinski WJ, Durham RA, LeVine H (2002) Modeling Alzheimer's disease and other proteopathies in vivo: is seeding the key? Amino Acids 23:87-93.

101. Walsh DM, Lomakin A, Benedek GB, Condron MM, Teplow DB (1997) Amyloid beta-protein fibrillogenesis. Detection of a protofibrillar intermediate. J Biol Chem 272:22364-22372.

102. Wang HW, Pasternak JF, Kuo H, Ristic H, Lambert MP, Chromy B, Viola KL, Klein WL, Stine WB, Krafft GA, Trommer BL (2002) Soluble oligomers of beta amyloid (1-42) inhibit long-term potentiation but not long-term depression in rat dentate gyrus. Brain Res 924:133-140.

103. Weidemann A, Konig G, Bunke D, Fischer P, Salbaum JM, Masters CL, Beyreuther K (1989) Identification, biogenesis, and localization of precursors of Alzheimer's disease A4 amyloid protein. Cell 57:115-126.

104. West MJ (1993) Regionally specific loss of neurons in the aging human hippocampus. Neurobiol Aging 14:287-293.

105. Wild-Bode C, Yamazaki T, Capell A, Leimer U, Steiner H, Ihara Y, Haass C (1997) Intracellular generation and accumulation of amyloid beta-peptide terminating at amino acid 42. J Biol Chem 272:16085-16088.

106. Wirths O, Breyhan H, Cynis H, Schilling S, Demuth HU, Bayer TA (2009) Intraneuronal pyroglutamate-Abeta 3-42 triggers neurodegeneration and lethal neurological deficits in a transgenic mouse model. Acta Neuropathol.

107. Wirths O, Multhaup G, Czech C, Blanchard V, Moussaoui S, Tremp G, Pradier L, Beyreuther K, Bayer TA (2001) Intraneuronal Abeta accumulation precedes plaque formation in beta-amyloid precursor protein and presenilin-1 double-transgenic mice. Neurosci Lett 306:116-120.

108. Yamaguchi H, Sugihara S, Ogawa A, Saido TC, Ihara Y (1998) Diffuse plaques associated with astroglial amyloid beta protein, possibly showing a disappearing stage of senile plaques. Acta Neuropathol (Berl) 95:217-222.

109. Yu G et al. (2000) Nicastrin modulates presenilin-mediated notch/glp-1 signal transduction and betaAPP processing. Nature 407:48-54.

7 Appendix

Table 1 A: Types of commissural neurons in layer III of the frontocentral cortex (Capetillo-Zarate et al., 2006)

Type I commissural neurons:	Pyramidal neurons with a highly ramified dendritic tree showing multiple secondary and tertiary branches
Type II commissural neurons:	Pyramidal neurons with a dendritic tree that branches distant from the cell soma, secondary and tertiary branches are usually not observed in 100µm thick sections
Type III commissural neurons:	Non-pyramidal commissural neurons

Table 2 Statistical analysis. Significant differences are marked in red.

A: Parameters for neurodegeneration in APP23 and APP51/16 mice

DiI-tracing of commissural neurons in frontal cortex: Mann-Whitney U-test (exact test) APP23 and APP51/16 mice were tested in comparison with their specific wild-type littermates, respectively

Age/ months	Mouse line	Type I neurons	Type II neurons	Type III neurons
5	APP23 mice	p = 0.023	p = 0.094	p = 0.944
5	APP51/16 mice	p = 0.833	p = 0.667	p = 0.117
11	APP23 mice	p = 0.004	p = 0.965	p = 0.274
11	APP51/16 mice	p = 0.630	p = 0.376	p = 0.776
15	APP23 mice	p = 0.001	p = 0.004	p = 0.093
15	APP51/16 mice	p = 0.905	p = 0.730	p = 0.111

Total number of CA1 neurons deterimed by unbiazed stereology: ANOVA with Games-Howell post-hoc test to correct for multiple testing
Wild-type mice vs. APP23 mice: $p < 0.001$
Wild-type mice vs. APP51/16 mice: $p = 0.669$

Frequency of dystrophic dendrites at the electron microscopic level: Mann-Whitney U-test with Bonferoni correction for multiple testing (exact test)
Wild-type mice vs. APP23 mice: $p = 0.038$
Wild-type mice vs. APP51/16 mice: $p = 0.819$

Number of synapses: Mann-Whitney U-test with Bonferoni correction for multiple testing (exact test)
Asymmetric Synapses
Wild-type mice vs. APP23 mice: $p = 0.042$
Wild-type mice vs. APP51/16 mice: $p = 0.650$
Symmetric Synapses
Wild-type mice vs. APP23 mice $p = 0.502$
Wild-type mice vs. APP51/16 mice $p = 0.355$

B: Deposition of Aβ, B10AP- and A11-positive aggregates and Aβ-levels in the APP23 and APP51/16 mouse brain

Age-related increase of Aβ-plaque and B10-plaque distribution as represented by the phase of Aβ-deposition in mice (Thal et al., 2006)

	APP23 mice	APP51/16 mice
Aβ-phase: Fischer's exact test/ Trend-test	p < 0.001 / < 0.001	p < 0.001 / < 0.001
B10AP-phase: Fischer's exact test/ Trend-test	p = 0.002 / = 0.008	p = 0.028 / = 0.011

Age-related increase of the Aβ load, the total $Aβ_{1-40}$ and $Aβ_{1-42}$ concentration in the brain as determined by ELISA

	APP23 mice	APP51/16 mice
Aβ load: ANOVA	p < 0.001	P = 0.008
$Aβ_{1-40}$: ANOVA	p < 0.001	p < 0.001
$Aβ_{1-42}$: ANOVA	p < 0.001	p = 0.012

Comparison of B10-positive material between 15-month-old wild-type, APP23 and APP51/16 mice. The p-values are calculated using the Fischer's exact test. The Bonferoni-correction was used to control for multiple testing.

	Wild-type vs. APP23	Wild-type vs. APP51/16	APP23 vs. APP51/16
B10AP phase of plaque-deposition	p < 0.003	p = 0.03	p < 0.003

C: Quantification of Aβ positive material in the monomeric band in the western blot after SDS-PAGE of mouse brain soluble fraction immunoprecipitated with 6E10, B10AP and A11 antibodies or antibody fragments.
The mean grey value of monomeric band was measured for each mouse model and age. The values were compared between different genotypes and ages by One way ANOVA corrected for multiple testing with Games-Howell post-hoc test.

	IP-B10AP	**IP-A11**
Wild-type (5m) vs. APP23 (5m)	p<0.001	p<0.001
Wild-type (5m) vs. APP51/16 (5m)	p<0.001	p=0.004
APP23 (5m) vs. APP51/16 (5m)	p<0.001	p<0.001
Wild-type (12m) vs. APP23 (12m)	p<0.001	p<0.001
Wild-type (12m) vs. APP51/16 (12m)	p<0.001	p<0.001
APP23 (12m) vs. APP51/16 (12m)	p<0.001	p<0.001
APP23 (5 m) vs. APP23 (12 m)	p=0.001	p<0.001
APP51/16 (5 m) vs. APP51/16 (12 m)	p=0.004	p=0.006
APP23 (5 m) vs. APP51/16 (12 m)	p<0.001	p<0.001

D: Deposition of B10AP- and A11-positive material in the human AD and control brain.

The presence of B10AP- and A11-positive dots, plaques or plaque-associated dots was associated with AD. The p-value is calculated using the Fisher's exact test.

	Presence of B10AP dots	Presence of B10AP plaques	Presence of A11-dots	Presence of plaque-associated A11 dots
AD vs. non-AD (= control and ADRP cases)	$p < 0.001$	$p < 0.001$	$p < 0.001$	$p < 0.001$

E: Quantification of Aβ-positive material in the monomeric band in the western blot after SDS-PAGE of human brain soluble fraction immunoprecipitated with B10AP and A11 antibodies.

The mean gray value of monomeric band was measured for each mouse model and age. The values were compared between different genotypes and ages by One way ANOVA corrected for multiple testing with Games-Howell post-hoc test.

	IP-B10AP	**IP-A11**
AD vs. Control	$p<0.001$	$p<0.001$
AD vs. ADRP	$p=0.004$	$p=0.004$
ADRP vs. Control	$p=0.339$	$p=0.011$

Tab. 3: List of human autopsy cases

a) Cases used for histological und immunohistochemical analysis

Case Number	Age	Gender	Diagnosis	CDR-Score	Braak-NFT-Stage	CERAD-Plaque-Score	Aβ-MTL-Phase
1	62	m	Control	0	0	0	0
2	62	m	Control	0	0	0	0
3	66	f	Control	0	0	0	0
4	61	m	Control	0	0	0	0
5	69	f	Control	0	0	0	0
6	66	m	Control	0	1	0	0
7	72	f	Control	0	1	0	0
8	66	m	Control	0	1	0	0
9	60	m	Control	0	1	0	0
10	74	m	Control	0	1	0	0
11	71	m	ADRP	0	1	0	2
12	71	m	Brain infarction, ADRP	0	1	0	3
13	63	f	Brain infarction, ADRP	0	3	1	4
14	83	m	Brain infarction, ADRP	0	3	0	2
15	72	m	ADRP	0	3	0	2
16	84	f	Brain infarction, ADRP	0	3	0	3
17	85	f	ADRP	0	3	1	4
18	66	f	ADRP	n.d.	2	0	2
19	86	m	Vascular Dementia, ADRP	0,5	2	0	2
20	88	m	AGD, ADRP	2	2	1	3
21	78	m	AD	1	4	1	3
22	68	f	AD	1	6	3	4
23	82	m	AD	2	3	2	3
24	89	f	AD	2	4	3	4
25	83	m	AD	3	4	2	4
26	87	f	AD	3	4	1	4
27	78	f	AD	3	5	3	4
28	83	m	AD	3	5	3	4
29	81	f	AD	3	5	1	4
30	89	f	AD	3	5	2	4
31	86	f	AD, AGD	3	6	3	4

b) Cases used for biochemical analysis

Case Number	Age	Gender	Diagnosis	CDR-Score	Braak-NFT-Stage	CERAD-Plaque-Score	Aβ-MTL-Phase
32	60	m	Control	0	0	0	0
33	66	m	Control	0	1	0	0
34	69	f	Control	0	1	0	0
35	71	f	Control	0	1	0	0
36	73	f	ADRP	0	2	0	1
37	68	f	ADRP	0	2	0	2
38	84	f	ADRP	0	2	0	3
39	77	f	ADRP	0	2	0	3
40	78	f	ADRP	0	2	0	3
41	71	m	ADRP	0	2	1	3
42	73	f	ADRP	n.d.	1	0	3
43	91	f	AD	3	4	1	3
44	62	f	AD	3	6	3	4
45	84	m	AD	3	6	3	4
46	79	f	AD	n.d.	4	2	3
47	64	f	AD	n.d.	6	3	4

8 Acknowledgement

I would like to express my gratitude to my supervisor, Prof. Dr. med. D. R. Thal, for giving me the opportunity to work on this project. I also thank him for contributing to my neuropathological and statistical knowledge as well as for confirming my neuropathological findings.

I thank Kathrin Pruy, Alice Yeates, Daniela Schwab for technical help. I am grateful to Irina Kosterin for providing Electron Microscopy data and further technical help, Estibaliz Capetillo-Zarate for providing EM-photoconversion data and tracing data for APP23+APP51/16 mice; D. Abramowski and M. Staufenbiel (Novartis Institutes for Biomedical Research Basel, Switzerland) for providing APP23 and APP51 mice and ELISA results; Sathish Kumar and Jochen Walter for technology transfer and providing antibodies; Haruyasu Yamaguchi (Gunma University School of Health Sciences Maebashi, Gunma, Japan); Christian Haass (DZNE-German Center for Neurodegenerative Diseases, Munich and Adolf-Butenandt-Institute, Biochemistry, Ludwig-Maximilians-University, Munich, Germany); and Marcus Fändrich (Max Planck Research Unit for Enzymology of Protein Folding and Martin-Luther University Halle-Wittenberg, Halle, Germany) for providing commercially not available antibodies.

I would thank Prof. Heiko Braak and Dr. Kelly Del Tredici from the Department of Neurology (Section Clinical Neuroantomy, Center for Clinical Research), University of Ulm for providing permission to reproduce some of the diagrams from previous publications and Dr. Kelly Del Tredici for reading my manuscript. Finally, I am very thankful to my family and friends who have continuously provided me with help and support.

This study was supported by DFG-grants TH624/4-2, TH624/6-1, Alzheimer Forschung Initiative Grant #10810 (received by DRT), SFB610 and the Landesexzellenz-Netzwerk „Biowissenschaften“ (Sachsen-Anhalt) (received by MF).

Ajeet Rijal Upadhaya

Curriculum Vitae

First Name:	Ajeet
Family Name:	Rijal Upadhaya
Date of Birth:	27.03.1979
Place of Birth:	Lalitpur, Nepal
Address:	Ochsensteige 4
	89075 Ulm
	Germany
Email:	ajeetrijal@hotmail.com

EDUCATION

School: 1983-1995 (Baal Vidhya Griha High School, Kathmandu, Nepal)

Higher Secondary Education: 1995-1997 Trichandra College, Kathmandu, Nepal

Bachelor degree in Microbiology 1998-2001, Tribhuvan University, Kathmandu Nepal

Bachelor in Biology (Biomedical Science): 2002 – 2005, FH-Bonn Rhein Sieg, Germany

Masters degree in Molecular Biotechnology (MSc): University of Bonn, Bonn, Germany (October 2005- September 2007)

PhD student at the University of Ulm, Germany, Institute of Pathology, Section Neuropathology, (since January 2008)

Thesis title: Amyloid beta-protein deposition and toxicity in animal models of Alzheimer's disease.

List of Publications:

1. Utter S, Tamboli IY, Walter J, **Rijal Upadhaya A**, Birkenmeier G, Pietrzik CU, Ghebremedhin E, Thal DR (2008) Cerebral small vessel disease-induced apolipoprotein E leakage is associated with Alzheimer disease and the accumulation of amyloid beta-protein in perivascular astrocytes. J Neuropathol Exp Neurol 67:842-856.

2. Rolyan H, Feike AC, **Rijal Upadhaya A**, Waha A, Van Dooren T, Haass C, Birkenmeier G, Pietrzik CU, Van Leuven F, Thal DR (2011) Amyloid-beta protein modulates the perivascular clearance of neuronal apolipoprotein E in mouse models of Alzheimer's disease. J Neural Transm.

3. **Rijal Upadhaya A**, Lungrin I, Yamaguchi H, Fändrich M, Thal DR (accepted for publication) High-molecular weight Aβ-oligomers and protofibrils are the

predominant Aβ-species in the native soluble protein fraction of the AD brain. J Cell Mol Med. doi:10.1111/j.1582-4934.2011.01306.x.

4. **Rijal Upadhaya A**, Capetillo-Zarate E, Kosterin I, Abramowski D, Kumar S, Yamaguchi H, Walter J, Fändrich M, Staufenbiel M, Thal DR (accepted for publication) Dispersible amyloid β-protein oligomers, protofibrils, and fibrils represent diffusible but not soluble aggregates: Their role in neurodegeneration in amyloid precursor protein (APP) transgenic mice. Neurobiol Aging.

5. Abramowski D, Rabe S, **Rijal Upadhaya A**, Reichwald J, Danner S, Staab D, Capetillo-Zarate E, Yamaguchi H, Saido T, Wiederhold K, Thal DR (accepted for publication) Transgenic expression of intraneuronal $A\beta_{42}$ but not $A\beta_{40}$ leads to cellular Aβ lesions, degeneration and functional impairment without typical Alzheimer's disease pathology. J Neurosci.